Strategies of the ubiquitous freshwater diatom *Achnanthidium minutissimum* in response to phosphate limitation

Doctoral thesis for obtaining

the academic degree Doctor of Natural Sciences

(Dr. rer. nat.)

Submitted by

Adrien Lapointe

at the

Universität Konstanz

Faculty of Sciences

Department of Biology

Konstanz, 2024

Day of the oral examination: 16/12/2022

1st speaker: Pr. Dr. Peter Kroth

2nd speaker: Pr. Dr. Graham J C Underwood

“To Catherine and Béatrice”

Contents

Summary **1**

Zusammenfassung **3**

Abbreviations **5**

Chapter 1. General Introduction **6**

The crucial role of phosphorus in nature 6
Global phosphorus sources and transports 8
Phosphorus cycle in lakes 9
Lake Constance and phosphorus availability 10
Diatom: a "chimeric organism" 11
Adaptations in diatoms to phosphorus limitation 13
Benthic diatoms: a sticky lifestyle 15
Achnanthidium minutissimum 17
Aims 18

Chapter 2. High throughput method for extracting polyphosphates from diatoms **19**

Abstract 19
Introduction 20
Materials and methods 21
Cultivation conditions 21
Extraction and purification of polyP 21
PolyP quantification 23
Determination of polyP recovery 25
Common lysis buffers and self-made gel filtration columns preparation 25
Statistical analysis and diagrams 27
Results 27
Comparison of different polyP extraction methods in *A. minutissimum* 27
PolyP extraction using common lysis buffers and self-made gel filtration columns 28
Characterization of the polyP extraction and quantification parameters using the Nexttec DNA isolation kit approach 30
Recovery of polyP after extraction and purification using the optimized Nexttec DNA isolation kit protocol 31
Scope of the newly established polyP extraction and purification method 32
Discussion 33
Conclusions 35

Acknowledgements 35

Chapter 3. Characterization of polyphosphate dynamics in the widespread freshwater diatom *Achnanthidium minutissimum* under varying phosphorus supplies. 36

Abstract 36
Introduction 37
Materials and methods 39
Growth conditions and experimental cultures 39
Screening for bacterial contaminations 40
Cell counts and growth rate 40
Quantification of dissolved extracellular phosphate 41
PolyP quantification 41
Size distribution of polyP from *Achnanthidium minutissimum* 42
Scanning electron microscopy 43
Stimulated Raman microscopy of *Achnanthidium minutissimum* 43
Vacuoles staining in *Achnanthidium minutissimum* 44
Data analysis 44
Results 45
Achnanthidium minutissimum possesses polyP-containing granules enclosed in vacuoles 45
Estimation of polyP chain-lenghts from *Achnanthidium minutissimum* 48
Impact of phosphate availability on diatom physiology 50
Discussion 55
Achnanthidium minutissimum stores polyP granules in vacuoles resembling acidocalcisomes organelles 55
The resistance of *Achnanthidium minutissimum* and reduction of polyP reservoirs under phosphate-limiting conditions 56
PolyP production of starved cells after phosphate resupply: the overplus mechanism 57
Conclusions 59
Acknowledgements 60

Chapter 4. An intimate view into the biofilm formation of *Achnanthidium minutissimum*: A first structural and biochemical characterization of the stalk 61

Abstract 61
Introduction 62
Material and methods 63
Growth conditions 63
Co-cultivation of the diatom with bacteria 63

Scanning electron microscopy (SEM) and energy-dispersive X-ray (EDX) spectroscopy 64
Transmission electron microscopy (TEM) 65
DAPI staining for fluorescence microscopy 65
DAPI-polysaccharides complex 65
Stimulated Raman spectroscopy 66
Results 66
DAPI shifting fluorescence in extra- and intracellular structures in *A. minutissimum* 66
Mapping of the atom distribution in *A. minutissimum* using energy-dispersive X-ray (EDX) analysis 68
DAPI shifting fluorescence 69
Characterization of the stalk ultrastructure in *A. minutissimum* 71
Discussion 72
Conclusion 75
Acknowledgements 75
Chapter 5. Effects of varying phosphorus supplies on the resilience and the biofilm formation of the freshwater diatom *A. minutissimum* 76
Abstract 76
Introduction 77
Material and methods 78
Organisms and cultivation conditions. 78
Co-cultivation of the diatoms with bacteria in different P supplies. 79
Quantification of dissolved extracellular phosphate 80
Staining and microscopy 81
Results 81
Dissolved extracellular phosphate 82
Growth of the diatoms in biofilm form 83
Stalk length 85
Discussion 86
Alkaline phosphatase activity: a marker of phosphorus stress in *A. minutissimum* 86
The role of stalk elongation in *A. minutissimum* 87
Conclusion 89
Acknowledgements 89
Chapter 6. General Discussion 90
A new method for extraction and quantification of polyP in diatoms: easy-to-use, specific and high throughput 90
Pre-conditioning history: the importance of phosphorus reserves 92

Extra- and intracellular P sensing in *A. minutissimum*? 94
The life of *A. minutissimum* in biofilm: "the tallest tree in the forest" 96
Conclusions and perspectives 99
Acknowledgements **102**
Author contributions **104**
Supporting information **106**
Chapter 2. High throughput method for extracting polyphosphates from diatoms 106
Chapter 3. Characterization of polyphosphate dynamics in the ubiquitous freshwater diatom *A. minutissimum* under varying phosphorus supplies. 109
Chapter 5. Effects of varying phosphorus supplies on the resilience and the biofilm formation of the freshwater diatom *A. minutissimum* 116
List of publications **117**
References **118**

List of Figures

Chapter 1. General Introduction

Figure 1. 1: Orthophosphate, an inorganic phosphate unit (P_i), is the primary phosphorus form in biology 6
Figure 1. 2: Diversity of phosphate compounds found in living organisms 7
Figure 1. 3: Photoautotrophic epilithic biofilms of Lake Constance 11
Figure 1. 4: Different lifestyles in *A. minutissimum* 18

Chapter 2. High throughput method for extracting polyphosphates from diatoms

Figure 2. 1: Comparison of the polyP extraction efficiencies from *A. minutissimum* using different methods 27
Figure 2. 2: PolyP extraction efficiencies from *A. minutissimum* using self-made methods ... 29
Figure 2. 3: Characterization of the polyP extraction, purification, and quantification parameters using the Nexttec DNA isolation kit 30
Figure 2. 4: Recovery of polyP standards 32
Figure 2. 5: PolyP quantification using the optimized Nexttec DNA isolation kit protocol and performed on various diatoms 33
Figure 2. 6: Workflow of the protocol for extraction, purification and quantification of polyP in diatoms 34

Chapter 3. Characterization of polyphosphate dynamics in the widespread freshwater diatom *Achnanthidium minutissimum* under varying phosphorus supplies

Figure 3. 1: Detection of granules containing phosphorus in an *Achnanthidium. minutissimum* cell 46
Figure 3. 2: Localization of the vacuoles in the diatom *Achnanthidium. minutissimum* 47
Figure 3. 3: PolyP detection in *Achnanthidium. minutissimum* cells using stimulated Raman scattering (SRS) microscopy 48
Figure 3. 4: Gel electrophoresis of polyP extracted from *Achnanthidium. minutissimum* cultivated in P-replete $P_{(+)}$ conditions 49

Figure 3. 5: Cultivation of *Achnanthidium. minutissimum* under different P availabilities 51
Figure 3. 6: SRS images of *Achnanthidium minutissimum* cells showing the dynamic of polyP granules and lipids in cells before and after medium resupply……..……54
Figure 3. 7: Schematic figure showing the P physiology of the diatom *A. minutissimum* in different nutrient availability scenarios 58

Chapter 4. An intimate view into the biofilm formation of *Achnanthidium minutissimum*: A first structural and biochemical characterization of the stalk

Figure 4. 1: DAPI staining revealing blue and yellow fluorescent structures in *A. minutissimum* co-cultivated with *Dyadobacter* sp. 32 66
Figure 4. 2: Shifts in DAPI signature emission spectra upon binding to DNA or stalks, frustules, and intracellular polyP granules.....67
Figure 4. 3: SRS images via stimulated Raman loss detection of *A. minutissimum* co-cultivated with *Dyadobacter* sp.32.....68
Figure 4. 4: SEM micrograph of *A. minutissimum* co-cultivated with *Dyadobacter* sp. 32.....69
Figure 4. 5: DAPI emission fluorescence spectra upon binding to sulphated polysaccharide and polyP 70
Figure 4. 6. *A. minutissimum* cell and its extracellular adhesives.....71
Figure 4. 7: Enlargement of the TEM micrograph shown in Figure 4. 6 C.....72

Chapter 5. Effects of varying phosphorus supplies on the resilience and the biofilm formation of the freshwater diatom *Achnanthidium minutissimum*

Figure 5. 1: Dynamics of physiological parameters in *A. minutissimum* co-cultivated with the bacterium *Dyadobacter* sp. 32, subjected to different P supplies 82
Figure 5. 2: Representative cellular sites of alkaline phosphatase (AP) activity in the diatom *A. minutissimum* labelled with ELF-97 84
Figure 5. 3: Representative bright-field micrographs of *A. minutissimum* cells producing stalks when co-cultivated with *Dyadobacter* sp. 32 under different P supplies.....85

Chapter 6. General Discussion

Figure 6. 1: Hypothetical scenario of *A. minutissimum* lifestyle in a freshwater epilithic phototrophic biofilm, based on the data collected during this thesis 98

Supporting information

Chapter 2. High throughput method for extracting polyphosphates from diatoms

Figure S2. 1: Standard curve of the OD 882 nm vs the concentration of phosphate (P).....107
Figure S2. 2: Preparation of self-made gel filtration columns using empty commercial spin columns.....108

Chapter 3. Characterization of polyphosphate dynamics in the widespread freshwater diatom *Achnanthidium minutissimum* under varying phosphorus supplies

Figure S3. 1: Ultrastructural SEM image of an *A. minutissimum* cell taken from the same sample containing the cell shown in Figure 3. 1A. 113
Figure S3. 2: *A. minutissimum* cells cultivated in $P_{(+)}$ condition. Diatom cells cultivated in $P_{(+)}$ conditions for 3 days (upper row) and 6 days (lower row). A) Bright-field micrographs. B) Chlorophyll fluorescence. C) BODIPY staining. D) Merged picture from B) and C).....114
Figure S3. 3: Correlation matrices of cell growth rate, extracellular P, polyP amount and cellular P uptake in $P_{(-)}$ and $P_{(+)}$ datasets.....114
Figure S3. 4: Dynamics of the polyP granules in *A. minutissimum* in different P availabilities.. 115

Chapter 5. Effects of varying phosphorus supplies on the resilience and the biofilm formation of the freshwater diatom *A. minutissimum*

Figure S5. 1: Percentage of disrupted cells labelled by ELF-97.....113
Figure S5. 2: Representative micrograph of cells stained by crystal violet after 1h of cultivation with *Dyadobacter sp. 32* 113

List of Tables

Supporting information

Chapter 2. High throughput method for extracting polyphosphates from diatoms

Table S2. 1: Comparison of the polyP determination methods 106

Chapter 3. Characterization of polyphosphate dynamics in the widespread freshwater diatom *Achnanthidium minutissimum* under varying phosphorus supplies

Table S3. 1: Protocol for cell fixation and embedding for SEM visualization.. 110
Table S3. 2: Final cell densities and growth rates of *A. minutissimum* after 15 days of cultivation under $P_{(+)}$ and $P_{(-)}$ conditions before medium exchange.. 110
Table S3. 3: Final cell densities and growth rates of *A. minutissimum* after 18 days of cultivation under $P_{(+/+)}$ or $P_{(-/+)}$ conditions 111
Table S3. 4: Rate of polyP synthesis and degradation , before media resupply for $P_{(+)}$ cultures, and after medium resupply at d 15 for $P_{(+/+)}$ cultures. 111
Table S3. 5: Rate of polyP synthesis and degradation, before media resupply for $P_{(-)}$ cultures, and after medium resupply at d 15 for $P_{(-/+)}$ cultures..... 111
Table S3. 6: Exogenous P_i uptake allocated to polyP synthesis, before media resupply for $P_{(+)}$ and $P_{(-)}$ cells, and after medium resupply at d 15 for $P_{(+/+)}$ and $P_{(-/+)}$ cells. 111

Summary

Diatoms are primary producers found in both marine and freshwater environments and are the most diverse group of microalgae. They contribute to ca. 20% of annual global carbon fixation and contribute to the biogeochemical cycles. Diatoms occupy a variety of environments, including the benthic habitat where they are often the most abundant eukaryotes. A crucial part of the biological success of the diatoms is their ability to form biofilm by excreting adhesive extracellular polymeric substances (EPS) structures, allowing them to attach to surfaces. Such a strategy allows the diatom and other microorganisms (eukaryotes, prokaryotes) to stay fixed on a substratum exposed to sufficient nutrients and light. Together, the consortium of microorganisms is encased in a polysaccharide matrix, which exerts considerable control over the movement of nutrients from the water column to the biofilm. A nutrient limitation may occur as the biofilm get denser, resulting in competition between microorganisms for nutrients. Phosphorus (P) is an essential nutrient utilized by the whole life kingdom for growth, energy transport and membrane synthesis. Despite the dramatic consequences of P starvation due to its scarcity in some aquatic environments, many microalgae can thrive in P-limited environments, including the benthic diatom *A. minutissimum*. Initially isolated from an oligotrophic lake (Lake Constance, Germany), the diatom can form a biofilm by producing a stalk made of polysaccharides in the presence of the bacterium *Dyadobacter* sp. 32. Works in laboratory cultures showed that the diatom in axenic or biofilm form can continue to divide for several days (ca. 2 weeks), after a transfer in a P-deplete cultivation medium. Such resistance implies the presence of P reserves within the diatom, sustaining the cell in P for several new generations. Several strategies are known in diatoms to cope with P-limited conditions, but most research to date has focused on the adaptations in marine phytoplankton and biogeochemical cycles. However, freshwater benthic diatoms such as *A. minutissimum* likely have developed strategies of survival in such environments. This thesis has the aim to understand the strategies of the ubiquitous diatom *A. minutissimum* for adapting under P limitation, in its planktonic as well as its biofilm form. Herein, we identified intracellular granules of polyphosphate (polyP), a variable-length chain of inorganic phosphate units linked by phosphoanhydride bonds. The identification was unambiguously supported via a combination of stimulated Raman spectroscopy as well as elemental electron microscopy analyses. We developed an easy-to-use method for extracting the polyP in diatoms based on gel filtration. We investigated the

physiology of the axenic diatom under variable exogenous P availability. We discovered that the diatom can thrive in fluctuating P conditions by rapidly accumulating polyP when extracellular P is available. The polyP reserves in diatoms were rapidly declining when cells were subjected to exogenous P depletion, suggesting the use of polyP for buffering cells in P. The biofilm formation was of particular interest as we investigated the biochemical composition of the stalk produced by the diatom. Using a combination of microscopy techniques, we revealed that the stalk of *A. minutissimum* is composed of sulphated polysaccharides, probably cross-linked by metal ions such as magnesium and iron. We identified further adaptations developed by the diatom in biofilm form under P-limited conditions. Notably, the ability of the cell to produce surface-associated alkaline phosphatase (AP), allowing the scavenging of organic P forms. The enzyme was suggested to be an indicator of the intracellular P stress of the diatom, as it was displayed by cells subjected to P limitation. Diatoms were able to elongate their stalk only in cultures where higher amounts of cells were displaying AP activity, suggesting an advanced depletion of their intracellular P reserved. This elongation was suggested to elevate the cells from the substratum, allowing better nutrient access than in a dense biofilm. Therefore, intracellular P resources, and notably polyP are proposed to play an important role in the adaptations of the benthic diatom to fluctuating P conditions.

Zusammenfassung

Diatomeen (Kieselalgen) sind Hauptproduzenten in Salz- und Süßwasser und die vielfältigste Gruppe der Algen. Sie tragen zu ca. 20 Prozent der jährlichen globalen Kohlenstofffixierung bei und treiben biogeochemische Kreisläufe an. Diatomeen leben in unterschiedlichen Umgebungen, einschließlich des benthischen Lebensraums. In diesem sind sie die am häufigsten vorkommenden Eukaryonten. Einen entscheidenden Teil des biologischen Erfolgs verzeichnen Diatomeen vor allem in der Bildung von Biofilmen. Dabei scheiden sie extrazelluläre, polymere Substanzen (EPS) aus, die klebende Strukturen bilden, mit denen sie sich an Oberflächen anhaften können. Solche Strategien ermöglicht es den Kieselalgen und anderen Mikroorganismen (Eukaryonten, Prokaryonten), auf einem Substrat zu haften, welches ausreichend Nährstoffen und Licht ausgesetzt ist. Zusammen ist das Konsortium von Mikroorganismen in eine Polysaccharidmatrix eingeschlossen, die beträchtliche Kontrolle über die Bewegung von Nährstoffen von der Wassersäule zum Biofilm ausübt. Sobald der Biofilm dichter wird, kann Nährstoffbegrenzung auftreten. Sie führt um die noch verfügbaren Nährstoffe zu einer Konkurrenz zwischen den Mikroorganismen. Phosphor (P) ist ein essentieller Nährstoff, der von allen Lebewesen für Wachstum, Energietransport und Membransynthese benötigt wird. Trotz der dramatischen Folgen des P-Mangels, aufgrund seiner Knappheit in einigen aquatischen Lebensräumen, können viele Mikroalgen (darunter benthische Diatomeen wie *A. minutissimum*) in P-armen Umgebungen gedeihen. Die ursprünglich aus einem oligotrophen See (Bodensee, Deutschland) isolierten Diatomeen können einen Biofilm bilden, indem sie in Gegenwart des Bakteriums *Dyadobacter* sp.32 Polysaccharid-Stiele produzieren. Arbeiten an den Laborkulturen haben gezeigt, dass sich Diatomeen in axenischer oder Biofilm-Form, auch nach einem Transfer in ein P-armes Kulturmedium, noch mehrere Tage (ca. 2 Wochen) weiter teilen können. Eine solche Resistenz setzt das Vorhandensein von P-Reserven innerhalb der Diatomeen voraus, die die Zelle mit P versorgen. Es sind mehrere Strategien bekannt, um mit P-begrenzten Bedingungen zurechtzukommen. Die meisten Forschungen haben sich bisher auf die Anpassungen in marinem Phytoplankton und die biogeochemischen Kreisläufe konzentriert. Allerdings haben auch benthische Süßwasserdiatomeen wie *A. minutissimum* sehr wahrscheinlich Strategien entwickelt, um in einer solchen Umgebung zu überleben. Ziel dieser Arbeit ist es, die Anpassungsstrategien der ubiquitären Kieselalge *A. minutissimum* unter P-Limitierung, sowohl in ihrer planktonischen, als auch in ihrer Biofilmform zu verstehen. In dieser Arbeit

identifizierten wir intrazelluläre Granula von Polyphosphat (polyP), die durch Phosphoanhydridbindungen vernetzte P-Ketten variabler Länge bilden. Durch eine Kombination aus stimulierter Raman-Spektroskopie und elementarer Elektronenmikroskopie wurde die Identifizierung von PolyP eindeutig bestätigt. Des Weiteren haben wir eine einfach zu handhabende, auf Gelfiltration basierende Methode zur Extraktion von PolyP in Diatomeen entwickelt. Die Untersuchungen konzentrierten sich auf die Physiologie der axenischen Diatomeen unter variabler exogener P-Verfügbarkeit. Forschungen zeigten, dass die Diatomeen unter schwankenden P-Bedingungen gedeihen können, indem sie schnell P-Reserven und vor allem PolyP ansammeln, sobald dies extrazellular gegeben ist. Die PolyP-Reserven in Diatomeen nahmen zu Beginn der P-limitierten Bedingungen rasch ab, was auf die Funktionsweise von PolyP als Puffer von P hindeutet. Die Biofilmbildung war von besonderem Interesse, da wir mit einer Kombination von Mikroskopietechniken das Vorhandensein sulfatierter Polysaccharid-Stielen biochemisch charakterisierten. Sie sind aller Wahrscheinlichkeit nach, durch Metallionen wie Magnesium und Eisen vernetzt. Wir untersuchten weitere Anpassungsmöglichkeiten der Diatomeen in ihrer Biofilmform und unter P-begrenzten Bedingungen. insbesondere die Fähigkeit der Zelle, oberflächenassoziierte alkalische Phosphatase (AP) zu produzieren. Diese ermöglichen das Abfangen von organischen P-Formen. Das Enzym könnte ein Indikator für den intrazellulären P-Stress der Kieselalge sein, da es von Zellen, die einer P-Limitierung ausgesetzt waren, gebildet wurde. Kieselalgen konnten ihren Polysaccharid-Stiel nur in Kulturen verlängern, in denen eine größere Anzahl von Zellen AP-Aktivität zeigte, was auf eine fortgeschrittene Abnahme ihrer intrazellulären P-Reserven schließen lässt. Die Verlängerung der Zellen hebt diese vermutlich vom Substrat ab und ermöglicht ihnen einen besseren Zugang zu den Nährstoffen als in einem dichteren Biofilm. Somit besteht die Annahme, dass die intrazellulären P-Ressourcen, insbesondere PolyP eine wichtige Rolle bei der Anpassung der benthischen Kieselalge an schwankende P-Bedingungen spielen.

Abbreviations

AM: *Achnanthidium* medium

ATP: adenosine triphosphate

AP: alkaline phosphatase

CM: cell membrane

CHO: carbohydrate

CLSM: confocal laser microscopy

d: days

ddH_2O: double distilled water

DAPI: 4',6-diamidino-2-phenylindole

DNA: deoxyribonucleic acid

EDX: energy-dispersive X-ray

EPS: extracellular polymeric substances

FCMG: frustule-cell membrane gap

FP: frustule pores

GITC: guanidine isothiocyanate

HPO: hymenate pore occlusion

LB: lipid body

LOQ: lower limit of quantitation

min: minutes

NMR: nuclear magnetic resonance

P: phosphorus

P_i: inorganic phosphate unit

PL: phospholipid

polyP: polyphosphate

$P_{(+)}$: phosphorus-replete

$P_{(-)}$: phosphorus-deplete

$P_{(+/+)}$: pre-conditioning in $P_{(+)}$ followed by a transfer in $P_{(+)}$

$P_{(+/-)}$: pre-conditioning in $P_{(+)}$ followed by a transfer in $P_{(-)}$

$P_{(-/-)}$: pre-conditioning in $P_{(-)}$ followed by a transfer in $P_{(-)}$

$P_{(-/+)}$: pre-conditioning in $P_{(-)}$ followed by a transfer in $P_{(+)}$

PPX: exopolyphosphatase

R: raphe channel

RNA: ribonucleic acid

s: seconds

S: stalk

SEM: scanning electron microscopy

SL: sulfolipid

SRS: stimulated Raman spectroscopy

TEM: transmission electron microscopy

VTC: vacuolar transporter chaperone

q_0: minimum phosphorus per cell

Chapter 1. General Introduction

The crucial role of phosphorus in nature

During his quest for the philosopher's stone, the German alchemist Hennig Brand in 1669 observed that a white solid obtained after heating a mixture of sand and charcoal with a tar-like substance produced after boiling human urine, can glow in the dark and ignite spontaneously in contact with air (Weeks, 1933). Consequently, he named this solid literally "light-bearing" from the Greek words "Phos" (light) and "Phorus" (bearing) (Benitez-Nelson, 2000), and so phosphorus (P) was discovered. The importance of P as a nutrient was recognized during the mid-1800s and was subsequently utilized as fertilizer for soils via dissolution by H_2SO_4. Large deposits of phosphorus rocks can be found in the Middle East, China, Russia, Morocco, and the USA. As an exploitable resource, estimations suggest phosphorus reserves will be depleted in less than a century (Brinck, 2009).

The most common forms of phosphorus are phosphates, based on anionic phosphorus (V) entity surrounded by four atoms of oxygen (PO_4). Orthophosphate is an inorganic (not bound to carbon) phosphate unit (P_i, Figure 1. 1), which is the basis for a multitude of complex inorganic or organic (bound to carbon) P compounds. Exceptions exist where one or more oxygen atoms are exchanged for other atoms like sulphur (S), Hydrogen (H), or Fluorine (F) (Kamerlin *et al.*, 2013).

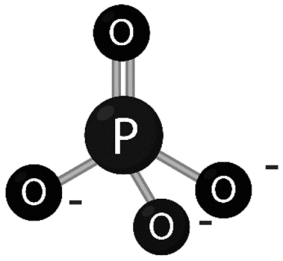

Figure 1. 1: Orthophosphate, an inorganic phosphate unit (P_i), is the primary phosphorus form in biology.

"Why nature chose phosphates?" A question that the biochemist Frank Westheimer asked when observing that "Phosphates are ubiquitous in biochemistry". He answered that phosphates "can do almost everything" (Westheimer, 1987). Indeed, when we look at a cell, phosphates exist in various states of protonation and esterification and can be found in inorganic form (orthophosphate, pyrophosphate polyphosphates) and organic form (DNA, lipids,

phosphonates) (Figure 1. 2). P compounds in cells play crucial roles in a multitude of cellular processes.

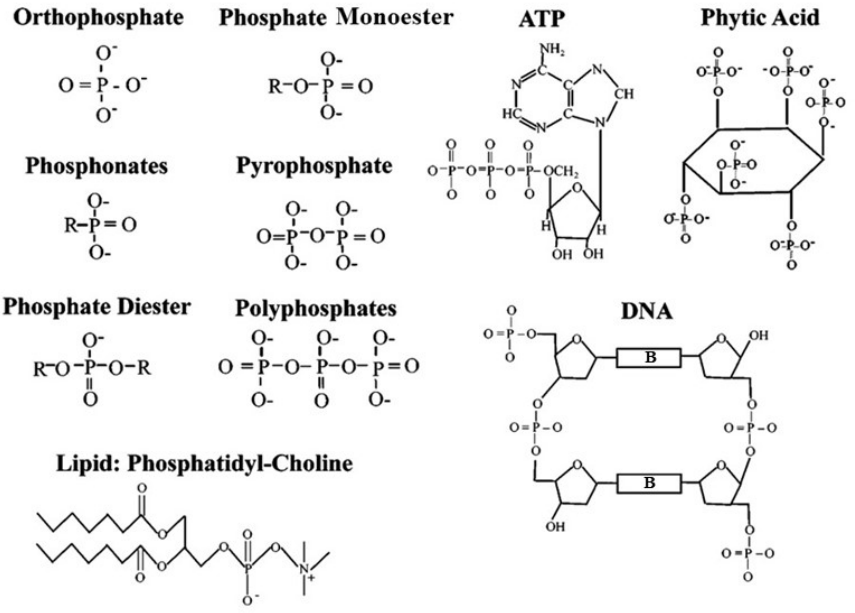

Figure 1. 2: Diversity of phosphate compounds found in living organisms. The B in the DNA molecule represents the base pairs. Modified from Paytan and McLaughlin (2007).

Starting at the cell membranes, phosphates are found in lipid membranes as phospholipids (PL) (Figure 1. 2); which contribute to 5-10% of cellular biomass in most cells (Harris, 2003). Looking at the nucleus, phosphate diesters contribute to ca. 9% of the mass of nucleic acids (DNA and RNA) and are crucial elements in the stability of the genetic information by linking together the nucleosides (Elser, 2012, Harris, 2003, Westheimer, 1987) (Figure 1. 2). Moreover, phosphates are also present in the structure of adenosine triphosphate (ATP), the molecule providing the principal source of biochemical energy for the cell (Figure 1. 2). The phosphoanhydride bond, which binds two phosphate groups in ATP is highly energetic and can be released via hydrolysis to support cellular metabolism. The ubiquity of phosphates within the cell is undeniable but it still does not answer why nature selected it in a myriad of cellular processes.

Most importantly, the key biological role of phosphates within the cell is their "importance of being ionized" (Davis, 1958). Electrostatic interactions between negative and positive charges were possibly the most primitive mode of interactions between molecules. According to Davis,

molecule ionization is an important biochemical feature that has created the right conditions for the evolution of life (Davis, 1958). Starting with cell membranes, the negative charges present in phospholipids due to the presence of the phosphate polar heads contribute to the repulsive forces that self-organize the lipid bilayer. The electrostatic repulsion between the negatively charged phosphates of an ATP is used as a source of biological energy in nature (Kamerlin et al., 2013). In addition to its structural role, the phosphate diesters backbone in DNA confers a negative charge to the molecule. This in turn provides protection of the DNA against hydrolysis as well as its containment within the lipid membrane, instead of being diffused through it and being lost from the cell. From a thermodynamics and geometry point of view, arsenate (As) ion ($[AsO_4]^{3-}$) was speculated to be a plausible candidate for replacing phosphate in the DNA (Denning & MacKerell Jr, 2011). However, arsenate esters might hydrolyze 7-10 orders of magnitude faster than phosphate esters (Šponer *et al.*, 2012), potentially making an As-DNA backbone more unstable than based on phosphate. Moreover, a computational investigation showed a superior match in terms of structure and interaction energy between proteins-DNA/RNA and phosphate than between proteins-DNA/RNA and As, suggesting that evolution has optimized the inter-relationship between protein and DNA/RNA based on phosphate compounds (Xu *et al.*, 2012).

Global phosphorus sources and transports

Like the carbon or nitrogen cycles, the phosphorus cycle comprises biological and non-biological environmental reservoirs interconnected through different pathways (Mackey *et al.*, 2019). P is the eleventh most abundant element in the Earth's crust (0.09% by weight), occurring in mineral and organic forms. Mineral P is generally formed after magmatic processes or through precipitations from solutions (Mackey et al., 2019), and can be microbially mediated (Diaz *et al.*, 2008). The composition of P minerals depends on the presence of ions within the solution during the precipitation. Apatite [$Ca_5(PO_4)^{3-}$(F, Cl, OH)] is the commonly occurring P mineral within Earth's crust. Additionally, P can be found adsorbed on iron-manganese oxide, or clay particles containing iron and aluminium oxyhydroxides. Collectively, the different P mineral deposits are called "phosphorites", to reflect the variation of their chemical compositions depending on the ions present in the solution during precipitation.

From the erosion of rocks, P-containing minerals reach terrestrial systems and are therefore present in soils. From here, rain leaches charged compounds, including those containing P. The

leaching of mineral P, but also the deposition of dust and aerosols containing P leads to dissolved phosphates entering the water table, where they enter water bodies and ultimately the ocean. Rivers contribute the majority of the P delivered to, and are also the largest source of P in the oceans (Mackey et al., 2019).

Phosphorus cycle in lakes

Lakes comprise 87% of surface liquid state freshwater on Earth (Gleick & Schneider, 1996), and are therefore crucial for Earth's ecosystems. Within the dissolved (particle size <0.2 μm) and particulate (particle size >0.2μm) P fractions entering lakes via rivers, phosphates can be in inorganic or in organic form. Of these forms, the inorganic phosphate unit (P_i) is preferentially assimilated by phytoplankton (Figure 1. 1 (Paytan & McLaughlin, 2007). Assimilated P_i is further transformed into organic phosphate compounds via primary production but also into more complex inorganic compounds such as polyphosphates (Figure 1. 2), (Cotner Jr & Wetzel, 1992). Subsequent events such as cell lysis or grazing of phytoplankton cells by detritivores or zooplankton, the immobilized organic and inorganic phosphate can rapidly return to the P pool of available P in the form of dissolved/particulate organic/inorganic phosphate compounds. Heterotrophic as well as autotrophic microbes use a specific group of enzymes called phosphatases to mineralize organic phosphate through a recycling process called the "microbial loop". Phosphatases comprise a broad range of enzymes depending on their affinity for substrate as well as their optimal pH activity. For example, alkaline phosphatases (AP) are phosphomonoesterases that hydrolyze a phosphate monoester bond, generating a P_i and an alcohol product (Cembella *et al.*, 1984).

Human activity also contributes to the P cycle in lakes. P runoff, caused by unabsorbed P from fertilizers and animal wastes, eventually reaches water ways, where they subsequently enter lakes (Carpenter *et al.*, 1998). This process is promoted by the alteration of the landscape by human activity which promotes increased drainage and runoffs resulting in greater amounts of P loading in waters. Consequently, increased P loads can stimulate large-scale macro/micro algal blooms (Michael Beman *et al.*, 2005), which can be harmful and cause anoxia, fish deaths, and more generally a loss of habitats as well as biodiversity (Tilman *et al.*, 2001).

The remaining P that was not assimilated into the microbial loop via planktonic primary is removed from a lake's water column through sedimentation, reaching the lakebed. Here, benthic organisms structured into autotrophic/heterotrophic assemblages forming biofilms can take up

the remaining P and metabolize it similarly to their planktonic counterparts. Thus, both benthic and planktonic microbes are crucial components of the P cycle in lakes.

Sediments act as an internal nutrient reserve. Like in soils, sediments contain insoluble phosphorites. P can be adsorbed onto iron or manganese oxyhydroxide. Unlike phosphorites, adsorbed P can be remobilized at the sediment-water interface in response to physical mixing or by oxido-reduction reactions that release P in a process called "internal P loading" (Koski-Vähälä & Hartikainen, 2001). Finally, decomposition through the P mineralization in aquatic detrital organic matter by microorganisms can also remobilize P from sediments.

Lake Constance and phosphorus availability

Lake Constance is situated at the northern edge (47"N 09"E) of the A1ps. The lake is shared by Austria, Germany, and Switzerland. The lake has mostly a glacial origin from the Alps. Therefore, the nutrient supply in the lake water is low (Petri, 2006). During the 20th century, the rising population around the lake was accompanied by the development of industrial and agricultural activities, which lead to the increasing discharge of pollution to the lake (Hartmann & Nümann, 1977). The increased amounts of P contained in fertilizers and detergents led to the eutrophication of the lake from the 1950s to the 1970s, with a peak of ca. 80 µg/L P_i. Due to the ban on P detergents and the investments in wastewater treatment plants, the re-oligotrophication phase was a great success and the P concentrations in the lake reached similar amounts to the pre-eutrophication period. Currently, P is the limiting nutrient within the lake with < 10 µg/L P_i (IGKB 2020). Due to the decrease of P, the productivity of the lake decreased and the water became clearer. In contrast to the low level of productivity in the water column, the substratum of the littoral of the lake is composed of rocks, which are covered with green-brownish biofilms dominated by pennate diatoms, producing adhesive EPS structures in the form of tubes and stalks for example (Figure. 1. 3A).

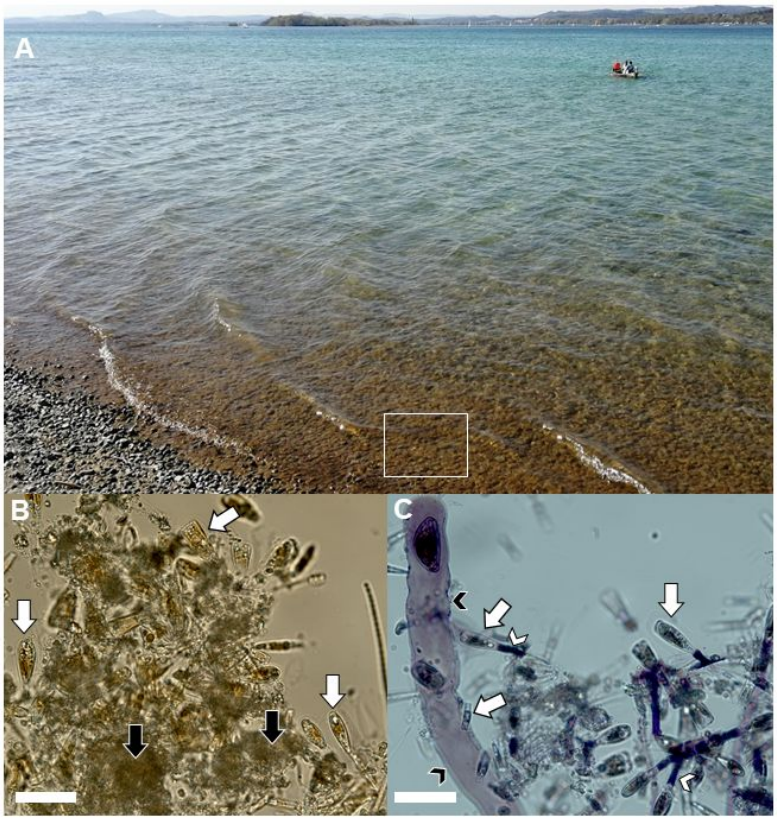

Figure 1. 3: Photoautotrophic epilithic biofilms of Lake Constance. A) Typical littoral zone of Lake Constance displaying rocks covered by a brownish layer of biofilms. A stone from the region indicated by the white square was taken to the lab. A section of the biofilm covering the stone was scraped away and observed under a microscope. B) Bright-field micrograph of the scraped biofilm showing various diatom species (white arrows) in sediment particles (black arrows). C) Crystal violet staining highlights EPS structures like tubes (black arrowheads) and stalks (white arrowheads), produced by the diatoms for attaching to the substratum. Scale bars: 20µm.

Diatom: a "chimeric organism"

Diatoms are eukaryotic unicellular photosynthetic microalgae found globally from tropical and subtropical regions to polar ecosystems, in both marine and freshwater habitats (Field *et al.*, 1998, Pierella Karlusich *et al.*, 2020). Marine diatom photosynthesis generates as much organic carbon as all the terrestrial rainforests combined (Field et al., 1998). Diatoms are the richest class of microalgae with at least 100 000 species according to estimates (Malviya *et al.*, 2016). Diatoms account for the majority (>50%) and are responsible for 40% of the marine primary productivity (Falkowski 1998), and 20% of annual carbon fixation (Pierella Karlusich et al., 2020). Diatoms may have influenced the global climate over geological times because of their

influence on the atmospheric CO_2-oceans fluxes (Armbrust *et al.*, 2004). The carbon generated serves as a base for the marine food web, sustaining the food chain necessary for fisheries on coastal waters.

Diatoms became dominant in aquatic systems 135 million years ago (Falciatore *et al.*, 2020). Their name derives from the Greek "cut in half" which refers to their two-part exoskeleton enclosing their cytoplasm. This exoskeleton, also called frustule, is an arranged amorphous biosilica structure forming pores. The porous structure of the frustule gives to the diatom mechanical strength (Hamm *et al.*, 2003), increasing surface area (Gordon *et al.*, 2009), and unique optical properties (Romann *et al.*, 2015).

Diatoms are the result of complex endosymbiotic events. The initial primary endosymbiosis event occurred ca. 1,5 billion years ago when a heterotrophic microorganism engulfed a cyanobacterium to form the photosynthetic plastids of the Archaeplastida. The resulting progenitor plant cell diverged into the ancestor of green algae, land plants, and red algae (Yoon *et al.*, 2004). In these newly formed groups, gene transfer from the cyanobacterial genome to the nucleus of the host occurred. 10% of the Archaeplastida genes have a cyanobacterial origin (Reyes-Prieto *et al.*, 2006). A secondary endosymbiotic event occurred about 500 million years later when a different heterotrophic cell engulfed a red alga and perhaps a green alga (Becker *et al.*, 2008). The progenitor cell led to a diverse array of algae, including the Heterokontophyta division, also known as stramenopiles, containing the diatom group. The red algal endosymbiont became the plastid of the diatoms group. Genes transfer continued from the genome of the endosymbiont to the host nucleus, with 170 red-algal genes being transferred in the nuclear diatom genome, mostly coding for plastid components (Bowler *et al.*, 2008). Meanwhile, the nucleus and mitochondria of the endosymbiont are lost, and horizontal gene transfer events from the bacterial donor enriched the Stramenopila genome. This complex evolutionary history has led to a "chimeric" diatom genome, consisting of genes originating from a variety of microorganisms.

Diatoms are generally classified based on their morphology and are separated into two lineages according to their symmetry, with centric and pennate diatoms. Centric diatoms (e.g., *Thalassiosira pseudonana*) have radial symmetry, while the pennate diatoms (e.g., *Phaeodactylum tricornutum*) have bilateral symmetry. First diatoms were centric and 120 million years ago, pennate species emerged (Armbrust, 2009). Some pennate diatoms have an additional morphological trait with the apparition of a longitudinal slit in the cell wall called a raphe (raphid diatoms), enabling their motility and attachment on surfaces. Raphid diatoms

outnumber the other diatom lineages in terms of diversity because their penchant to colonize and adapt to a variety of habitats (like sea-ice in polar oceans to the benthic lifestyle in freshwater ecosystems) has led to a vast amount of speciation. Benthic diatoms are of particular focus for the following of this thesis because they have successfully colonized surfaces by forming biofilms.

The "chimeric" diatom genome is likely a key factor in explaining the diversity of diatoms, as well as their survival strategies in dynamic aquatic environments (Bowler et al., 2008). Given their ecological importance and their extreme diversity, diatoms are a good subject for studying the drivers of adaptations to biotic and abiotic changes, occurring in aquatic environments. In the last two decades, the development of the molecular "omic" approaches greatly improved our comprehension of carbon (Kroth *et al.*, 2008), nitrogen (Levitan *et al.*, 2015), iron (Groussman *et al.*, 2015) as well as P metabolism in diatoms (Dyhrman *et al.*, 2012). Among this panel of nutrients, P is commonly regarded as the ultimate limiting nutrient in ocean and freshwater systems, as any nitrogen deficit can be virtually compensated by nitrogen fixation (Martiny *et al.*, 2019, Tyrrell, 1999). Diatoms have developed a panel of adaptations for facing P limitation to achieve high growth rates, comprising the modulation of P transporters, P scavenging, lipidome rearrangement, and cellular P storage (Lin *et al.*, 2016).

Adaptations in diatoms to phosphorus limitation

The first adaptation of diatoms to P limitation is the "scavenging" of organic P compounds. This adaptation relies on the use of alkaline phosphatases (AP) enzymes, which hydrolyse organic P compounds released after cell lysis due to grazing activities for example and produce a P_i which is readily assimilated by the cell (Paytan & McLaughlin, 2007). Molecular analyses revealed that the expression of genes encoding AP in *P. tricornutum* is modulated according to the external P concentration (Dell'Aquila & Maier, 2020). The AP activity in *P. tricornutum* is localized to the cell wall (Flynn *et al.*, 1986), and is also released extracellularly under P limitation (Lin *et al.*, 2013). In addition, a putative AP was shown to be associated with the endoplasmic reticulum (ER) and the plastid membrane, suggesting internal P scavenging occurring during the phospholipid (PL) degradation pathway, as proposed in Dell'Aquila et al. (2020). In addition to AP, diatoms may also produce extracellular nucleotidases, with transcripts upregulated under P limitation (Alipanah *et al.*, 2018). To increase the chance of capturing the orthophosphates released during AP activity, cells increase the amount of high-

affinity P_i transporters on their plasma membrane. Under P limitation, the increasing amounts of P_i transporters at the cell surface have been shown to increase the maximum nutrient-uptake (Vmax) in *P. tricornutum* (Caceres *et al.*, 2019). Ambient P concentrations control the regulation of the high-affinity P_i transporters in *P. tricornutum* by down-regulating the expression of these transporters after a P_i resupply (Cruz de Carvalho *et al.*, 2016). Taken together, hydrolysation of organic P compounds and synthesis of high-affinity P_i transporters contribute to the optimization of P bioavailability and uptake by diatoms under P limitation.

Remodelling of a cell's lipidome in response to environmental changes is a common process in microorganisms (Benning *et al.*, 1995, Huang *et al.*, 2019). Marine phytoplankton populations can substitute non-P-containing lipids for PL in their membranes under P limitation (Van Mooy *et al.*, 2009). That is, the sulfolipid (SL) sulfoquinovosyldiacylglycerol (SQDG) substitutes the phospholipid phosphatidylglycerol (PG) and betaine class lipids like diaglyceryl-hydroxymethylN,N,N-trimethyl-β-alanine (DGTA) substitutes phosphatidylcholine (PC). Substitution of SL for PL is a marker of P-stress in oligotrophic environments (Martin *et al.*, 2014). It is also known that diatoms biosynthesized large reserves of non-P-containing triacylglycerol under P stress (Brembu *et al.*, 2017). The onset of membrane lipid remodelling in the diatom *T. pseudonana* occurs only 24h after the cultivation of the diatom during P limitation (Martin *et al.*, 2011). Such a response allows cells to reduce their P demands (ca. 17 %), allowing a growth advantage by prioritizing nucleic acids for which no P substitute exists. (Hunter *et al.*, 2018). Recent work showed that the membrane lipid remodelling response was accompanied by a minor PL net breakdown in *T. pseudonana* under P limitation, while the majority of PL remained intact and was diluted among progeny cells. However, the breaking down of PL to available P was sufficient for covering DNA synthesis during the time course of the experiment (ca. 3 days) (Hunter et al., 2018). Thus, membranes PL are a P reservoir in diatoms, sustaining cells under P limitation, but other P reserves exist in microalgae.

In addition to efficient nutrient acquisition and lipid membrane breakdown and remodelling, microalgae can store P in the form of P-rich inclusions known as polyphosphate (polyP). PolyP is a chain of P_i (from three to several hundred) linked by phosphoanhydride bonds (Brown & Kornberg, 2004) (Figure 1. 2). PolyP has diverse physiological roles, including stress responses (nutrient, osmotic, or heat), stationary-phase adaptations, protein binding, metal complexation, energy, and P reserves (Rao *et al.*, 2009). Among the multiple roles of the molecule in microorganisms, the dynamics of polyP in response to changing P availability is of particular interest (Kornberg *et al.*, 1956, Harold, 1966). Regarding *de novo* polyP synthesis, two separate

processes exist. The first of these is called “luxury uptake of P” where cells accumulate polyP under conditions of P supplies above the P requirement. Luxury uptake of P is a process, which is believed to occur typically in habitats where cells have abundant P supplies (Orchard *et al.*, 2010, Sforza *et al.*, 2018). In contrast, the second process of polyP accumulation is termed “overplus response”, where cells living in P limited habitats, experience an exogenous P pulse resulting in a rapid uptake of the nutrient and a dramatic increase in polyP production (Liss & Langen, 1962). The latter process has been extensively studied in phytoplankton in ocean and freshwater habitats (Aitchison & Butt, 1973, Kulaev *et al.*, 2004, Sicko-Goad & Jensen, 1976, Sanz-Luque *et al.*, 2020, Rier *et al.*, 2016, Eixler *et al.*, 2019). The presence of polyP granules has been previously mentioned in the pennate *Navicula pupula* and the centric diatom *Melosira varians* respectively (Mann, 1985, Crawford, 1973). In *P. tricornutum*, the polymer was found to vary in size after osmotic stress with longer polyP chains produced after a hyperosmotic shock, suggesting that synthesis and degradation of polyP may adjust the intracellular osmotic pressure under varying extracellular osmotic conditions (Leitão *et al.*, 1995). Recent investigations on the polyP production through “omic” approaches revealed that the polyP synthesis gene (VTC) of *T. pseudonana* (Dyhrman et al., 2012) and *P. tricornutum* (Dell'Aquila & Maier, 2020), was upregulated under P limitation. So far in diatoms, the location of polyP production within the cell as well as its biochemical characterization, and the quantitative dynamics (luxury uptake of P, degradation, overplus response) have not yet been addressed yet.

Benthic diatoms: a sticky lifestyle

Diatoms are the most frequent early algal colonizers of natural substrata in water and are often considered the most abundant group of organisms within the benthic communities (Wetherbee *et al.*, 1998). Diatoms in the water column cannot actively seek a surface to attach, although a surface-sensing mechanism has been suggested to be activated after initial adhesion (Cooksey & Cooksey, 1988). Instead, diatoms are carried to surfaces passively by gravity or by the action of currents. First contact with the substratum activates a set of processes including stabilization and re-orientation of the cell (Wetherbee et al., 1998). Following the initial adhesion, benthic diatoms can adopt one of the two following lifestyle strategies: diatoms can move on the surface by “gliding”, thus becoming motile (Wetherbee et al., 1998) or become sessile and attach to one position for an extended period and form a biofilm.

Photoautotrophic biofilms refer to a community of surface-attached microorganisms (eukaryotes and prokaryotes), with photosynthetic microalgae (cyanobacteria and diatoms) playing a major role in producing organic molecules through photosynthesis (Underwood & Kromkamp, 2000). In marine environments, photoautotrophic biofilms develop in the intertidal zone, forming a brownish colour due to the abundance of diatoms, and acting as a stabilizer of sediments (Underwood & Paterson, 2003). This benthic lifestyle confers advantages compared to pelagic microbes, namely stability, light, and nutrient access (Letáková *et al.*, 2018), and confers tolerance to environmental stresses. For example, diatoms living in biofilms show better tolerance to salinity stress (Steele *et al.*, 2014) and pollution (Morin *et al.*, 2008) as well as a reduced risk of desiccation (McKew *et al.*, 2011). Moreover, biofilm formation can be triggered by unfavourable environmental conditions, for example, sea-ice diatoms can produce extracellular carbohydrates (CHO) as a strategy to acclimate to cold stress under saline conditions (Aslam *et al.*, 2012).

Many of the advantages that a biofilm confers to the cells originate from its extracellular polymeric substances (EPS) secretions. EPS are described as secreted substances of different chemical and physical natures (Sutherland, 1988). Diatoms can secrete more or less sophisticated EPS structures (Bahulikar & Kroth, 2007), made of polysaccharides that sometimes are composed of specific adhesives molecules (Lachnit *et al.*, 2019) in the form of capsules, pads, tubes, and stalks (Bahulikar & Kroth, 2007, Hoagland *et al.*, 1993). The latter structures are of particular interest to this thesis. The formation of stalks is a common phenomenon in benthic diatoms and is a crucial component of their attachment. Stalks are extruded from the siliceous cell wall and are composed of fine fibrils more or less organized, depending on the diatom species. Stalks can measure from a few to several hundred micrometres, like the stalks produced by the invasive diatom *Didymosphenia germinata* (Whitton *et al.*, 2009). This diatom possesses complex stalks comprising several layers of arranged fibrils (Ehrlich *et al.*, 2016). Diatom stalks are composed of acidic, mainly carboxylated or sulphated polysaccharides (Wustman *et al.*, 1997); and their composition can vary among species (Bahulikar & Kroth, 2007, Wustman et al., 1997). In natural biofilms, along with ensuring the colonization of surfaces, stalks allow cells to elevate above the substratum, thus allowing access to better nutrients and light conditions (Molino & Wetherbee, 2008, Chiovitti *et al.*, 2006, Lewis *et al.*, 2002). For example, the stalk length of *D. germinata* is affected by light and nutrient availability, with diatom stalks elongating after cells experience P limitation (Kilroy & Bothwell, 2011). Although such behaviour allows diatoms to improve

their growth, it can have a serious impact on oligotrophic rivers invaded by *D. germinata* which forms widespread mats. Extensive stalk production may contribute to 90% of the biomass in oligotrophic rivers (Bray *et al.*, 2017).

Thus, diatoms can acclimate to nutrient fluctuations by adjusting their nutrient uptake system and intracellular P metabolism. In addition, they play a crucial role in biofilm formation and environmental factors can control biofilm development. Disentangling these acclimation responses is a critical step in bridging the gap between diatom cellular physiology and biofilm formation under varying environmental conditions.

Achnanthidium minutissimum

The freshwater diatom *Achnanthidium minutissimum* (renamed from *Achnanthes minutissima*, Kützing; Czarnecki 1994) is the primary organism in this thesis. This benthic, pennate diatom is considered to be one of the most common diatom taxa in the world, occurring in alkaline, and acidic, oligotrophic and hypertrophic freshwater (Potapova & Hamilton, 2007), as well as in elevated ionic (Na and Cl) concentrations habitats (Thienpont *et al.*, 2012). The diatom has a peculiar lifestyle by secreting insoluble EPS forming adhesive structures (stalks and capsules) when grown xenically (in presence of natural satellites bacteria living within the biofilm). In contrast, when diatom grows axenically (after removal of bacteria by antibiotic treatment), diatoms only produce soluble CHO (Windler *et al.*, 2015). In the presence of a specific strain of the genus "*Dyadobacter*", designated as *Dyadobacter sp.32*, the diatoms produce a stalk allowing the cells to attach to surfaces (Figure 1. 4). Both the diatom *A. minutissimum* and *Dyadobacter sp.32* have been isolated from photoautotrophic, epilithic biofilms taken from the littoral zone of Lake Constance (Windler *et al.*, 2012). Considering the low P availability in the lake, the benthic diatom must have developed adaptations to resist and adapt to such an environment.

The diatom *A. minutissimum* being widespread in a variety of habitats makes it an excellent candidate for studying diatom adaptations to varying nutrient availability. Moreover, the fact that the diatom can be cultivated in the laboratory both in benthic and planktonic modes allows a comprehensive understanding of the consequences of cellular adaptations to nutrient stress associated with biofilm formation.

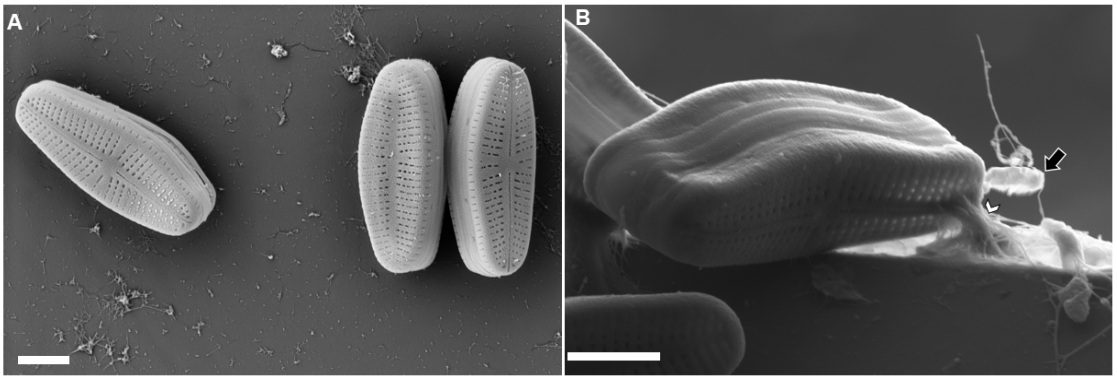

Figure 1. 4: Different lifestyles in *A. minutissimum*. A) Scanning electron micrograph of axenic *A. minutissimum* cells (image produced by Katrin Leinweber at the Electron Microscopy Centre of the University of Konstanz). B) Scanning electron micrograph of *A. minutissimum* cell co-cultivated with bacteria *Dyadobacter sp.32*. The diatom in the presence of the bacteria (black arrow) attaches to the surface and forms a biofilm by producing a stalk (white arrowhead). Scale bars: 2 µm.

Aims

The main goal of this study was to investigate the cellular adaptations of benthic diatoms to varying P availability with a focus on their P reserves dynamics, namely polyP, and the consequences for their biofilm development.

The production and the dynamics of P storages is mainly an unexplored topic in diatoms. Therefore, polyP production was probed using *A. minutissimum* as a model system. The effects of varying P availability on *A. minutissimum* were investigated from different viewpoints, by examining intracellularly its physiology as well as extracellularly its biofilm formation, in the hope to understand better the adaptations of benthic diatoms in biofilm.

Taken together, this thesis builds toward understanding the adaptations of benthic diatoms to thrive in nutrient-varying environments.

Chapter 2. High throughput method for extracting polyphosphates from diatoms

Adrien Lapointe, Dieter Spiteller and Peter G. Kroth

Published in Endocytobiosis and Cell Research, 2022

https://zs.thulb.uni-jena.de/receive/jportal_jparticle_01216927

Abstract

Polyphosphates (polyP) are widely distributed in living organisms and have crucial cellular functions. Little is known about the physiological roles of polyP in algae, especially in diatoms. Therefore, we have developed a standardized method for polyP extraction and quantification from diatoms, using the freshwater model organism *A. minutissimum* and further marine diatoms to validate the method. Investigating the efficiency of polyP extraction methods, we found that a commercial DNA isolation kit yielded best results. The method is based on separation of polyP from lower molecular weight compounds using gel filtration spin columns. Moreover, we demonstrate that self-made gel filtration spin columns and extraction buffers can also extract polyP from *A. minutissimum* efficiently. Under defined conditions, samples spiked with polyP of chain-lengths between 45 to 700 P_i moieties consistently resulted in a recovery of more than 70% of the initially loaded polyP. PolyP was quantified with an ascorbate-antimony-molybdate assay that detects phosphates (P_i) by hydrolysis of a specific exopolyphosphatase (PPX). The method detects as little as 3 µM polyP in high throughput analyses using 96-well plates. This sensitive, rapid and straightforward method is ideal to characterize the physiological role of polyP in diatoms.

Keywords: Diatoms, polyphosphates extraction, gel filtration column, exopolyphosphatase, ascorbate-antimony-molybdate assay, 96-well plate

Introduction

Polyphosphates (polyP) are a naturally occurring polymers consisting of three to several hundreds of phosphate units (inorganic phosphate, P_i) condensed by high-energy phosphoanhydride bonds. In eukaryotic microalgae and cyanobacteria, polyP play an important role in a number of physiological processes, including acclimation to nutrient deprivation (Falkner & Falkner, 2011), DNA synthesis (Murata *et al.*, 2016), heat stress (Barcytė *et al.*, 2020), metal ion sequestration (Sicko-Goad & Lazinsky, 1986), and osmotic stress (Leitão et al., 1995). PolyP recently received attention because of their implication for biogeochemical cycling in marine ecosystems (Orchard et al., 2010, Martin *et al.*, 2018, Martin et al., 2014).

Here, we describe an efficient extraction of polyP from the diatom *Achnanthidium minutissimum* (Round, 2004, Hlúbiková *et al.*, 2011, Potapova & Hamilton, 2007), and compare it to published methods for polyP extraction. Available protocols for polyP analyses in biological samples follow in principle similar workflows, comprising extraction and quantification. PolyP quantification based on the fluorescence of 4',6-diamidino-2-phenylindole (DAPI)-polyP interaction was developed by Aschar-Sobbi et al. (2008), and revisited by Martin and Van Mooy (2013). The latter protocol includes a brief boiling step of the samples in order to inactivate enzymes, followed by protein digestion with proteinase K. This method has often been used for extraction and quantification of polyP from cyanobacteria and marine environmental samples (Li et al. 2019; Martin et al. 2014; Zhang et al. 2015). Although being sensitive (detection limit < 1µM), it requires multiple extractions, and interference of DAPI with nucleic acids may be problematic (Omelon et al. 2016). Other quantification procedures have been designed for polyP analyses in *Saccharomyces cerevisiae* (Bru *et al.*, 2016a, Christ & Blank, 2018a) and bacteria (Pokhrel *et al.*, 2019), including enzymatic hydrolysis of polyP with the exopolyphosphatase enzyme (PPX), followed by colourimetric quantification of the released P_i. In this study, we developed a straightforward high throughput method for polyP quantification from diatoms combining and optimizing existing polyP quantification steps.

Materials and methods

Cultivation conditions

The freshwater diatom *A. minutissimum* (Kützing) Czarnecki (strain MW1), was isolated from photoautotrophic, epilithic biofilms in Lake Constance (47°41´N; 9°11`E, Germany) and purified from associated bacteria using the antibiotic imipenem (Windler et al., 2012). The diatoms were cultivated at 20°C, under a 16:8 light:dark cycle with a light intensity of 70 µmol m^{-2} s^{-1} and with constant shaking at 130 rpm. Diatoms were cultivated in "*Achnanthidium* medium" ((AM, (Windler, 2014)), a modified, 'basal' version of "Bacillariophycean medium" (BM), (Schlösser, 1994) but without soil extract. Vitamins, silica/selenate, and trace metals ion solution were supplemented as described for F/2 medium (Guillard, 1975). *A. minutissimum* was cultivated in P_i-replete AM (55 µM P_i as K_2HPO_4). Marine diatoms were cultivated in artificial seawater medium (ASW) (Tropic Marin), supplemented with Guillard's F/2 (Sigma-Aldrich) with modifications (Guillard, 1975). *Phaeodactylum tricornutum* (CCMP 2561) was cultivated in half salt ASW (16 g/l NaCl), without silica and Tris, and adjusted to pH 7.0. *Thalassossira pseudonana* (CCMP 1335) was cultivated in full salt ASW (33 g/l NaCl) with addition of silica ($Na_2SiO_3 \cdot 9H_2O$) but without Tris, and adjusted to pH 7.0. The two marine diatoms were incubated at 20°C with a 12:12 h light/dark regime, with a light intensity of 70 µmol $m^{-2}s^{-1}$ and with constant shaking at 130 rpm.

Extraction and purification of polyP

A. minutissimum was cultivated in 2 l AM and the cultures were weekly diluted with fresh AM to keep the culture in the log phase (ca. $1 \bullet 10^6$ cells/mL). Marine diatoms were cultivated in 100 mL of the respective medium, and kept in log phase. For harvesting, aliquots of 30 mL were centrifuged (5000 g, 5 min), and the supernatant was discarded. Cells were subsequently resuspended with 1 mL of fresh AM and transferred to a 2 mL tube. After pelleting the cells (5000 g, 2 min), the supernatant was discarded and the pellets were frozen in liquid nitrogen. Each tube contained ca. 3×10^7 cells, and was stored at -80°C.

All chemicals used were brought to room temperature prior to use unless stated otherwise. For the five different polyP extraction protocols, four replicates as well as the corresponding negative controls (blanks containing only the corresponding buffers) were utilized for each method (except for Method 4 where only three replicates were used).

Method 1: Extraction and purification of polyP from *A. minutissimum* with Nexttec DNA isolation kit

The samples were resuspended in the lysis buffer containing 140 µL of buffer G and 10 µL of proteinase K, as described by the manufacturer (Biozym, Hessisch Oldendorf, Germany). Samples were incubated for 1 h at 56°C at 1200 rpm. After centrifugation (5 min, 18000 g), the supernatant was transferred to a pre-conditioned column provided in the kit, and left for 3 min at room temperature for elution. After centrifugation of the column (700 g, 1 min), the eluate containing polyP was stored at -80°C until polyP quantification.

Method 2: Extraction and purification of polyP from *A. minutissimum* with phenol/chloroform extraction and ethanol precipitation (Bru et al., 2016a)

Samples were resuspended in 400 µL AE buffer (50 mM sodium acetate, 10 mM Na_2EDTA, pH 5.3) at 4°C. Samples were mixed with 300 µL phenol and 40 µL 10% SDS four times by inversion, vortexed for 5 s, and incubated at 65°C for 5 min in a thermomixer. After cooling the samples to room temperature, 300 µL of chloroform were added and the sample mixed and vortexed as before. After centrifugation (13000 g, 2 min), the aqueous phase was transferred into a new tube containing 350 µL chloroform. After mixing and vortexing, the samples were centrifuged again, and the resulting upper aqueous phase transferred into a new tube. 2µL of 10 mg/mL RNAse (Sigma-Aldrich Chemie GmbH, Taufkirchen, Germany), and DNAse (Sigma-Aldrich Chemie GmbH, Taufkirchen, Germany) were added, and the samples were incubated for 1 h at 37°C. The mixture was transferred to pre-cooled tubes (-20°C) containing 1 mL of absolute ethanol and 40 µl of 3 M sodium acetate (pH 5.3), and incubated for 3 h at -20°C to precipitate the extracted polyP. After centrifugation (13000 g, 20 min, 4°C), the supernatant was discarded and 500 µL of 70% ethanol were added. Samples were centrifuged for 5 min, and the supernatant discarded. After a final centrifugation step for 1 min at 13000 g, the last drops of ethanol in the tube were removed with a pipette. The pellet was left for 10 min under a gentle air flow to evaporate the residual ethanol. The resulting white pellet (polyP) was dissolved in 400 µL of ddH_2O water and stored at -80°C until polyP quantification.

Method 3: Extraction and purification of polyP from *A. minutissimum* with phenol/chloroform but without ethanol precipitation (Christ & Blank, 2018a)

Samples were resuspended in 400 µL of sterile filtered (0.2 µm) ME-buffer (25 mM MOPS, 2.5 mM Na_2EDTA, pH 7.0). After 20 s of vortexing, the resuspended cells were briefly centrifuged (5 s, 1000 g) to remove drops of sample from the lid and 300 µL of ROTI®Phenol

(Carl Roth GmbH, Karlsruhe, Germany) were added. After 20 s of vortexing, samples were incubated (45°C, 10 min). After a brief centrifugation (1000 g, 5 s), 1 mL of chloroform were added to each sample followed by 20 s of vortexing. The tubes were briefly centrifuged, and their lids were filled with autoclaved silicone vacuum grease (Beckman instruments, Inc. Palo Alto, USA), which acts as an aqueous/organic phase barrier. After centrifugation (18000 g, 5 min), the aqueous phase above the silicone vacuum grease containing polyP was entirely transferred to another tube and kept at -80°C until polyP quantification.

Method 4: Extraction and purification of polyP from *A. minutissimum* with boiling and nuclease/proteinase K treatment, modified from (Martin & Van Mooy, 2013)

Samples were sonicated for 15 s in 500 µL of Tris buffer (20 mM, pH 7.0), boiled for 20 min in a thermomixer (100°C, no shaking) and incubated for 2 h with 40 µL of 20 mg/mL of proteinase K (37°C, 300 rpm). Because we did not quantify the extracted polyP by DAPI staining, we omitted nuclease treatment to reduce the fluorescence of DAPI as recommended by the authors. Samples were centrifuged (16100 g, 1 min), and the supernatant was collected and stored at -80°C until polyP quantification.

Method 5: Extraction and purification of polyP from *A. minutissimum* with guanidine isothiocyanate followed by column purification (Pokhrel et al., 2019)

Samples were resuspended in 250 µl GITC (Sigma-Aldrich Chemie GmbH, Taufkirchen, Germany) (guanidine isothiocyanate, chaotropic salt) lysis buffer (4 M GITC, 50 mM Tris-HCl, pH 7.0) and incubated for 10 min in 95°C. After cooling to room temperature, 250 µl of 95% ethanol were added, and the samples were vortexed for 10 s. The resulting mixture was transferred into a NucleoSpin silica column (Macherey-Nagel, Düren, Germany), and centrifuged (30 s, 16100 g). After discarding the flow-through, the column was rinsed with 750 µl of a mixture containing Tris-HCl (5 mM, pH 7.5), NaCl (50 mM), EDTA (5 mM), 50% ethanol, and centrifuged (30 s, 16100 g). The flow-through was discarded and 150 µl of Tris-HCl (50 mM, pH 8.0) was added in the column. After five min of incubation the column was centrifuged (2 min, 8000 g) and the eluate was kept at -80°C until polyP quantification.

PolyP quantification

PolyP quantification was performed in a 96-well plate following the protocol developed by (Christ & Blank, 2018b) with modifications. The purified polyP samples and blanks were

diluted with ddH_2O prior to quantification to yield a final polyP concentration in the well ranging between 3 to 100 µM P_i (see below). Quantification was performed by enzymatic hydrolysis of polyP with the recombinant *Escherichia coli* exopolyphosphatase (PPX, MyBioSource, Inc., San Diego, USA). As the polyP chains in diatoms did not contain short chain-length of two to four P_i moieties (polyP-2 to polyP-4), we omitted the use of the pyrophosphatase described in Christ and Blank (2018b). Briefly, 100 µL of a diluted polyP extract were pipetted into two different wells of a 96-well plate. In the first well, a volume of 50 µL of enzyme reaction buffer (magnesium acetate 15 mM, Tris 60 mM, ammonium acetate 150 mM, pH 7.7) was added. In the second well, 49 µL of enzyme reaction buffer containing 1 µL PPX (1 mg/mL) of PPX was pipetted. Elsewhere in the microplate, 100 µL P_i standard (K_2HPO_4) (0 to 100 µM) and 50 µL of enzyme reaction buffer were added in triplicate. The microplate was incubated at 37°C for 1 h in a plate reader (Infinite® 200 PRO, TECAN). After incubation, P_i concentrations were measured using the ascorbate-antimony-molybdate assay described by Christ and Blank (2018b). Briefly, 50 µL of P_i detecting reagent containing ammonium heptamolybdate (2.4 mM), H_2SO_4 (600 mM), antimony potassium tartrate (0.6 mM) and ascorbic acid (88 mM) were added to the wells. After 2 min of incubation at room temperature and gentle shaking of the microplate, the absorbance of the samples was determined at 882 nm in the microplate reader. The lowest amount of polyP that could be determined with suitable precision and accuracy was given by the limit of quantitation (LOQ) and was calculated according to the Equation 1 (σ is the standard deviation of the 0 µM P_i standard value given in µM, and S the value of the slope of the P_i standard curve where an example is given in (Figure S2. 1) (ICH Guideline, 1996):

$$LOQ = (10 * \sigma)/S \quad (1)$$

For every microplate measured, a P_i calibration curve was performed as indicated above, and the calculations given in Equation 1 lead to an LOQ value of ca. 3 µM P_i. Therefore, we only considered polyP concentrations detected between LOQ and the upper limit of detection (100 µM P_i). The polyP content in each cell was calculated using Equation 2:

$$PolyP\ amount\ (fg\ Pi.cell^{-1}) = \frac{polyP\ sample\ (M) * dilutions * volume\ cell\ extract\ (L) * M_{Pi}\ (g.mol^{-1}) * 10^{15}}{\text{cell number}} \quad (2)$$

The absorbance of each well was corrected by subtracting the value by the mean value of the blank wells containing 0 µM P_i standard. For each replicate, the polyP content was calculated

by subtracting the amount of P_i determined in the sample treated with PPX by the amount of Pi determined in the well without PPX and referred to as "polyP sample" in Equation 2. PolyP was specified as P_i equivalent with a molecular weight of: M_{Pi} 94.97 g mol^{-1}. For each different diatom culture a pre-assay was performed using only one sample to determine the correct dilution to apply on the cell extract, in order to achieve a final P_i concentration between 3 to 100 µM. Naturally, this dilution step was omitted for sample with P_i concentrations < 6 µM, which would result in a concentration lower than the LOQ after the two-fold dilution occurring in the well. For example, a polyP extract was first diluted five-fold with ddH_2O. It was subsequently diluted by two-fold in the wells at the end of the assay and the resulting value in "dilutions" in Equation 2 was 10.

Determination of polyP recovery

The efficiency of polyP extraction was determined for defined amounts (8 and 30 nmol) of standard polyP differing in their number of phosphate units, (polyP-6, polyP-45, Sigma-Aldrich), (polyP-14, polyP-60, polyP-130, RegeneTiss Incorporated) and (polyP-700, Kerafast). PolyP standards were dissolved in ddH_2O. For each polyP standard of either 8 or 30 nmol, diatom samples were resuspended in 200 µL ddH_2O and divided into two subsamples of 100 µL each. One subsample was spiked with 50 µL of polyP standard to reach a final concentration of either 8 or 30 nmol and was called spiked sample. The other subsample was diluted with the same volume of ddH_2O and was called unspiked sample.

PolyP in spiked and unspiked samples were identically extracted and purified using Method 1 (see *Material and Methods*), and the recovery of each standard was quantified after 1 h of incubation with PPX using the Equation 3 (C is the polyP concentration of the different samples in fg P_i/cell calculated using Equation 2):

$$PolyP\ recovery\ (\%) = ((C_{spiked\ sample} - C_{unspiked\ sample}) * 100)/C_{added} \quad (3)$$

Common lysis buffers and self-made gel filtration columns preparation

The composition of the lysis buffer of the Nexttec kit and the nature of its spin column resin is not publicly available. Thus, we tried different size exclusion resins and prepared two lysis buffers containing two different common detergents and proteinase K.

The first buffer contained sodium dodecyl sulfate (SDS) (SDS 0.02% w/v, proteinase K, 0.4 mg/mL, 30 mM Tris-HCl, pH 8.0), while the second contained Triton X-100 (Triton X-100 0.001% w/v, proteinase K 0.4 mg/mL, 30 mM Tris-HCl, pH 8.0). The concentrations of the detergents were equal to the tenth of their critical micellar concentration (CMC) (Singh and Tyagi, 2015), to avoid any micelles to pass through the gel filtration column. We observed that micelles produced by higher concentrations of detergents could interfere with PPX at concentration > CMC (data not shown). To prepare the size exclusion columns, we disassembled all the components (collection tube, plastic ring, membrane discs) (Figure S2. 2B) of commercial spin columns (GENECLEAN® Turbo Cartridges, MP Biomedicals Germany GmbH) (Figure S2. 2A), leaving only the lower filter disc to support the gel filtration matrix (Figure S2. 2C). The column and its collection tube were washed in 0.1 M NaOH for 5 min, three times with sterile ddH_2O, and dried under a gentle air flow. We prepared three different columns using Bio-Gel P-6 (Biorad), LH-20 (Cytiva), and Sephadex® G-50 (Merck) size exclusion resins. 500 µL of an overnight swollen matrix in Tris-HCl buffer (30 mM, pH 8.0) were transferred into the cleaned spin columns and the excess buffer was removed by centrifugation (350 g, 1 min). The process was repeated several times until the bed height reached 1 cm, which corresponded to ca. 0.4 g of the swollen resins after removing the excess buffer (Figure S2. 2D). The spin columns were preconditioned with 350 µL of Tris-HCl buffer (30 mM, pH 8.0) and stored at 4°C until further use. For polyP extraction, 150 µL of the two different lysis buffers containing SDS and Triton X-100 were used to resuspend the diatom samples. In parallel, other diatom samples were resuspended with the Nexttec DNA isolation kit lysis buffer following Method 1 (see *Material and Methods*). All the samples were incubated for cell lysis in the same manner as for Method 1 (1 h, 56°C 1200 rpm) (see *Materials and Methods*). Subsequently, lysed cells were centrifuged (5 min, 18000 g), each supernatant containing the cell extract was transferred in another tube, and stored at 4°C before use. Before applying the cell extracts onto the different columns, a Nexttec DNA isolation kit column was conditioned as described in Method 1. In parallel, the different self-made gel filtration columns were centrifuged (1 min, 350 g) and the eluate was discarded. Carefully, 100 µL of the extracts obtained after lysis of cells using SDS buffer were applied into the middle of each column. After 3 min of incubation, the columns were centrifuged (700 g, 1 min) and the eluate of each column containing the polyP was transferred into a 1.5 mL tube and kept at -80°C until quantification. This process was repeated for the other extracts obtained after using Triton X-100 and the Nexttec DNA isolation kit lysis buffers. Before adding the samples, the four

different columns were carefully washed three times with 350 µL of 0.1 M NaOH and then equilibrated three times with 350 µL of Tris-HCl buffer (30 mM, pH 8.0).

Statistical analysis and diagrams

Statistical analyses were performed using the analyzing tools in GraphPad Prism software. Diagrams were drawn using Biorender.com.

Results

Comparison of different polyP extraction methods in *A. minutissimum*

In order to develop a polyP quantification protocol optimized for diatoms, we compared several published polyP extraction protocols (Bru et al. 2016; Martin and Van Mooy 2013; Christ and Blank 2018a; Pokhrel et al. 2019) and a new approach using a commercial DNA isolation kit based on size exclusion. PolyP extracted from *A. minutissimum* using the different methods were all hydrolyzed by PPX, and the released P_i was quantified by the same colourimetric assay (Figure 2. 1).

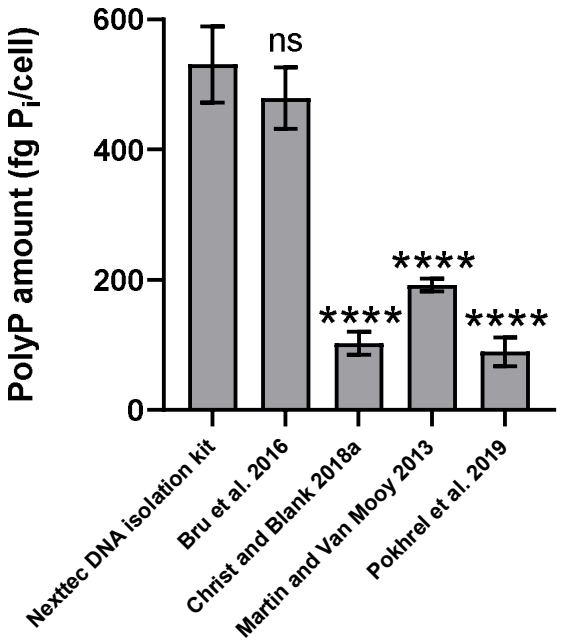

Figure 2. 1: Comparison of the polyP extraction efficiencies from *A. minutissimum* using the following methods: Lysis buffer with proteinase K and purification by gel filtration spin column

using the Nexttec DNA isolation kit, phenol/chloroform extraction and purification by ethanol precipitation (Bru et al. 2016), phenol/chloroform extraction without ethanol precipitation (Christ and Blank 2018a), boiling extraction and proteinase K treatment (Martin and Van Mooy 2013), extraction using guanidine isothiocyanate followed by silica spin column purification (Pohkrel et al. 2019). The amounts of polyP extracted from *A. minutissimum* are given in fg P_i/cell after enzymatic hydrolysis. Data represent means, and standard deviations are given as error bar of n = 4 replicates except for Martin and Van Mooy (2013) where n = 3. Asterisks indicate significant differences (one-way ANOVA, $^{****}p < 0.0001$) and ns indicates no significant difference of polyP levels.

Extractions using the DNA kit as well as the phenol/chloroform approach with ethanol precipitation yielded the highest amounts of polyP corresponding to 531 ± 59 and 479 ± 47 fg P_i/cell, respectively. Although the Nexttec DNA isolation kit extracted 10% more polyP than the phenol/chloroform extraction from Bru et al. (2016), there was no significant difference between the two extraction steps ($p>0.05$). The subsequent purification of the extract by ethanol precipitation seems to be critical for extracting polyP from the diatom, as the phenol/chloroform extraction without ethanol precipitation by Christ and Blank (2018a) extracted five times less polyP than the method from Bru et al. (2016) with 103 ± 18 fg P_i/cell. Regarding improvement of the protocol by Martin and Van Mooy (2013), we tested, whether only one extraction using Tris-boiling may be sufficient to obtain the entire polyP from the cells if boiling time, proteinase K concentration and incubation time were increased. However, the respective yield in this case was only slightly higher (192 ± 9 fg P_i/cell), but 40% less efficient than the size exclusion separation using DNA kit spin columns. Finally, extractions using GITC with silica spin column yielded the lowest amount of polyP corresponding to 89 ± 22 fg P_i/cell.

PolyP extraction using common lysis buffers and self-made gel filtration columns

The Nexttec DNA isolation kit requires two steps, cell lysis using a specific lysis buffer (Nexttec buffer), followed by polyP purification using a gel filtration spin column (Nexttec column).

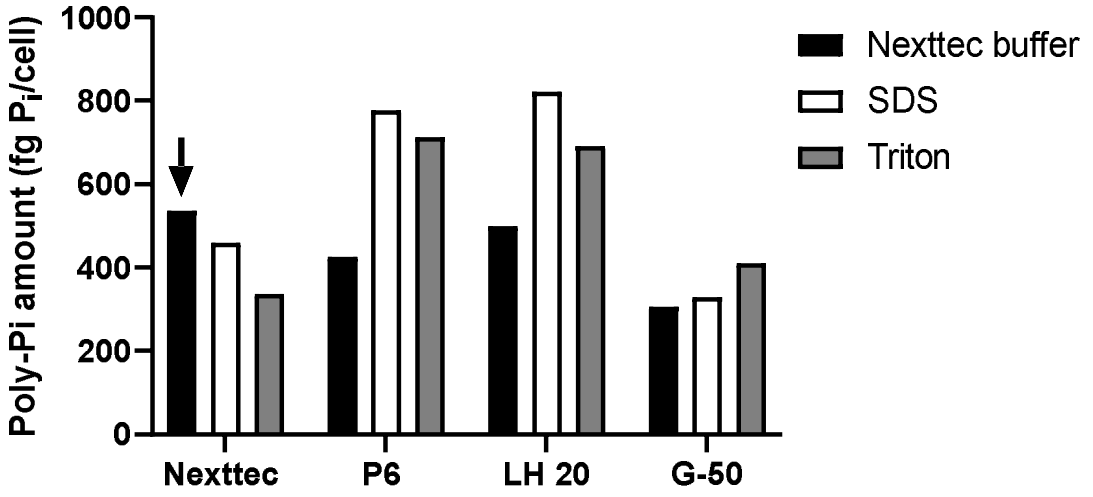

Figure 2. 2: PolyP extraction efficiencies from *A. minutissimum* using a combination of different lysis buffers ((Nexttec DNA isolation kit (Nexttec buffer), 0.01% (w/v) sodium dodecyl sulfate (SDS) and 0.002% (w/v) Triton X-100 (Triton)) with three different self-made gel filtration column (P-6, LH-20 and G-50) and one pre-packed column provided in the Nexttec DNA isolation kit (Nexttec). The black arrow represents the amount of polyP yielded after extracting and purifying a sample following the DNA kit isolation protocol. The amounts of polyP extracted from *A. minutissimum* are given as fg P_i/cell after enzymatic hydrolysis. Each bar represents the polyP amounts from one sample (n = 1) subjected to an extraction and purification using one of the three lysis buffers combined with one of the four columns.

Therefore, we tested whether these steps are reproducible using commonly used lysis buffers and self-made gel filtration spin columns. We examined the efficiency of two lysis buffers combined with three different gel filtration columns for extracting polyP from *A. minutissimum*, and used the results obtained with the Nexttec DNA isolation kit approach as a reference (Figure 2. 2). Using Triton X-100, SDS, or Nexttec buffers combined with the G-50 column resulted in 23, 38, and 42% lower polyP yields than obtained with the DNA isolation kit. However, a combination of Triton X-100 with either a P-6 or LH-20 column led to an increase of polyP yield by 25 and 22% respectively compared to the Nexttec DNA isolation kit. Yields were even about 31 and 34% higher when SDS was applied in combination with the same columns. These results confirm that quantification of polyP from the diatom works well with self-made gel filtration spin columns and buffers.

Characterization of the polyP extraction and quantification parameters using the Nexttec DNA isolation kit approach

For the further optimization of the polyP analysis, we addressed the reproducibility of the Nexttec DNA isolation kit (Method 1). We first tested whether increasing the extraction time may influence polyP yields. *A. minutissimum* samples were subjected to both a regular 1 h extractions as well as an extended overnight extractions (15 h) (Figure 2. 3A).

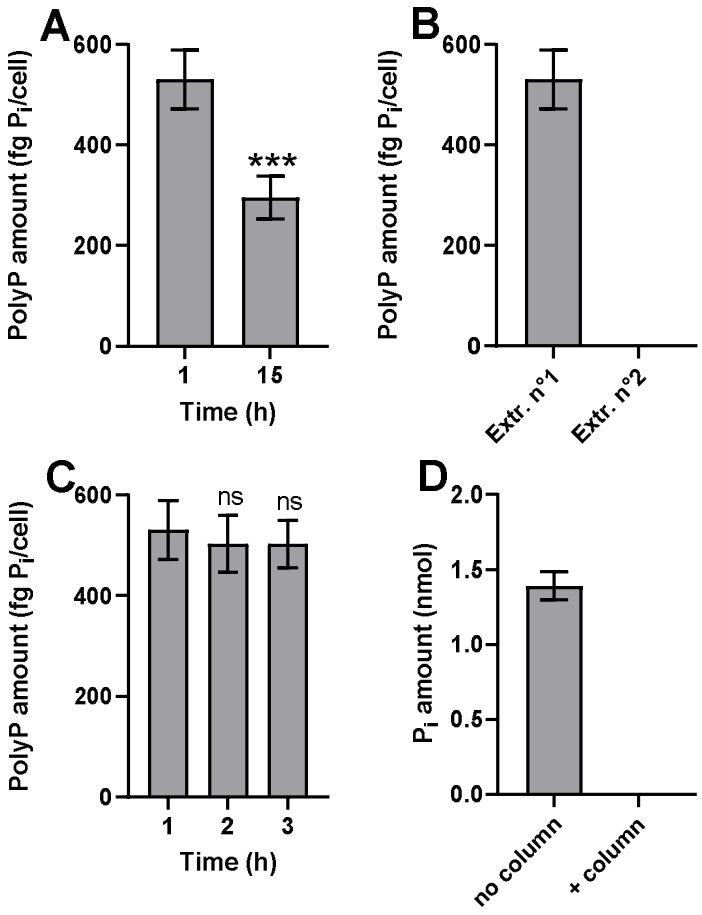

Figure 2. 3: Characterization of the polyP extraction, purification, and quantification parameters using the Nexttec DNA isolation kit. The amounts of polyP extracted from *A. minutissimum* are given in fg P_i/cell after enzymatic hydrolysis. A. Comparison of P_i yields after 1 or 15 h of incubation with the lysis buffer. B) Yields after a first extraction of 1 h of the sample followed by a second extraction of 1 h using fresh lysis buffer. C) Yields after 1 h of extraction, but with different times of enzymatic treatment. D) Enzymatic hydrolysis of 8 nmol of adenosine 5'-triphosphate (ATP) without or with column purification. Data represent means, and standard deviations are given as error bar of n = 4 replicates. Asterisks indicate significant difference of polyP amounts compared to the reference yield indicated in the first column of A, B and C (unpaired t-test, $^{***}p < 0.001$; C, one-way ANOVA, ns: not significant).

The 15 h extraction yielded less polyP (0.3 fg P_i/cell) compared to the 1 h extraction (Figure 2. 3A), suggesting that a prolonged time at 56°C may promote polyP degradation. Additionally, we tested whether further extractions of the cell pellet could enhance the extraction efficiency, however, after a second round of extraction, no additional polyP was detected (Figure 2. 3B). In addition, an increase of the incubation time with PPX did not yield more P_i, indicating that incubation for 1 h with the described enzyme concentration is sufficient (Figure 2. 3C). Moreover, with the aim to exclude other potential sources of hydrolyzed P_i, we tested whether potentially co-isolated adenosine 5'-triphosphate (ATP) or DNA could also be hydrolyzed by PPX. A direct incubation of 8 nmol ATP in presence of PPX resulted in very minor ATP hydrolysis, releasing 1.4 ± 0.1 nmol P_i within 1 h (Figure 2. 3D). When ATP was subjected to Nexttec spin column purification, no P_i was released after its subsequent incubation with PPX, suggesting that ATP was retained within the column. Similarly, we tested whether 8 nmol of a DNA PCR fragment obtained from *A. minutissimum* could be hydrolyzed by PPX but no P_i was detected with or without column purification (data not shown).

Recovery of polyP after extraction and purification using the optimized Nexttec DNA isolation kit protocol

Because the Nexttec isolation method showed convincing results after about one hour of polyP extraction and purification and an additional hour of PPX treatment, we further challenged the accuracy of the extraction by supplementing the diatom samples with known amounts of polyP standards of different P_i unit lengths, preceding the extraction (Figure 2. 4). After extraction and purification, we observed that 8 nmol of added standard consisting of polyP containing 130 and 700 P_i units (polyP-130 and polyP-700 respectively), were recovered at 67 ± 9% and 78 ± 4%, respectively, while the shorter standards polyP-6 and polyP-14 were recovered much less efficiently: 21 ± 7% and 55 ± 2%, respectively (Figure 2. 4A). Chains of more than 14 P_i residues yield a minimum recovery of 60%. Moreover, the recovery depends on the initial amount of polyP. Increasing the concentration of polyP standard to 30 nmol, which corresponds to ca. 20% of the polyP found in diatom samples, resulted in different recovery rates of standards. PolyP ranging from 45 to 700 P_i units were recovered best with an average recovery of 77 ± 4%, while shorter standards like polyP-14 were recovered less well with 63 ± 2% recovery. The polyP-6 standard was recovered with only 27 ± 2% recovery (Figure 2. 4B).

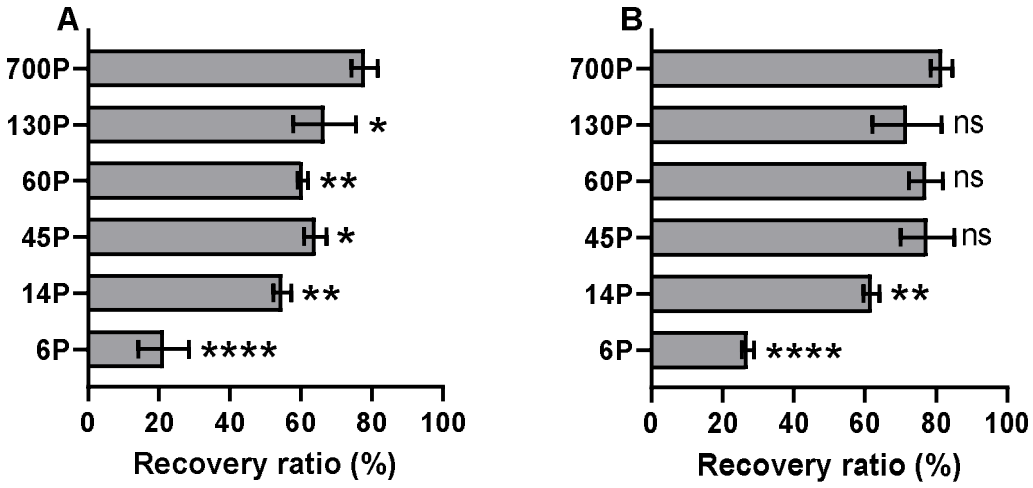

Figure 2. 4: Recovery of polyP standards of different sizes (6-700 P_i units) using the Nexttec DNA isolation kit. The amounts of polyP extracted from *A. minutissimum* are given as fg P_i/cell after enzymatic hydrolysis. Prior to extraction, each diatom sample was split in two subsamples (equal volume). One subsample was supplemented with 8 nmol (A) or 30 nmol (B) of a polyP standard containing 6, 14, 45, 60,130 or 700 P_i units. The other subsample was supplemented with ddH_2O. Both subsamples were extracted and purified using the Nexttec DNA isolation kit, and their polyP concentrations were determined. The recovery of the polyP standards was calculated using equation 3. Data represent means, and standard deviations are given as error bar of n = 4 replicates. Asterisks indicate a significant difference of polyP amounts compared to the amounts recovered for the standard of 700 P_i units. A and B, one-way ANOVA, $^{*}p < 0.05$; $^{**}p < 0.01$; $^{***}p < 0.001$; ns: not significant.

Scope of the newly established polyP extraction and purification method

Finally, we tested the optimized method on other representative diatoms. We chose two marine species, *P. tricornutum* and *T. pseudonana,* which are considered as model laboratory strains (Bowler et al. 2008; Armbrust et al. 2004). PolyP was found in all diatoms tested. *P. tricornutum* and *T. pseudonana* yielded 16 ± 5 and 70 ± 10 fg P_i/cell, respectively (Figure 2. 5). With 531 ± 59 fg P_i/cell, polyP amounts in *A. minutissimum* were 33 times higher than in *P. tricornutum*.

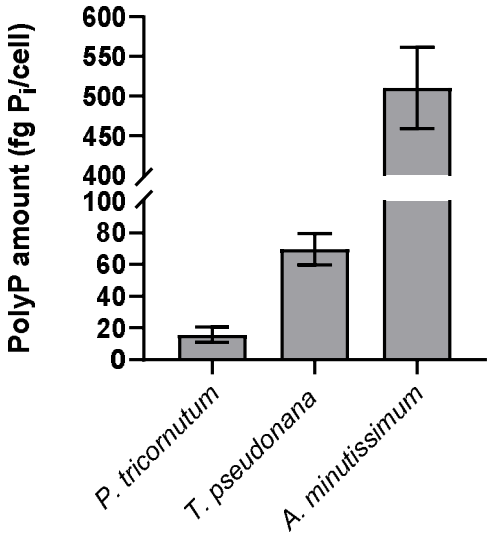

Figure 2. 5: PolyP quantification using the optimized Nexttec DNA isolation kit protocol and performed on the marine algae P. tricornutum, T. pseudonana, as well as on the freshwater diatom *A. minutissimum*. Data represent means, standard deviations are given as error bar of n = 3 replicates.

Discussion

We developed a straightforward method for the extraction of polyP from diatoms. Several methods for polyP extraction and purification exist, in particular for microorganisms (Bru et al. 2016; Martin and Van Mooy 2013; Pokhrel et al. 2019). When studying the diatom *A. minutissimum*, comparison of different approaches indicated that extraction using either the Nexttec DNA isolation kit consisting of a lysis buffer containing proteinase K and gel filtration columns, as well as a phenol/chloroform extraction followed by ethanol precipitation gave the best yields of polyP. However, when comparing both approaches, polyP can be extracted five times faster using the Nexttec DNA isolation kit, thanks to less handling steps, and without the use of hazardous solvents, such as phenol (Table. S1). Hence, this method is ideal for routine measurements of polyP.

A practical advantage of the polyP purification by gel filtration is its single elution step, which simplifies considerably the time and the handling process. In comparison, polyP purification by silica spin columns requires several elution steps (Ault-Riche *et al.*, 1998, Lee *et al.*, 2018), and polyP purification by ethanol precipitation takes at least 3 h to recover polyP (Bru et al. 2016). Gel filtration columns have the drawback to retain small molecular weight compounds such as

short polyP, such as polyP-6, while long fragments ranging from polyP-14 to polyP-700 are directly eluted. However, because polyP from *A. minutissimum* range mostly between ca. 130 to 500 P_i units (Lapointe et al. unpublished), this is not problematic here. In contrast, silica matrices were reported to fail recovering polyP shorter than 60 P_i units (Ogawa et al. 2000), hindering a comprehensive analysis of organisms producing polyP ≤ 60 P_i units. Accordingly, gel filtration is the method of choice for recovering a wide range of polyP chains in a single step (Ohtomo and Saito 2005; Ohtomo and Saito 2008). Furthermore, we demonstrated that self-made spin columns (P-6 or LH-20 resin) in combination with common detergents, such as Triton X-100 or SDS lead to very good polyP extraction, indicating that polyP could be purified without using a commercial kit (Figure 2. 6). As the purification by gel filtration removes low molecular weight compounds like salts or pigments, the colourless eluate can be used for spectroscopic analysis like the ascorbate-antimony-molybdate assay. In addition, the high purity of the sample is critical for polyP enzyme-based quantifications. Ohtomo and Saito (2005) used gel filtration resins (BioGel P-2 and P-6) with fractionation range of about polyP-20 to remove the urea contained in the extraction buffer from arbuscular mycorrhizal fungi polyP samples, allowing a comprehensive polyP quantification via the polyphosphate kinase (PPK) (Ault-Riché et al. 1998).

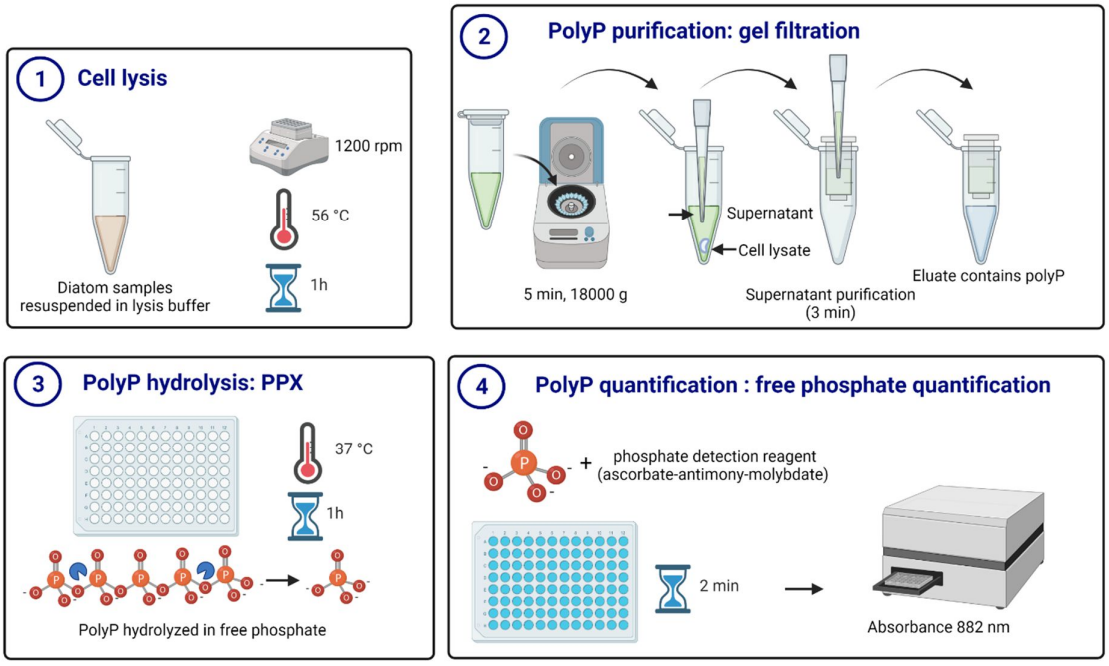

Figure 2. 6: Workflow of the protocol for extraction, purification and quantification of polyP in diatoms.

Because gel filtration elutes other macromolecules along with polyP, quantification requires enzyme assays that are specific for polyP. While the DAPI staining has been found to interact with other molecules (Omelon et al. 2016), PPX (Werner et al. 2005; Bru et al. 2016) and PPK (Ault-Riché et al. 1998; Ohtomo and Saito 2005) assays allow a specific quantification of polyP. The polyP quantification using PPK converts polyP to ATP that is subsequently quantified by a luciferase assay (Ault-Riché et al. 1998). Although this PPK assay is very sensitive (picomolar range), the enzyme can only detect polyP with > 38 P_i units (Ault-Riché et al. 1998). Alternatively, PPX is well suited for short-chain polyP quantification, although it is less sensitive (> 3 µM). It cleaves down to polyP-3 (with ca. 50% efficiency) (Ohtomo and Saito 2008), enabling the quantification of a wider polyP range than PPK. Using our current column gel filtration, PPX can only detect chain-length ≥ 14 P_i units, which is still better than the PPK chain-length detection limit. Although there is a functional interaction between linear DNA and PPX during quantification (Bru et al. 2016), using excess PPX (1 µg/well) overcomes this issue (Pokhrel et al., 2019). Finally, the use of PPX in the micro-assay developed by Christ and Blank (2018b) is well suited for specific and fast quantification of polyP in high throughput.

In summary, our straightforward method for polyP quantification will be a valuable tool to reveal the physiological role of polyP in diatoms in different growth situations.

Conclusions

The described method allows to quantify a wide range of polyP, ranging from polyP-14 to polyP-700, in diatoms. The approach is fast, specific, and can be performed in high throughput.

Acknowledgements

This work was supported by the DFG (Deutsche Forschungsgemeinschaft)-298726046/GRK2272 (RTG R3). We are grateful to RegeneTiss Incorporated (Tokyo, Japan) for the kind gift of the polyP standards.

Chapter 3. Characterization of polyphosphate dynamics in the widespread freshwater diatom *Achnanthidium minutissimum* under varying phosphorus supplies.

Adrien Lapointe, Imaiyan Chitra Ragupathy, Paavo Bergman Mustafa Kocademir, Michael Laumann, Dieter Spiteller, Andreas Zumbusch, and Peter G. Kroth

Published Journal of Phycology, 2024

https://doi.org/10.1111/jpy.13423

Abstract

Polyphosphates (polyP) are ubiquitous biomolecules that play a multitude of physiological roles in many cells. We have studied the presence and role of polyP in a unicellular alga, the freshwater diatom *Achnanthidium minutissimum*. This diatom stores up to 2.0 pg·cell^{-1} of polyP, with chain lengths ranging from 130 to 500 inorganic phosphate units (P_i). We applied energy dispersive X-ray spectroscopy, Raman/fluorescence microscopy, and biochemical assays to localize and characterize the intracellular polyP granules that were present in large apical vacuoles. We investigated the fate of polyP in axenic *A. minutissimum* cells grown under phosphorus (P), replete ($P_{(+)}$), or P deplete ($P_{(-)}$) cultivation conditions and observed that in the absence of exogenous P, *A. minutissimum* rapidly utilizes their internal polyP reserves, maintaining their intrinsic growth rates for up to 8 days. PolyP-depleted *A. minutissimum* cells rapidly took up exogenous P a few hours after P_i resupply and generated polyP three times faster than cells that were not initially subjected to P limitation. Accordingly, we propose that *A. minutissimum* deploys a succession of acclimation strategies regarding polyP dynamics where the production or consumption of polyP plays a central role in the homeostasis of the diatom.

Keywords: *Achnanthidium minutissimum,* diatom, electron microscopy, phosphate uptake, polyphosphate, stimulated Raman scattering microscopy.

Introduction

Phosphorus (P) is an essential element playing an important role in all living organisms (Paytan and McLaughlin 2007). Phosphorus in form of phosphate (P_i) is incorporated into vital biomolecules such as nucleic acids and, therefore, is crucial for the storage, replication, and transcription of genetic information. In addition, P_i is critical for the effective production of ATP for intracellular energy storage and for structural components such as phospholipids for membrane formation. If P availability becomes limited, primary production in the ocean (Benitez-Nelson 2000) and lake ecosystems (Li et al. 2019) can be strongly affected.

It is known that microalgae have developed adaptive responses to cope with low ambient P, including enzymatic use of extracellular dissolved organic P, a decrease in cellular P demands, and cellular P storage (Lin et al. 2016). The benthic diatom *Seminavis robusta* actively moves towards P sources (Bondoc et al. 2019). Under high-P conditions, microalgae can store excess P_i intracellularly by the formation of inorganic polyphosphates (polyP), and use it to alleviate future P limitation (Sanz-Luque et al. 2020). These are linear polymers composed of inorganic phosphate units linked by energy-rich phosphoanhydride bonds comprising from three up to several thousand phosphate monomers. PolyP exists ubiquitously in all kingdoms of life (Brown and Kornberg 2004, Docampo et al. 2005, Sanz-Luque et al. 2020). Displaying a granular shape, polyP was initially called “metachromatic granules” (Babes, 1895), or “volutin granules” (Meyer, 1904), and later renamed polyP granules (Wiame, 1947). This inorganic polymer was first isolated from yeast (Lieberman 1890) and much later from microalgae (Fisher 1971). PolyP fulfills a large number of functions (Rao et al. 2009, Xie and Jakob 2019): In bacteria, polyP is involved in stress resistance, biofilm formation, quorum-sensing, and virulence (Rao et al. 1998, Rashid et al. 2000). In *Saccharomyces cerevisiae*, polyP was observed to chelate metal ions, preventing metal ion-induced cellular damage (Trilisenko et al. 2017) and to be important for yeast cell survival upon DNA damage (Bru et al. 2017) and for the accumulation and metabolism of P_i in yeast (Ogawa et al. 2000).

Although the function of polyP in microalgae under P limitation has attracted attention in recent years (Li and Dittrich 2019, Solovchenko et al. 2020, Plouviez et al. 2021), only a handful of studies have focused on polyP production in diatoms. Diatoms constitute one of the most diverse and ecologically important groups of eukaryotic phytoplankton. They exist in all aquatic systems, and they are responsible for about one-fifth of global photosynthesis (Armbrust 2009). PolyP production by diatoms plays a key role in the sequestration of P within the marine sediment and contributes to the formation of calcium-phosphate apatite (Diaz et al. 2008).

However, studies focusing on polyP occurrence and production in diatoms are scarce. In *Phaeodactylum tricornutum*, the subject of polyP amounts and sizes has been described as a function of osmotic conditions (Leitão et al. 1995). Volutin granules were observed in raphid (Mann, 1985), as well as in centric diatoms (Bedoshvili et al. 2018). Taking into account nutrient variations, a few studies have focused on the regulatory mechanisms that link changes in the environmental phosphate concentrations to polyP synthesis in diatoms (Dyhrman et al. 2012). Therefore, to understand the mechanisms of polyP dynamics in diatoms, more systematic studies detecting and monitoring polyP dynamics under different P availabilities are required.

In this study, we therefore investigated the role of polyP in the freshwater diatom *Achnanthidium minutissimum,* a species that is observed widely not only in alkaline and acidic but also in oligotrophic and hypertrophic environments (Round 2004, Potapova and Hamilton 2007, Hlúbiková et al. 2011). Because of its ubiquity in different aquatic habitats, *A. minutissimum* serves as an excellent model for shedding light on the effects of P availability on polyP accumulation in freshwater diatoms. We hypothesized that *A. minutissimum* builds up polyP stocks under high P availability to overcome later P-limitation. To test this hypothesis, we cultured *A. minutissimum* in either P-rich or P-limited conditions over 10 days, and subsequently resupplied the cells with a P-rich medium. We monitored cell growth, phosphate uptake and polyP detection within cells at the different growth stages.

Materials and methods

Growth conditions and experimental cultures

The freshwater diatom *Achnanthidium minutissimum* (Kützing) Czarnecki (strain MW1), was isolated from photoautotrophic, epilithic biofilms in Lake Constance (47°41´N; 9°11`E, Germany). The associated bacteria were removed using the antibiotic imipenem (Windler et al. 2012). Cultures of axenic diatoms were cultivated at standard conditions at 20°C, under a 16:8 light:dark cycle with a light intensity of 70 µmol m^{-2} s^{-1} and with constant shaking at 130 rpm. Diatoms were cultivated in *Achnanthidium* medium (AM, (Windler 2014)), a modified, basal version of Bacillariophycean medium (BM), (Schlösser 1994), lacking soil extract. Vitamins, silica, selenate, and trace metal ions solution were supplemented as described for F/2 medium (Guillard 1975). For the study, two different inorganic phosphate (P_i) (K_2HPO_4) treatments within AM were compared with ca. 53 µM P_i accounting for P-replete ($P_{(+)}$) and no addition of K_2HPO_4, accounting for P-deplete ($P_{(-)}$) conditions. Cells were cultivated in glasswares which were washed once beforehand with 0.1 M HCl and thrice with double distilled water (ddH2O).

A stock culture of axenic *A. minutissimum* (5 L) was grown in AM $P_{(+)}$ under standard conditions described above; half of the culture was discarded weekly and replaced by the same volume of new AM $P_{(+)}$. This semi-batch culture approach maintained the stock culture cells in expontential phase growth, with cell densites between ca. 400 000 to 1.0×10^6 cells/mL. Before starting experiments, 55 mL of the stock culture was sampled and split into the following subsamples: 25 mL for polyP size distribution, 25 mL for scanning electron microscopy (SEM) analyses, 500 µL for vacuolar membrane visualization, and 1 mL for stimulated Raman scattering (SRS) (description of the procedures below). The rest of the stock culture was left overnight under the same standard conditions described above, but without shaking to allow cell sedimentation. Consecutively to the overnight sedimentation, the supernatant was discarded and cells were resuspended with 200 mL of new AM $P_{(+)}$. Cells were resuspended by gentle shaking and split into two equal volumes of 100 mL and centrifuged (5000 g, 5 min). The supernatant was discarded and cell pellets were resuspended carefully with 400 mL of either new AM $P_{(+)}$ or AM $P_{(-)}$. Subsequently, 100 mL of each four $P_{(+)}$ samples were transferred to four 3.0 L flasks (VWR, Borosilicate Erlenmeyer, Germany) containing each 1900 mL of AM $P_{(+)}$, and 100 mL of each four $P_{(-)}$ samples were transferred to four 3.0 L borosilicate flasks containing each 1900 mL of AM $P_{(-)}$. Starting cell concentrations in each culture were about 130×10^3 cells/mL. Cells were cultivated for 15 d as described above. Aliquots were taken 0, 2, 4, 6, 8, 10, 12, and 15 days after inoculation. After sampling on day 15, 420 mL and 240 mL

of $P_{(+)}$ and $P_{(-)}$ cultures, respectively were discarded, and the remaining cells were supplemented with new AM $P_{(+)}$ up to a volume of 2 L to reach a similar cell concentration of ca. 200 000 cells/mL in both treatments. Additional aliquots were taken after the resupply on day 15 as well as on days 16, 17, and 18. Each aliquot consisted of 160 mL of sample and was subjected to the same procedures for measuring the parameters as described below, except for the aliquots taken on day 15 after the resupply with AM $P_{(+)}$ which consisted of only 1mL used for measuring the cell number and the exogenous P concentration in the cultures.

Screening for bacterial contaminations

On days 0, 10, and 18, small aliquots (500 µL) were taken from the cultures and screened for bacterial contamination using the fluorescent nucleic acid staining SYBR Green I (Cambrex, Rockland, ME USA) (Windler et al. 2012). During the experiments, no bacterial contamination was observed.

Cell counts and growth rate

To quantify cell density, 100 µL of resuspended cells were taken from the original aliquots, and cells were counted using a Coulter-counter (Beckman, Multisizer 4 Coulter cell counter®, Germany). The growth rate was estimated from cell concentration measurements during exponential phase using the following equation (Levasseur et al. 1993):

$$\mu(d^{-1}) = \frac{\ln(C_x \div C_{x-n})}{t_x - t_{x-n}}$$

where µ is the growth rate, C is cell concentration (cells/mL), t is time (day), x is the harvesting day point and x-n is the preceding harvesting day point. For example, for calculating the growth rate occurring between days 2 and 4, t_x was 4 and t_{x-n} was 2.

Quantification of dissolved extracellular phosphate

Following the cell counts, original aliquots were centrifuged (5000 g, 5 min), and 1 mL of the supernatant was taken for analysis of dissolved orthophosphate (P_i) concentration using a colourimetric assay. The analysis was carried out in a 96 well-plate using the ascorbate-antimony-molybdate assay described by Christ and Blank (2018). 150 µL of each sample were pipetted into one well of a 96 microplate. Elsewhere in the microplate, 150 µL of the phosphate standard K_2HPO_4 (0 to 100 µM P_i) were added in triplicate. Then, 50 µL of the phosphate detection reagent containing ammonium heptamolybdate (2.4 mM), H_2SO_4 (600 mM), antimony potassium tartrate (0.6 mM), and ascorbic acid (88 mM) were added to the wells. After 2 min of incubation at room temperature and gentle mixing, the absorbance of the samples was determined at 882 nm. The lowest amount of P_i that could be determined with suitable precision and accuracy was given by the limit of quantitation (LOQ, ca. 3 µM Pi) (ICH Guideline, 1996), see also equation 1 in (Lapointe et al. 2022).

PolyP quantification

The rest of the supernatant of the centrifuged original aliquots was discarded and cells were resuspended in either 1 mL of ddH_2O, or 2 mL when samples were needed for stimulated Raman scattering (SRS) microscopy. In the latter case, the resuspended cell volume was pipetted into two tubes of 1 mL each. Subsequently, the first tube containing the sample for polyP quantification was centrifuged (5000 g, 5 min) and the supernatant was discarded. The second tube was subjected to SRS microscopy. Cell pellets generated for polyP analyses were frozen in liquid N_2 and kept at -80 °C. PolyP was extracted, purified, and quantified following the protocol described in Lapointe et al. (2022). Extraction and purification were performed using a DNA isolation kit based on cell lysis and gel filtration. For quantification, the purified polyP within the samples was specifically hydrolysed to P_i by the recombinant *Escherichia coli* exopolyphosphatase (PPX, MyBiosource, Inc., San Diego, California, USA) in a 96-well plate, following the protocol developed by Christ and Blank (2018) with modifications (Lapointe et al. 2022). 100 µL of a diluted polyP extract were pipetted into two different wells of a 96-well plate. One well was supplemented with 50 µL of enzyme reaction buffer (magnesium acetate 15 mM, Tris 60 mM, ammonium acetate 150 mM, pH 7.7). The other well was supplemented with 49 µL of enzyme reaction buffer and 1 µL PPX (1 mg/mL). K_2HPO_4 standards were pipetted elsewhere on the microplate (see quantification of dissolved extracellular phosphate section). After 1h of incubation at 37°C in a plate reader (Infinite® 200 PRO, TECAN), P_i concentrations were measured using the ascorbate-antimony-molybdate assay described above

(see quantification of dissolved extracellular phosphate section), and the polyP content in each well was calculated using equation 2 in Lapointe et al. (2022). The LOQ was measured as described above.

Size distribution of polyP from *Achnanthidium minutissimum*

PolyP was extracted and purified from the stock culture sample containing 25 mL of *A. minutissimum* cells cultivated in AM $P_{(+)}$ using the protocol described above. The purified extract was split into two subsamples of equal volume. In a 96-well plate, 100 µL of each subsample was transferred into two wells and subjected to polyP quantification, with the exception that the phosphate detection reagent was added for only one subsample. This procedure allowed the determination of the polyP concentration in the starting culture sample (ca. 5 nmol), and the production of an extracted and purified polyP sample for PPX treatment and a control. PolyP was separated on a 20% acrylamide TBE-urea gel (5.8 M urea, 10 mL 30% acrylamide/bisacrylamide (19:1), 3 mL 5 x TBE, 1.8 mL ddH_2O, 150 µL 10% ammoniumperoxosulfate, 15 µL TEMED). 5 µL of the polyP standards (405 pmol P) containing average chain-length polyP of 14, 60, 130 (polyP-14, -60, -130, RegeneTiss Incorporated, Nagano, Japan) and 700 (polyP-700, Kerafast, Boston, USA) P_i units, as well as 5 µL of the extracted and purified polyP sample with and without PPX treatment were mixed with 5 µL of 2 x loading dye (2 x TBE, 6% Ficoll 400, 0.04 bromophenol blue), and loaded on the acrylamide gel. Finally, 10 µL of 10 bp (O'RangeRuler 10 bp DNA Ladder, Thermoscientific, Germany) and 100 bp DNA ladders (Invitrogen, Germany) were loaded as size references. The gel was run at 150V for about 45 min at room temperature. PolyP was visualized by negative DAPI staining (Smith and Morrissey 2007). The size range of polyP chain-length was estimated by comparing DNA ladder bands and polyP standards as described in Smith et al. (2018).

Scanning electron microscopy

The second sample from the stock culture containing 25 mL of *A. minutissimum* cells cultivated in AM $P_{(+)}$ was centrifuged (5000g, 5 min). The cell pellets were packed by capillarity into cellulose capillaries (200 µm diameter, Leica microsystems). Within a petri dish containing ca. 5 mL of AM $P_{(+)}$, the capillaries were cut carefully using a scalpel for sealing each side. Capillaries were sequentially transferred to fixing buffer, and subsequently. dehydrated using ca. 1 mL of increasing ethanol concentrations, followed by an additional dehydration using ca. 1 mL of an acetone gradient. Cells were embedded in an increasing gradient of modified SPURR resin dissolved in absolute acetone. SPURR was prepared using the catalyst DMAE (Ted Pella, INc., Redding, California, USA), NSA (Serva, Heidelberg, Germany), and ERL 4221 (EMS, Hatfield, Pennsylvania, USA). After acetone was completely evaporated, capillaries were transferred to silicone moulds that were filled up with fresh resin mixture and left for polymerization for 2 d at 65 °C. A detailed fixation protocol is found in Table S3. 1. The samples were sectioned using a diamond knife (Diatome, Biehl, Switzerland). The resulting 500 nm sections were placed upon droplets of ddH_2O water on indium tin oxide-coated coverslips. Samples were sputtered with carbon (C) to a thickness of 10 nm (Balzers SCD030; Oerlikon Balzers, Balzers, Liechtenstein). Sections were analysed by energy-dispersive X-ray spectroscopy (SEM-EDX) in a Zeiss Auriga FESEM (Zeiss, Oberkochen, Germany) equipped with an X-Max $20mm^2$ detector (Oxford Instruments, Abingdon, UK).

Stimulated Raman microscopy of *Achnanthidium. minutissimum*

To visualize polyP granules in *A. minutissimum*, the cells were imaged using SRS microscopy (Cheng and Xie, 2015). SRS measurements of *A. minutissimum* were carried out using a Leica SP8 microscope with SRS capability (Leica Microsystems, Mannheim, Germany). For the analysis, the 1 mL stock culture sample (see cell concentration and growth rate section) as well as the 1 mL experiment aliquots (see polyP quantification section) were processed as follows. Each sample was centrifuged (5000 g, 1 min) and the supernatant was discarded. The cell pellet was resuspended with 40 µL of 1% w/v of a low-gelling agarose solution (Sigma Aldrich, Taufkirchen, Germany) to prevent the movement of cells during analysis (Moudrikova et al. 2017). A small drop (10 µL) of the sample was pipetted between two glass coverslips (24*60 mm, Menzel-Gläser, Heidelberg, Germany) and sealed with an imaging spacer (SecureSeal, Sigma Aldrich, Taufkirchen, Germany). Before analysis, samples were subjected to photobleaching of the carotenoids. Regions containing diatoms were subjected to the maximum

power of the microscope's 488 nm laser for 15-20 min. polyP granules were detected by SRS imaging at 1166 cm^{-1}. If necessary, several frames were made from each sample in different areas of the bleached sample to obtain data from at least 100 cells. A Python script was used to automatically determine the percentage of cells containing at least one visible granule on the SRS pictures based on the bright pixels. These data were used to calculate the relative area covered by the polyP granules within each cell containing granules. Spontaneous Raman spectra were recorded using a commercial Raman microscope (MonoVista CRS, S&I, Warstein, Germany) with excitation at 488 nm.

Vacuoles staining in *Achnanthidium minutissimum*

For visualization of vacuolar structures in *A. minutissimum*, we used the fluorescent membrane marker MDY-64 (Molecular probes, Leiden, Netherlands), following the protocol of Huang et al. (2016) with modifications. Cells were incubated in 2 µM MDY-64 in the dark for 2 min at room temperature, and fluorescence was analysed using an epifluorescence microscope Olympus BX51(Olympus Europe, Hamburg, Germany) equipped with a Zeiss AxioCam MRm digital camera system (Carl Zeiss MicroImaging GmbH, Göttingen, Germany).

Data analysis

GraphPad Prism 9.1.2 was used to conduct all statistical analyses. All data were checked for normality and homoscedasticity. We used t-tests for comparing two groups of data and the analysis of variance (ANOVA) when more than two groups of data were compared. A dataset combining mean values of growth rate, external P concentration, polyP concentration and P uptake was made for each $P_{(-)}$ and $P_{(+)}$ treatment, before and after resupply with P. We generated a Spearman's rank correlation coefficient for each datasets separately, as well as for the combined $P_{(+)}$ and $P_{(-)}$ dataset, to assess significant relationships between the above-mentioned variables.

Results

Achnanthidium minutissimum possesses polyP-containing granules enclosed in vacuoles

To study the presence of polyP granules in diatoms, we performed scanning electron microscopy (SEM) of a section containing *Achnanthidium minutissimum* cells cultivated in P-replete (P(+)) conditions and observed spherical structures (Figure 3. 1A, green arrowhead). These granules appeared to be filled with electron dense material and localized in the two apices of the diatom. Granules were enclosed in an uncharacterized area differing from the rest of the cellular components by poor electron density (Figure 3. 1A, blue arrowhead). Using the same SEM sample, we employed energy dispersive X-ray analyses (EDX) to investigate the molecular composition of the granules and detected an increased amount of phosphorus (P) and calcium (Ca) in the granules (Figure 3. 1B), when compared to other areas of the cell (Figure 3. 1C). Both P and Ca appeared to be distributed homogenously within the granules, and the P peak was much stronger than the Ca peak (Figure 3. 1BC, Figure S3. 1BC), indicating that the granules contained higher amounts of P than Ca.

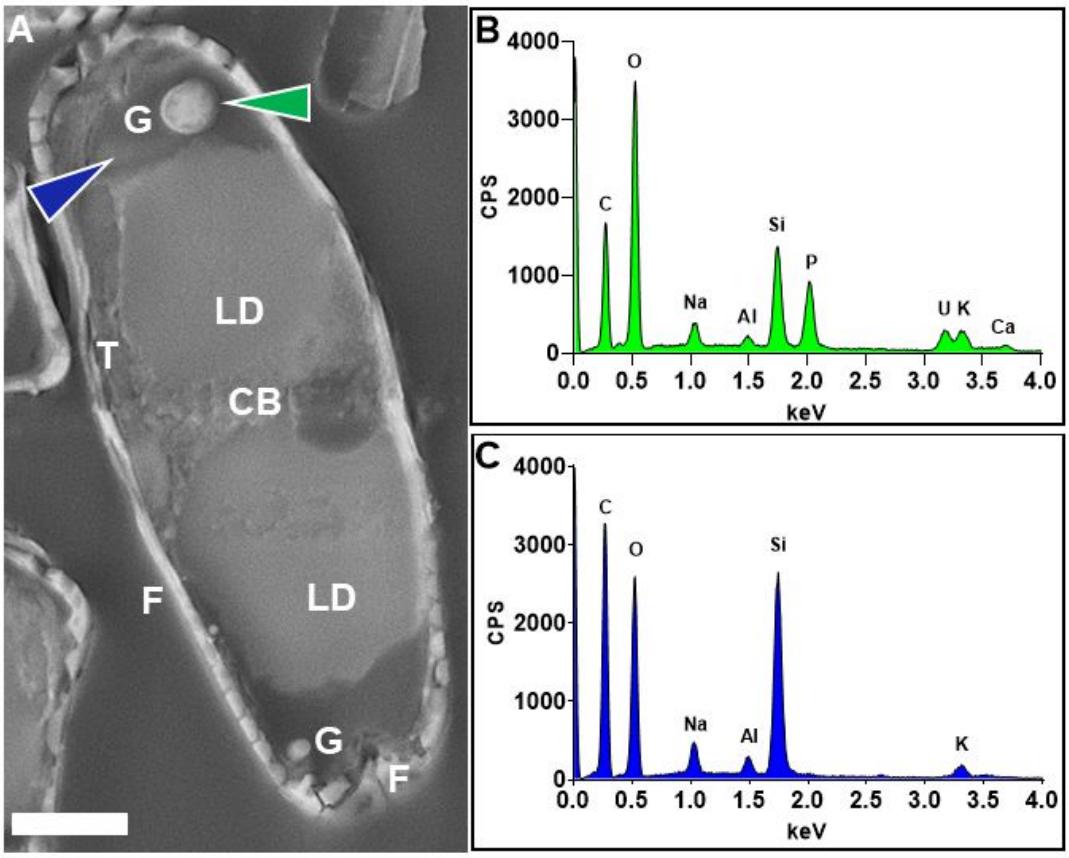

Figure 3. 1: Detection of granules containing phosphorus in an *Achnanthidium minutissimum* cell. A) Ultrastructural sectional SEM image of *A. minutissimum* containing a cytoplasmic bridge (CB), thylakoids (T), lipid droplets (LD), electron-dense granule (G), and (F) frustule. B) EDX spectrum of the electron-dense granule (recorded from the area indicated by the green arrowhead). The peaks at 2.01 and 3.69 keV indicate phosphorus (P) and calcium (Ca), respectively. C) EDX spectrum of a cellular area with no granule (recorded from the area indicated by the blue arrowhead) showing the absence of P and Ca peaks. These data are representative of cells cultivated in P-replete ($P_{(+)}$) conditions. The scale bar (white) represents 1 µm.

The locations of the granules within the *A. minutissimum* cells was investigated by epifluorescence microscopy using MDY-64, which specifically stains vacuolar membranes (Figure 3. 2). Most of *A. minutissimum* cells in the sample contained one or two large vacuoles (Figure 3. 2). The two apical vacuoles were located in the same cellular area as the P-containing granules observed by SEM and EDX (Figure 3. 2B), one on each apex of the cell and in close contact with large circular structures (Figure 3. 2A), confirmed as lipid droplet by BODIPY staining (Figure S3. 2).

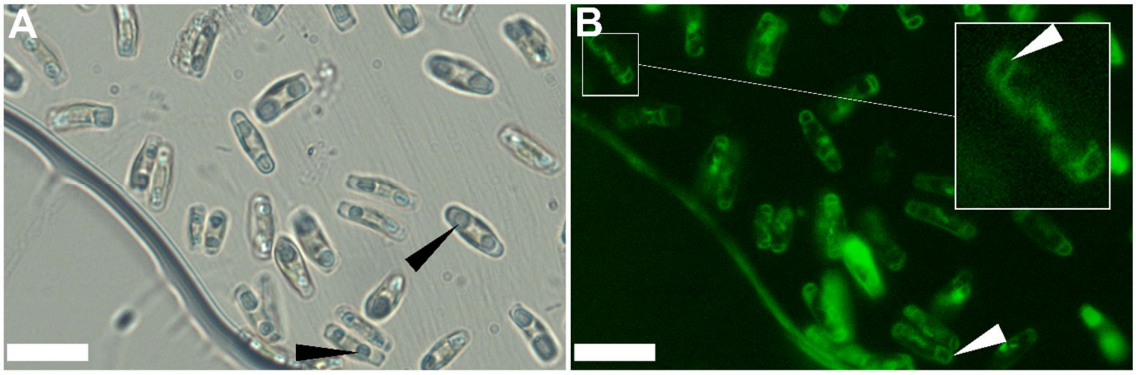

Figure 3. 2: Localization of the vacuoles in the diatom *Achnanthidium minutissimum*. A) Bright-field micrograph of *A. minutissimum* cells containing lipid droplets (black arrowheads). B) Epifluorescence of a marker for vacuole membrane (MDY-64) indicates the location of the vacuoles (white arrowheads). These data are representative of cells cultivated in P-replete ($P_{(+)}$) conditions.Scale bars represent 10 µm.

We furthermore investigated the molecular state of the P moieties detected in the granules using stimulated Raman scattering (SRS) based microscopy (Figure 3. 3), allowing the specific imaging of polyP, represented by a strong peak in the area of 1145-1177 cm (De Jager et al. 1998, Fernando et al. 2019). The SRS spectra of polyP and lipids of *A. minutissimum* cells cultivated in $P_{(+)}$ conditions are shown and compared to spontaneous Raman spectra of the polyP and fatty acid standards (hexametaphosphate and oleic acid) in Figures 3B and 3C, respectively. The granules (Figure 3. 3A, green pixels) revealed an intense peak at 1166 cm^{-1} (Figure 3. 3B), representing polyP.

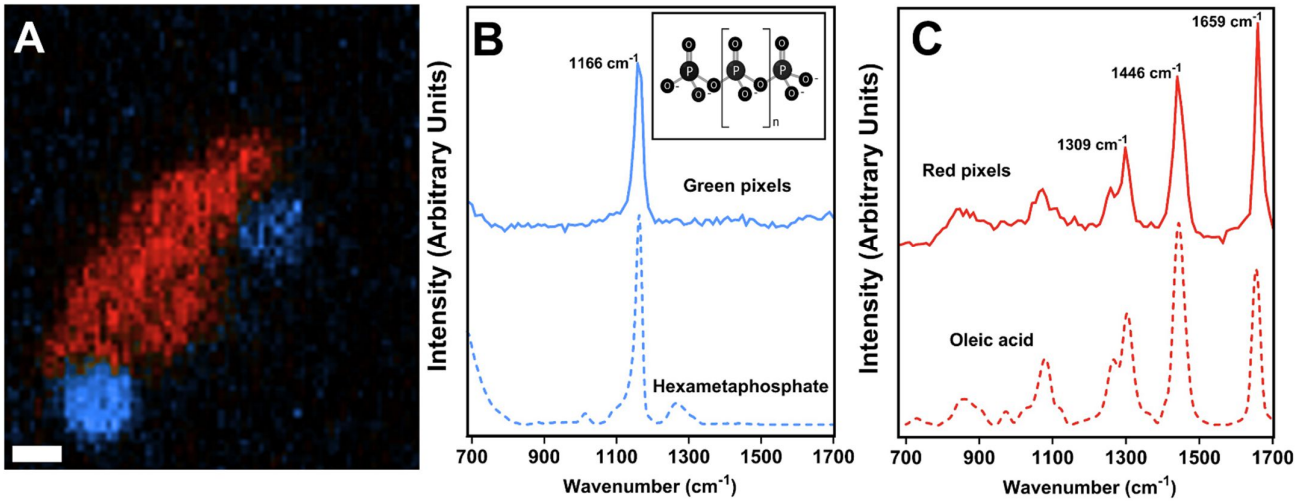

Figure 3. 3: PolyP detection in *Achnanthidium minutissimum* cells using stimulated Raman scattering (SRS) microscopy. A) SRS map of *A. minutissimum* cells showing the distribution of polyP (blue pixels) and lipids (red pixels; scale bar: 1µm). B) Spontaneous Raman spectrum of a polyP standard of sodium hexametaphosphate of 96% purity (Sigma Aldrich, Taufkirchen, Germany; green dotted line), and SRS spectrum of intracellular granules (solid blue line), showing a maximum at 1166cm^{-1}. A structure of linear polyP is shown in the upper right (n=1 to several 100 of P_i). C) Spontaneous Raman spectrum of oleic acid as a lipid standard (oleic acid, red dotted line) and SRS spectrum of the lipid distribution within the diatom (solid red line), showing three major maxima at 1309, 1446, and 1659cm^{-1}. These data are representative of polyP-rich cells cultivated in P-replete ($P_{(+)}$) conditions. These data are representative of polyP-rich cells cultivated in P-replete ($P_{(+)}$) conditions.

Estimation of polyP chain-lenghts from *Achnanthidium minutissimum*

To determine the lengths of the polyP chains in *Achnanthidium minutissimum*, polyP from cells cultivated in P(+) condition was isolated and purified using an optimized size exclusion method(Lapointe et al., 2022) and subjected to acrylamide TBE-urea electrophoresis. The polyP sample was compared to defined polyP standards and DNA size markers (Smith et al., 2018) (Figure 3. 4).

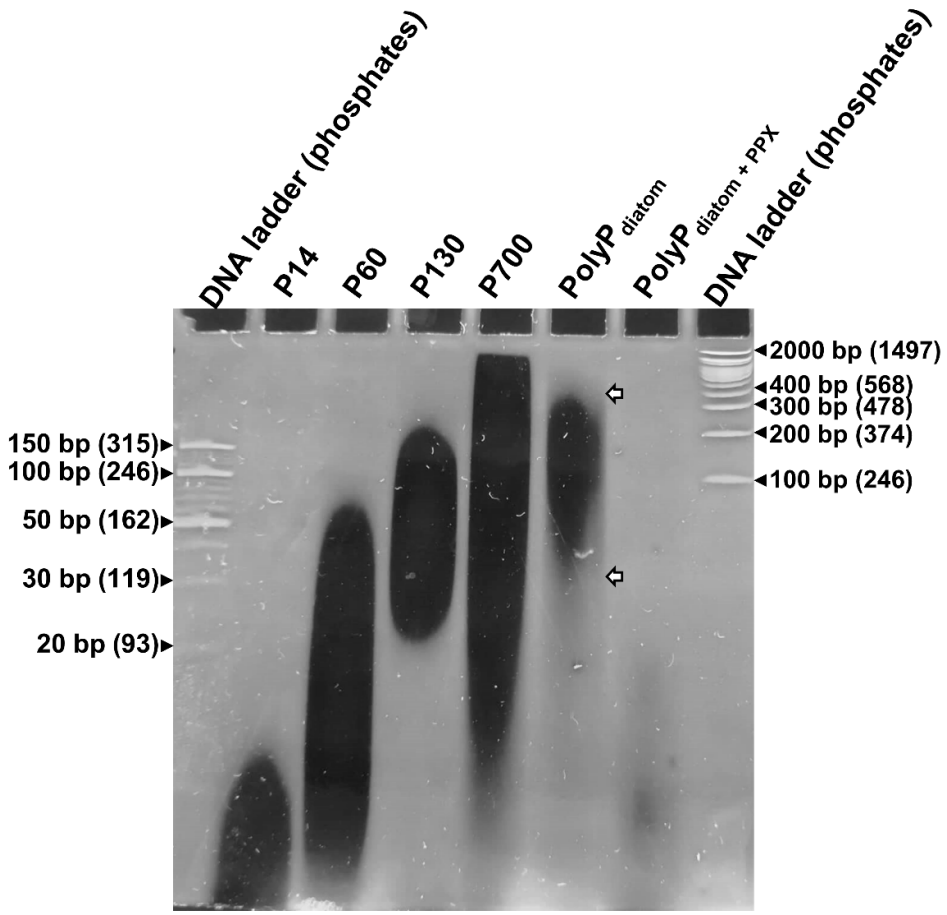

Figure 3. 4: Twenty percent TBE-urea gel electrophoresis of polyP extracted from *Achnanthidium minutissimum* cultivated in P-replete $P_{(+)}$ conditions. PolyP is stained with DAPI. The lanes show (from left to right) a 10bp DNA marker, the polyP standards polyP-14, 60, 130, and 700 P_i, polyP extracted from *A. minutissimum* (PolyP *diatom*), polyP extracted from the diatom and treated with exopolyphosphatase (PPX) (PolyP $_{diatom+PPX}$), and a 100bp DNA marker (Invitrogen). Labels of DNA ladders indicate the size of the ladders in base pairs (bp) as well as their equivalent in Pi units (in brackets) for polyP length determination following the calculation of Smith et al. (2018). White arrows indicate the upper and lower limit of the polyP range extracted from the diatom.

The polyP standards consist of heterogeneous mixtures of chain lengths resulting in a smear instead of a single band. The polyP fraction of *A. minutissimum* comprised polyP chain lengths of 130 to 500 P_i units (Figure 3. 4). Treating the samples with PPX, which cleaves polyP from the terminal ends and releases a P_i, resulted in complete degradation of the polyP fraction, confirming its identity.

Impact of phosphate availability on diatom physiology

To study responses to different phosphate (P_i) availabilities, we cultured *A. minutissimum* under P replete ($P_{(+)}$) and deplete ($P_{(-)}$) conditions. The lag phase of cells grown in $P_{(+)}$ and in $P_{(-)}$ conditions both occurred within 2 d and was followed by an exponential growth phase from day 2 to day 10 (Figure 3. 5A). In both conditions, the cells entered the stationary phase on day 10 (Figure 3. 5A). The final cell density on day 15 was 2.3 times higher for *A. minutissimum* cultivated in $P_{(+)}$ compared to cells in $P_{(-)}$ conditions before resupplying in AM $P_{(+)}$. Cells cultivated in $P_{(-)}$ conditions grew for 8 days even though there was no exogenous P detectable (Figure 3. 5A). Only between days 4 to 6, the growth rates of cells grown in $P_{(-)}$ and $P_{(+)}$ conditions differed significantly (Student test: $t(6) = 3.799$, $p = 0.090$) (Table S3. 2). After a 5 d stationary phase, cultures were resupplied with $P_{(+)}$ cultivation medium on day 15. Cells having experienced either $P_{(+)}$ or $P_{(-)}$ conditions (referred to as $P_{(+/+)}$ cells and $P_{(-/+)}$ cells) both simultaneously resumed growth after a lag phase of about 24h, and cultures started to divide again at day 17 (Figure 3. 5). $P_{(-/+)}$ and $P_{(+/+)}$ cells yielded slightly but significantly lower final cell numbers for $P_{(-/+)}$ cells with $2.41\times10^6 \pm 0.19\times10^6$ cell/mL than for $P_{(+/+)}$ cells with $3.02\times10^6 \pm 0.23\times10^6$ cell/mL, respectively (Table S3. 3). The extracellular P_i concentration in $P_{(+)}$ cultures started from 53.3 ± 0.77 µM P_i, at day 0 in $P_{(+)}$ cultivation medium (Figure 3. 5B). $P_{(+)}$ cells started to take up P_i during the lag phase with rates of 3.93 ± 1.21 pg P_i/cell/day from day 0 to day 2 (Figure 3. 5D). During cell division, levels of P_i uptake per cell were about 5 times lower than during the lag phase with 0.67 ± 0.19 pg P_i /cell/day and 0.57 ± 0.04 pg P_i /cell/day from day 2 to 4 and day 4 to 6, respectively (Figure 3. 5D). At day 6, levels of exogenous P in $P_{(+)}$ cultures were below the limit of quantification (LOQ, < 3 µM P_i) (Figure 3. 5B). In $P_{(-)}$ cultures, there were no detectable amounts of exogenous P_i from day 0 to day 15 (Figure 3. 5B).

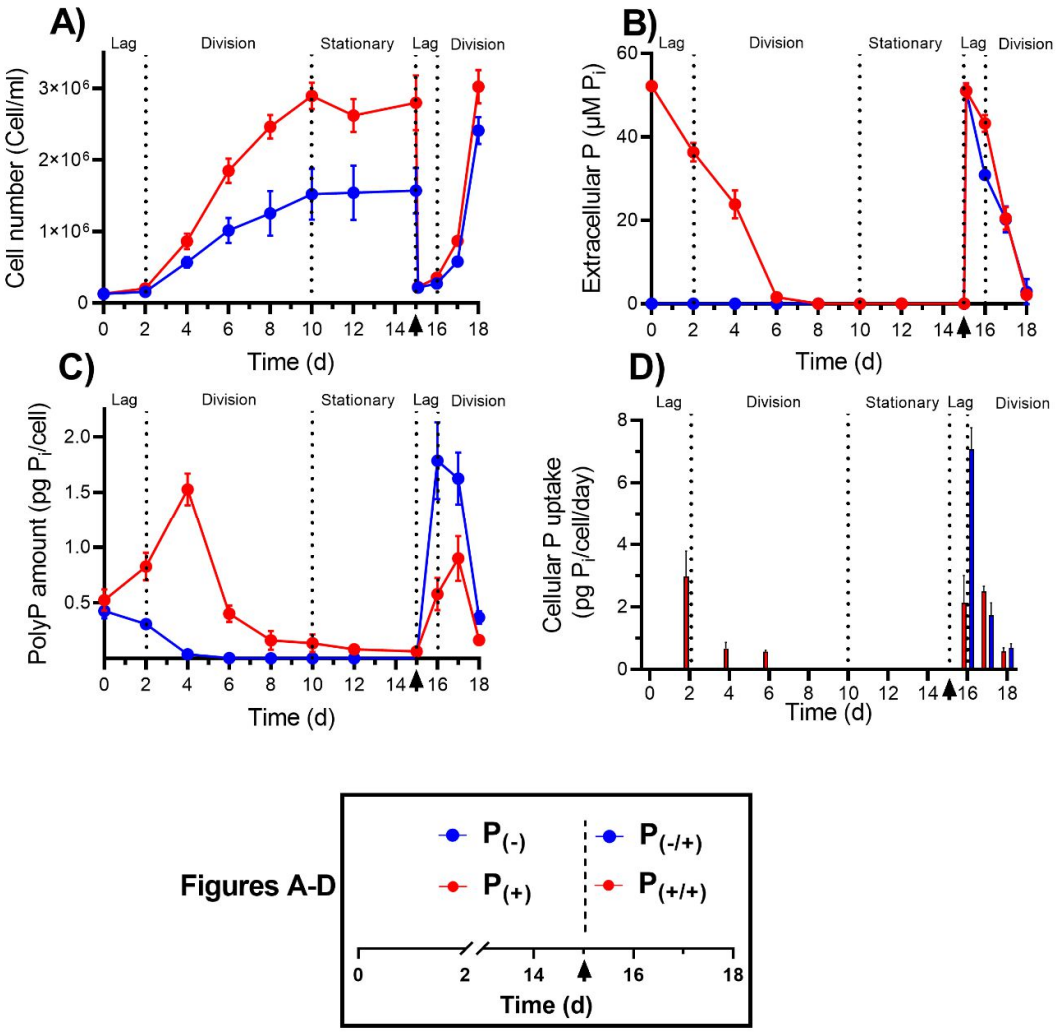

Figure 3. 5: Cultivation of *Achnanthidium minutissimum* under different P availabilities. Cells were cultivated for 15 days in either P-replete ($P_{(+)}$) or P-deplete ($P_{(-)}$) cultivation medium. Black arrows represent the time point of resupply with $P_{(+)}$ cultivation medium in $P_{(+)}$ and $P_{(-)}$ cultures (day 15), and cells were annotated $P_{(+/+)}$ and $P_{(-/+)}$, respectively. $P_{(+/+)}$ and $P_{(-/+)}$ cultures were incubated for 3 more days. A) Cell growth (cell/mL), B) Dissolved extracellular P concentrations in the cultivation medium (µM P_i), C) Changes in cellular polyP content (pg P_i/cell), D) Changes in P uptake (pg P_i/cell/day). Error bars indicate the standard deviation of n=4 replicates. On day 15, data from C correspond to before the resupply in AM $P_{(+)}$ cultivation medium, and A and B show data from before as well as after medium resupply with a difference of ca. 120 min between measurements.

During the first 48 h of the lag phase, polyP amounts in $P_{(+)}$ cells increased at a rate of 0.14 ± 0.09 pg P_i/cell/day, further increasing during cell division to 0.32 ± 0.08 pg P_i/cell/day until day 4 (Figure 3. 5C, Table S3. 4). On day 6, when exogenous P_i levels were no longer detectable, polyP concentrations per cell in the same cultures declined by 4-fold with a similar rate as the previous increase. At the beginning of the stationary phase, polyP amounts in $P_{(+)}$ cells were

low but still detectable with 0.15 ± 0.01 pg P_i/cell and remained stable until the resupply with $P_{(+)}$ cultivation medium at day 15 (ANOVA: $F_{3,11} = 1.511$; $p = 0.266$) (Figure 3. 5C). In $P_{(-)}$ cells, cellular amounts of polyP were stable during the lag phase (Student test: $t(6) = 2.995$, $p = 0.058$), and immediately declined at a rate of 0.13 ± 0.02 pg P_i/cell/day at the onset of cell division from day 2 to day 4. During the same period, polyP concentration being 42 times lower than in $P_{(+)}$ cells, but still detectable with 0.04 ± 0.01 pg P_i/cell on day 4 (Figure 3. 5C). Already at day 6, polyP was no longer detectable in $P_{(-)}$ cells (Figure 3. 5C).

After phosphate supplementation on day 15, $P_{(+/+)}$ and $P_{(-/+)}$ cultures responded differently. Within the 24 h lag phase, $P_{(-/+)}$ cells generated 3 times more polyP with 1.80 ± 0,30 pg P_i/cell compared to 0.60 ± 0.10 pg P_i /cell in $P_{(+/+)}$ cells (Figure 3. 5C, Table S3. 5). This strong increase in polyP stocks in $P_{(-/+)}$ cells measured 24h after P_i resupply was accompanied by a faster exogenous P_i uptake per cell during the same period, taking up exogenous P 3-fold faster than $P_{(+/+)}$ cells with an uptake rate of 2.13 ± 0.87 pg P_i/cell/day compared to 7.07± 0.68 pg P_i/cell/day, respectively (Figure 3. 5D). Between day 2 and 4, ca. 20% of the P uptake was allocated to polyP production in $P_{(+)}$ cells and 24h after phosphate supplementation ca. 30% of the P uptake was allocated to polyP synthesis of $P_{(-/+)}$ cells, against ca. 20% for $P_{(+/+)}$ cells (Table S3. 6) The strong capability to take up extracellular P_i in $P_{(-/+)}$ cells changed at the onset of cell division at day 17. During this period, the extracellular P_i uptake in $P_{(-/+)}$ cells decreased by 4-fold with an uptake rate of 1.74± 0.4 pg P_i/cell/day and were 1.4 times lower than $P_{(+/+)}$ cells (Figure 3. 5D). The amounts of polyP in $P_{(-/+)}$ cells at day 17 remained high and were comparable to those observed before the start of cell division at day 16 (Student test: $t(6) = 0.774$, $p = 0.468$) (Figure 3. 5C). At day 18, cells were continuing to divide and the uptake rates of P_i in both $P_{(+/+)}$ and $P_{(-/+)}$ cells decreased to reach similar levels with 0.58± 0.11 pg P_i/cell/day and 0.69± 0.13 pg P_i/cell/day (Student test: $t(6) = 1.276$, $p = 0.249$) (Figure 3. 5D). Extracellular P_i was depleted in both cultures on day 18 (Figure 3. 5B). Similarly to the observations for $P_{(+)}$ cells at day 6, P_i starvation at day 18 was accompanied by a decrease of polyP amounts which was 2-fold higher in $P_{(-/+)}$ than in $P_{(+/+)}$ cells (1.3 ± 0.2 pg P_i/cell/day and 0.7 pg P_i/cell/day) (Figure 3. 5D).

The Spearman's rank correlation coefficient matrix from the combined as well as separated $P_{(+)}$ and $P_{(-)}$ datasets revealed statistically significant strong positive relationships ($R > 0.6$) among polyP concentration, P_i uptake, and external P_i concentration (Figure S3. 3ABC). We also observed similar correlations when datasets were treated separately with the strongest correlation found between external P_i concentrations and the P_i uptake in $P_{(-)}$ treatment (Figure

S3. 3A). There were no significant correlations between growth rate and polyP concentration, P_i uptake, or external P_i concentration in either the separated or the combined dataset (Figure S3. 3ABC).

Using the same cultivation samples, polyP granules dynamics within the diatoms were followed by SRS image analysis. The SRS data (Figure 3. 6) confirm the quantitative polyP analyses as shown in Figure 3. 5C.

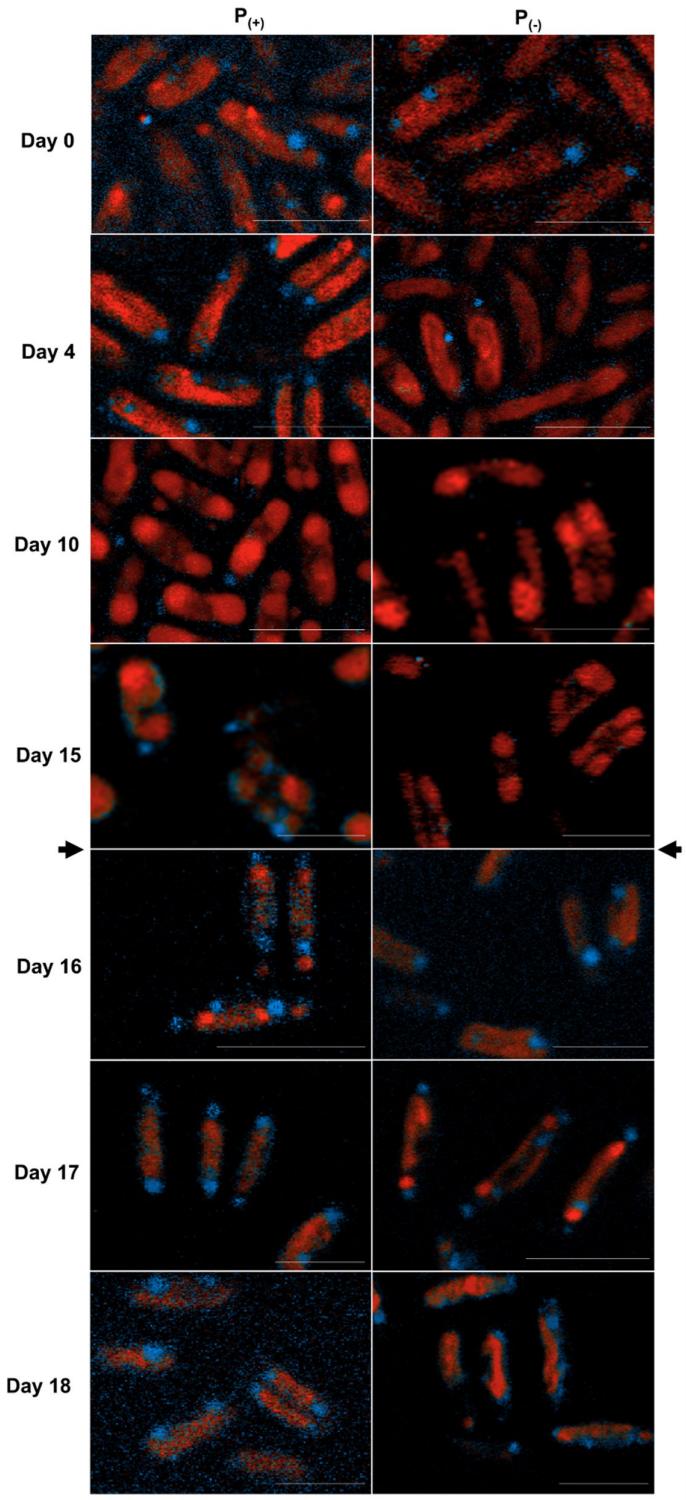

Figure 3. 6. SRS images of *A. minutissimum* cells showing the dynamic of polyP granules (blue pixels) and lipids (red pixels) in cells before and after medium resupply. On day 15, data correspond to before the resupply in $P_{(+)}$ cultivation medium. The scale bars correspond to 10 μm.

Granules were visible on day 0 in 50% of $P_{(-)}$ cells and 53% of $P_{(+)}$ cells (Figure S3. 4A), and the percentage of surface area per cell occupied by the polyP granules was similar for both treatments at 6% (Figure S3. 4B). On day 4, 79% of $P_{(+)}$ cells were displaying polyP granules and only 9% of $P_{(-)}$ cells, and granules were occupying a higher surface area in $P_{(+)}$ cells with ca. 7.00% compared to 4.23% in $P_{(-)}$ cells. On days 10 and 15, polyP granules were almost absent from $P_{(-)}$ cells with only 4 and 3% of cells containing granules, respectively. In contrast, in $P_{(+)}$ cells, although polyP amounts were low when extracellular P concentrations were below the LOQ, 18 and 12% of cells were displaying visible granules on days 10 and 15, respectively (Figure 3. 6). Only 24 h after phosphate resupply, polyP granules were present in 84 and 80% in both types of cells, respectively (Figure 3. 5 and S3. 4A). However, the percentage of surface area occupied by granules in cells was higher in $P_{(-/+)}$ than in $P_{(+/+)}$ cells with 8.33% compared to 5.36%, respectively (Figure S3. 4B). At day 17, a majority of $P_{(-/+)}$ and $P_{(+/+)}$ cells were still having granules with 80 and 75%, respectively. At day 18, when extracellular P concentrations were below the LOQ, but cells were still growing, the amount of cells displaying polyP granules decreased, to 44 and 34% for $P_{(-/+)}$ and $P_{(+/+)}$ cells, respectively (Figure S3. 4A). Similarly, the percentage of surface area occupied by the granules also decreased to 5.19 and 4.68% in both $P_{(-/+)}$ and $P_{(+/+)}$ cells, respectively (Figure S3. 4B).

Discussion

Achnanthidium minutissimum stores polyP granules in vacuoles resembling acidocalcisomes organelles

Raman spectroscopy, EDX microscopy, and biochemical analysis revealed that in the diatom Achnanthidium minutissimum, polyP is stored in granular form, located within cell vacuoles. The localization of the polyP granules in A. minutissimum confirms classical observations in raphid pennate diatoms describing two large apical vacuoles containing spherical "volutin granules," also known as polyP granules (Mann 1985). The vacuoles contain polyP-Ca-rich granules and share anatomical and chemical features with acidocalcisomes (Docampo et al. 2005). These acidic organelles are considered to be major storage compartments in microorganisms for phosphorus compounds (orthophosphate, pyrophosphate, polyP), as well as cations (calcium, magnesium, iron ions) (Docampo et al. 2005). The green alga *Chlamydomonas reinhardtii* also possess acidocalcisomes, these contain polyP and Ca^{2+} ions and are surrounded by a membrane containing a vacuolar proton-translocating inorganic

pyrophosphatases (V-H+-PPase) and a vacuolar proton ATPase (V-H+-ATPase;VHA), which generates a low pH in the organellar lumen (Ruiz et al. 2001). It has recently been demonstrated that the *T. pseudonana* VHA is localized in the membranes of chloroplasts (Yee et al. 2023), silica deposition vesicles (SDVs), as well as vacuoles (Yee et al. 2019). In addition, the vacuolar transport chaperone complex (VTC1-4) is important for polyP synthesis within yeast vacuoles (Secco et al. 2012), and in *C. reinhardtii* (Plouviez et al. 2021). The diatom *Phaeodactylum tricornum* encodes for homologs of VTC (PtVTC 1-4), but only the PtVTC2 was located in the vacuolar membrane region (Schreiber et al. 2017), while the homologs PtVTC1, PtVTC3 and PtVTC4 showed no vacuolar localization (Dell'Aquila et al. 2020). Sequence analyses of cDNA extracts indicated that *A. minutissimum* possesses homologs of VHA and V-H+-PPase, as well as the four subunits of the VTC complex (Dow, 2019). However, the localization of the VTC subunits as well as these proton pumps in *A. minutissimum* is unknown, and further studies are required to analyse the composition of these apical vacuoles containing polyP granules.

The resistance of *Achnanthidium minutissimum* and reduction of polyP reservoirs under phosphate-limiting conditions

Based on the results presented here, we propose a scenario of cell responses to varying P availabilities, (Figure 3. 7) described below.

Although the cell density in cultures under $P_{(+)}$ and $P_{(-)}$ conditions was different at the end of the exponential phase, cells cultivated in $P_{(-)}$ conditions continued to divide for another 8 days in the absence of available exogenous P and were able to resume P uptake and growth very quickly once P became available. This reflects the capability of this diatom to survive under varying external P availability, suggesting the presence of a metabolic poise that allows growth maintenance under short-term external P starvation. Applying SRS microscopy and biochemical analyses, we observed that dividing *Achnanthidium minutissimum* in $P_{(+)}$ conditions accumulated polyP when extracellular P_i concentrations declined. Microorganisms subjected to $P_{(+)}$ conditions can accumulate P_i from the environment in excess of that required for growth and store it as a reserve by synthesizing polyP chains when the external concentration of P is becoming limited (Kuhl 1974). Such a response is called "luxury uptake" (Eixler et al. 2006, Li and Dittrich 2019), and is thought to be essential for microorganisms to survive periods of scarce P availability In addition, yeast lacking the vacuolar transporter chaperone gene (VTC4), which is responsible for the synthesis of polyP from ATP, have shown

reduced growth when cultivated under $P_{(-)}$ conditions, suggesting that polyP is involved in cell survival during P stress(Hothorn et al. 2009). With no exogenous P available, we observed cellular polyP stocks in both $P_{(+)}$ and $P_{(-)}$ conditions decreased quickly as the cells were dividing, suggesting that polyP stocks in *A. minutissimum* may be used to sustain anabolic processes such as DNA synthesis (Figure 3. 7). Thus, the depletion of polyP stocks acquired in $P_{(+)}$ conditions in *A. minutissimum* cells may contribute to the P requirements for sustaining cellular processes under $P_{(-)}$ conditions.

After polyP stock depletion in $P_{(-)}$ conditions, the cells continued dividing for 4 more days. When subjected to P stress, diatoms and microalgae can reduce their cellular P demand by remodeling membrane lipids (Figure 3. 7). The response is associated with a reduction of membrane phospholipids (PL) in favor of other lipids like betaine and sulfur-containing lipids (Van Mooy et al. 2009, Martin et al. 2014, Huang et al. 2019). This process results in a decrease in the cellular P demands (Martin et al. 2011, Hunter et al. 2018), sparing ca. 17% of the total P cell demand in marine microalgae (Van Mooy et al. 2009). A minor membrane PL degradation has been detected during lipidome remodelling in *T. pseudonana* under P limitation, and the released P can support cell growth for additional 3 days (Hunter et al. 2018). Although the role of lipid membrane remodeling in alleviating external P limitation in *A. minutissimum* is still speculative and needs further analyses, it is reasonable to assume that the diatom uses other P reservoirs after the depletion of its polyP stocks.

PolyP production of starved cells after phosphate resupply: the overplus mechanism

Within the first 24 h following the resupply of cultures with P_i, *A. minutissimum* cells that were initially supplemented with $P_{(-)}$ medium ($P_{(-/+)}$), show a 3-fold faster extracellular P uptake rate than cells that were initially supplemented with $P_{(+)}$ medium ($P_{(+/+)}$) (Figure 3. 7). Such a phenomenon in other microalgae has been termed “overplus response” (Liss and Langen 1962, Harold 1964, Aitchison and Butt 1973, Plouviez et al. 2021). A rapid P uptake by $P_{(-/+)}$ proves that *A. minutissimum* can drastically increase its P assimilation rate. For the uptake of extracellular P through the plasma membrane and its transport to organelles, P_i-transporters are essential. Transcriptomic data analyses revealed that in *T. pseudonana* and *P. tricornutum*,

theexpression of P_i transporters genes is increased when the cells experience P deficiency (Dyhrman et al. 2012, Yang et al. 2014, Alipanah et al. 2018).

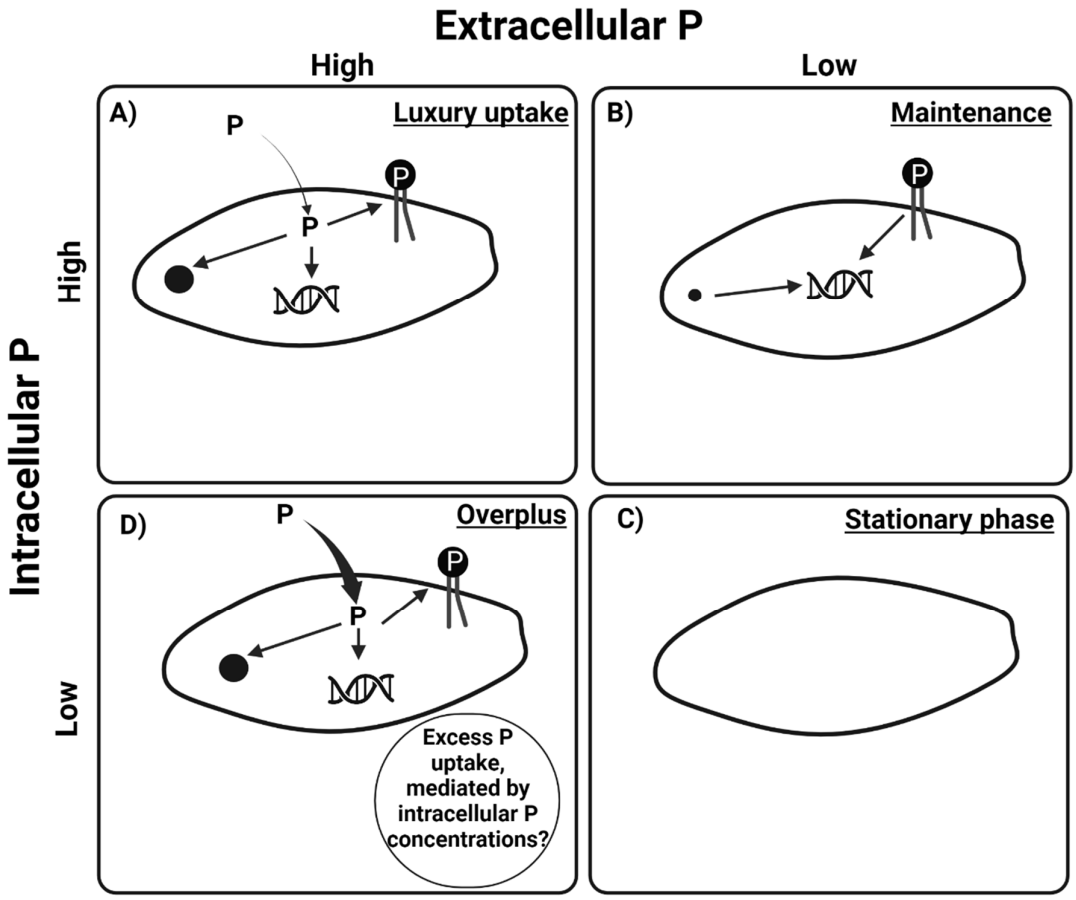

Figure 3. 7: Schematic figure showing the phosphorus (P) physiology of the diatom *Achnanthidium minutissimum* in different nutrient availability scenarios, based on the data collected in this study. A) In the presence of exogenous P, the diatom stored excess P not required for growth in polyP granules through the luxury uptake of P. B) In the absence of exogenous P, the diatom used its polyP reserves to sustain its cellular P requirements, and growth was maintained. After the depletion of polyP reserves, further growth was sustained by other cellular P storages, e.g., phospholipids. C) Growth of the diatom eventually halted when cellular P reserves were depleted. D) Once the diatoms with low P reserves were resupplied with exogenous P, they took up large amounts of P and stored the P as polyP through the overplus response. Depending on the availability of external P, the diatom could either undergo a new low-P availability phase and use its P storages to maintain its growth or could transition to a luxury uptake phase where it stored excess P in polyP. Curved black arrows indicate the uptake of exogenous P. Straight black arrows indicate the phosphorus transfer processes. Black spheres indicate the polyphosphate (polyP) granules. The DNA symbol represents the diatom growth.

The rapid P uptake per cell in *A. minutissimum* $P_{(-/+)}$ cells was accompanied by a dramatic increase in their polyP levels. This is also consistent with the observation of overplus responses in cyanobacteria (Li and Dittrich 2019) and *C. reinhardtii* (Plouviez et al. 2021). Overplus responses are likely to play an important role in P retention in cells experiencing temporally variable P supply (Rhee 1972). The usage of the P stored after overplus response for growth continuation was shown in stream periphyton communities (Rier et al. 2016), as well as in cyanobacteria (Falkner and Falkner, 2011). Similarly, in our study, it is reasonable to assume that *A. minutissimum* may also use the P stored (e.g. polyP stock) during the overplus response for sustaining growth under external P limitation. Hence, we suggest that *A. minutissimum* can respond rapidly to environmental P fluctuations by adjusting its P-uptake and polyP reserve metabolism. A remaining question is why the Pi uptake in $P_{(+/+)}$ cells remains low 24 h after the resupply with $P_{(+)}$ cultivation medium, even though cells experienced phosphorus limitation and growth cessation beforehand. Since P uptake rates in microalgae are dependent on the cellular P concentration (Rhee 1973, Caceres et al. 2019), it is likely that $P_{(+/+)}$ cells still possessed P reserves, other than polyP which prevented the diatom overplus response. The further identification of these reserves as well as the investigation of their co-dynamics under P limitation would greatly improve the understanding of the diatom P homeostasis.

Conclusions

The freshwater diatom *Achnanthidium minutissimum* can accumulate polyP through the "luxury uptake" and "overplus response," which are processes well documented in algae and other aquatic microorganisms but poorly understood in diatoms. These two strategies would provide a physiological advantage to the diatom in that it would be able to store P when it was available and later use it for growth when external P was depleted, for example in P-varying ecosystems. Further studies are needed to understand the relevance of polyP in diatoms. In this regard, SRS microscopy applications have a strong potential for fast detection of polyP in diatom samples. In addition, studies need to be conducted to unravel the molecular pathways of polyP synthesis to better understand its regulation in diatoms.

Acknowledgements

We are grateful for the financial support by the DFG (Deutsche Forschungsgemeinschaft)-GRK2272 (RTG R3). MK was supported by a Philipp–Schwartz stipend from the Alexander von Humboldt foundation. Part of this work received funding from the European Union's Horizon 2020 research and innovation program under grant agreement no. 812922. We thank RegeneTiss Incorporated (Tokyo, Japan) for the kind gift of the polyP standards. Open Access funding enabled and organized by Projekt DEAL.

Chapter 4. An intimate view into the biofilm formation of *Achnanthidium minutissimum*: A first structural and biochemical characterization of the stalk

Adrien Lapointe, Paavo Bergman, Michael Laumann, Imaiyan Chitra Ragupathy, Mustafa Kocademir and Peter G. Kroth

Manuscript not published

Abstract

Achnanthidium minutissimum is a cosmopolitan benthic freshwater diatom that forms biofilms on submerged surfaces by producing structures in the form of stalks and capsules made of extracellular polymeric substances (EPS). Although the diatom stalk allows its permanent adhesion to the substrata, its ultrastructure as well as its mechanism of production are not well known. By a combination of fluorescence and electron microscopy techniques, we demonstrate that the stalk is made of interwoven fibrils formed at the apex of the frustule, consisting of polysaccharides. The stalks contain sulphur, probably in the form of sulphate, associated with ion metals such as magnesium and iron, which are proposed to cross-bridge the polysaccharides. The sulphated polysaccharides can be labelled with DAPI, inducing a shifting of its emission fluorescence spectra, similarly to polyP-DAPI interactions. Fibrillar precursors are produced in an extracellular space between the frustule and the cell. . Fibrils are extruded through nanometer-scale pores in the siliceous cell wall and accumulate at the outer part of the frustule. The cell membrane appears to be thicker at the stalk production site, compared to the rest of the cell

Keywords: *Achnanthidium minutissimum*; diatom, biofilm, stalk, fluorescence microscopy, scanning electron microscopy, transmission electron microscopy, stimulated Raman spectroscopy

Introduction

Diatoms are unicellular photosynthetic eukaryotic microalgae that are often the most dominant eukaryotic member of phototrophic biofilms, thanks to their ability to colonize new substrata (Wetherbee et al., 1998). In diatoms, adhesion to substrata occurs by the production of mucilaginous extracellular polymeric substances (EPS) and can be retrieved in the form of stalks, tubes, apical pads, or capsules (Hoagland et al., 1993).

The biofilm-forming diatom *A. minutissimum* is ubiquitous in freshwater environments (Hlúbiková et al., 2011, Pinseel *et al.*, 2017, Potapova & Hamilton, 2007). The diatom was isolated from an epilithic phototrophic biofilm from Lake Constance (47°35′N 9°28′E, Germany) (Bruckner *et al.*, 2008), and later purified from its natural associated bacteria (Windler et al., 2012). The resulting axenic *A. minutissimum* cells no longer form a biofilm and remain planktonic. Once diatoms are co-cultivated with the bacterium *Dyadobacter* sp. 32 isolated from the same location as *A. minutissimum*, biofilm formation is restored. Bacteria were found to produce unknown soluble extracellular info-chemicals which trigger the secretion of insoluble extracellular EPS structures such as stalks and capsules in *A. minutissimum* (Windler et al., 2015).

The fluorescent probe 4',6-diamidino-2-phenylindole (DAPI) is commonly used to label DNA in fluorescence microscopy. When complexed to DNA, DAPI is attached specifically to the hydrogen bonds between the A-T base pairs and the amidino groups of the minor grove of the DNA (Kapuscinski, 1995). The fluorescent probe is also known to reveal EPS structures like stalks and capsules in microorganisms (Bahulikar & Kroth, 2007). Scanning electron microscopy (SEM) allows the detailed observation of fine structures as well as different cellular components. While the ultrastructure of the capsule of *A.minutissimum* has already been studied through SEM in *A.minutissimum* (Leinweber & Kroth, 2015), only a few structural information is available for its stalk and further investigations are needed to better characterize its biofilm formation. In this study, we analysed the microstructure and the composition of the stalk produced by *A. minutissimum* using a combination of DAPI fluorescence staining as well as SEM coupled with energy-dispersive X-ray (EDX) and stimulated Raman spectroscopy.

Material and methods

Growth conditions

The freshwater diatom *A. minutissimum* (Kützing) Czarnecki (strain MW1), was isolated from photoautotrophic, epilithic biofilms in Lake Constance (47°41´N; 9°11`E, Germany) (Bruckner et al., 2008), and its associated bacteria were removed using the antibiotic imipenem (Windler et al., 2012). A seed culture of axenic cells was cultivated in 150 mL in "*Achnanthidium* medium" (AM,(Windler, 2014)) in a vented cell culture flask (Sarstedt, Newton, NC, USA) at 16°C, under a 16:8 day/night cycle at a light intensity of 70 µmol photons m^{-2} s^{-1}. AM is a modification of the BM medium "Bacillariophycaean medium" (Schlösser, 1994), lacking the soil extract component. Vitamins, silica, selenate, and trace metals ion solution were supplemented as described for F/2 medium (Guillard, 1975). Weekly, cultures were diluted with new AM to maintain the culture in log-phase (ca. 1.0×10^6cell/mL). Cultures were gently shaken daily for 5 s to allow gas exchange within the flask.

Dyadobacter sp. 32 was isolated from a xenic *Cymbella microcephala* Grunow strain D-32 culture (Bruckner et al., 2008), which originated from photoautotrophic, epilithic biofilms from the same sampling site as *A. minutissimum* (47°410 N; 9°110 E, Germany). A 5 mL bacteria cell stock was originally cultivated at 20 °C in AM supplemented with 10 mM of glucose with shaking (130 rpm) until reaching an OD_{600nm} of 0.2.

Co-cultivation of the diatom with bacteria

In the following, *A. minutissimum* cultivated together with *Dyadobacter* sp. 32 is termed a "co-culture". 10 mL of the log-phase seed of axenic diatoms culture were inoculated in a vented cell culture flask containing 40 mL of new AM. Starting diatom cell concentration was 200×10^3 cells/mL. The bacteria culture was centrifuged (5000 g, 5 min), the supernatant was discarded and cells were resuspended in 5 mL of new AM lacking glucose. Subsequently, 300 µL of the bacterial culture was inoculated in the vented cell culture flask containing the diatom culture. Flask was gently shaken to resuspend cells and three wells of a sterile 6 well-plate (Sarstedt, Newton, North Carolina, USA), each containing a sterile Thermanox disk of ca. 1 cm in diameter (Miles Laboratories Inc., Elkhart, Indiana, USA), were filled with 3 mL of the co-culture following the procedure described in Leinweber et al. (2015). Additionally, 1.5 mL was transferred in (x 2) wells of a sterile chambered coverslip (Ibidi GmbH, Gräfelfing, Germany). The well-plate and the chambered coverslip were sealed with parafilm. Cells in the flask as well

as in the 6 well-plate and the chambered coverslip were cultivated for 10 days at 16°C, under a 16:8 day/night cycle at a light intensity of 70 µmol photons m^{-2} s^{-1}. Daily, cultures were gently shaken for 5 s to allow gas exchange within the flask and the wells. On day 10 of cultivation, biofilm cells grown on the cell-culture flask were detached by sonication for 10-20 s using an ultrasonic bath (Transsonic T700, Elma, Germany). After resuspending the cells, they were transferred to 50 mL falcon tubes and centrifuged (5000g, 5min). Subsequently, 45 mL of the supernatant were removed and the 5 mL left were used to resuspend the cells carefully. Three tubes of 1.5 mL were filled with 1 mL of the resuspended cells. On day 10, cells in the tubes as well as the Thermanox and the chambered coverslips containing the attached grown biofilms were subjected to the following microscopy procedures.

Scanning electron microscopy (SEM) and energy-dispersive X-ray (EDX) spectroscopy

Thermanox disks were delicately removed from the 6-well plates using ethanol-sterilized tweezers and washed carefully with new AM. Subsequently, disks were transferred to new wells, covered with 1 mL AM and subjected to the following protocol for fixation, dehydration, and sputtering of the biofilm sample. Diatom cells were fixed on the Thermanox disks with a 1 mL mixture containing 1 mL 4% glutaraldehyde, 20 mM $CaCl_2$, and 20 mM $MgCl_2$ in 0.2 M Na-HEPES buffer at pH 7 on ice for 10 min. Later, the supernatant was delicately discarded and disks were covered with 2 mL of 2% glutaraldehyde, 10 mM $CaCl_2$, and 10 mM $MgCl_2$ in 0.1 M Na-HEPES buffer at pH 7 on ice for 20 min. The supernatant was discarded and disks were washed with 10 mM $CaCl_2$ and 10 mM $MgCl_2$ in 0.1 M Na-HEPES buffer at pH 7 on ice for 10 min. This procedure was repeated once. The supernatant was removed and dehydration was conducted with 30% and 50% EtOH, on ice for 7 and 15 min respectively, followed by 70% EtOH at 4 ◦C over night, 80% EtOH at RT for 20 min, 90, and 96% EtOH at RT for 20 min each and finally with 100% EtOH twice for 20 min. After critical point drying in CO_2 (Balzers CPD030; Oerlikon Balzers, Balzers, Liechtenstein), samples were finally sputtered with carbon (C) to a thickness of 5 nm (Balzers SCD030; Oerlikon Balzers, Balzers, Liechtenstein). After fixation, dehydration and C-sputtering, the biofilm-covered Thermanox disks were imaged and analysed with a Zeiss “AURIGA” scanning electron microscope equipped with an X-Max 20mm2 EDX-detector (Oxford Instruments, Abingdon, UK).

Transmission electron microscopy (TEM)

A first tube containing 1 ml of the detached biofilm was subjected to the same protocol as in Chapter 3 for cell fixation, dehydration, embedding, and sectioning (see chapter 3, Materials and methods, scanning electron microscopy). Imaging was done with a Zeiss Omega 912 (Zeiss, Oberkochen, Germany).

DAPI staining for fluorescence microscopy

One additional tube containing 1 mL of the detached biofilm was briefly centrifuged (5000 g, 1 min) and the supernatant was discarded. Cells were resuspended in 99 µL of new AM medium. Subsequently; cells in the tube and the chambered coverslip were stained with 100 µM DAPI (final concentration), and incubated for 15 min in the dark at room temperature. Cells in the tube were observed with an epifluorescence microscope, under a UV filter set (Olympus; 365 nm excitation and >420 nm emission filter) using an Olympus BX51 microscope (Olympus Europe, Hamburg, Germany). Fluorescence of cells in the 2-well chambered coverslip was observed by confocal laser scanning microscopy (CLSM) (405 nm excitation, 410 to 630 nm emission recording in lambda scan mode) using a Zeiss LSM 700 (Zeiss, Oberkochen). Emission spectra of DNA, stalks, frustules, and polyP granules were collected in triplicate in three different cells, by selecting the area of interest using the "Spline contour" tool, available in the Zen blue software. Intensities of each wavelength recorded from the emission spectra of the three replicates were averaged, resulting in an averaged spectrum for DNA, stalk, frustule, and polyP. Using the GraphPad Prism software, each spectrum was normalized by defining the smallest and highest averaged wavelength as 0 and 100%, and subsequently plotted.

DAPI-polysaccharides complex

Because DAPI can interfere with molecules other than DNA like polyP (Omelon *et al.*, 2016) or EPS (Wustman et al., 1997), we recorded a series of fluorescence emission spectra of standard polyP (polyP-45, Sigma-Aldrich, Taufkirchen, Germany), dextran (Sigma-Aldrich, Taufkirchen, Germany), dextran sulfate (VWR, Ulm, Germany), and double distilled water (ddH_2O) solutions. Briefly, 1 mL of 2.5 µM of standard polyP, dextran, or dextran sulfate dissolved in ddH_2O water was transferred into a plastic cuvette (Brand, Wertheim, Germany). Subsequently, samples were stained with 1.4 µM DAPI (final concentration) and incubated for

at least 2 min in the dark at room temperature. All measurements were performed using an Horiba Scientific FluoroMax-4 spectrofluorometer with the following parameters: 405 nm excitation and 460-600 nm emission wavelength, in 1 nm increments and integrated for 0.1 s, with an integration time of 0.5 s. Fluorescence intensity data were normalized and plotted following the same procedure as described above (see Material and methods, DAPI staining for fluorescence microscopy section).

Stimulated Raman spectroscopy

The remaining tube containing the detached biofilm was briefly centrifuged (5000 g, 1 min) and the supernatant was discarded. Before observation under SRS, cells were subjected to the same protocol described in chapter 3 (see chapter 3, Material and methods, Stimulated Raman spectroscopy of *A. minutissimum* section).

Results

DAPI shifting fluorescence in extra- and intracellular structures in *A. minutissimum*.

When excited at 365 nm, DAPI bound to DNA in *A. minutissimum* displays a typical blue fluorescence. In addition, the fluorescent probe is also bound to frustules and stalks, displaying a shifted fluorescence appearing yellow (Figure 4. 1B).

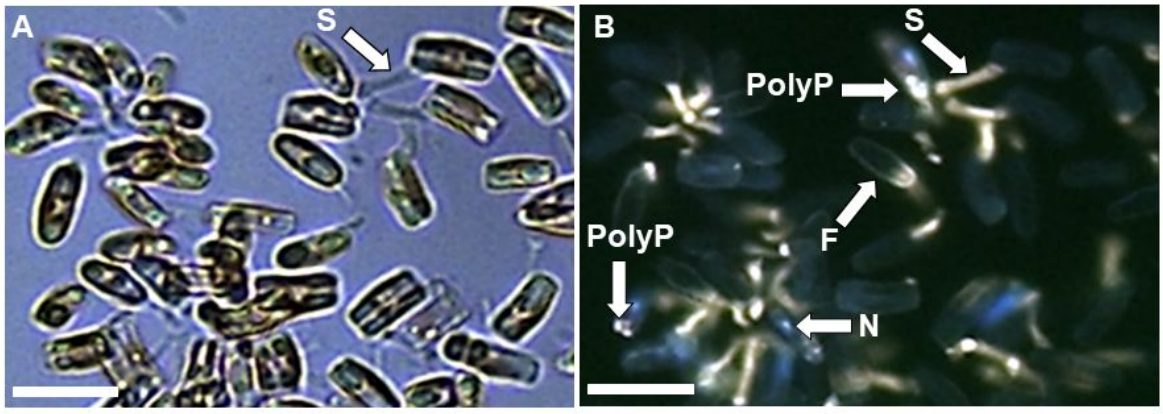

Figure 4. 1: DAPI staining (excitation: 365 nm) revealing blue and yellow fluorescent structures in *A. minutissimum* co-cultivated with *Dyadobacter* sp. 32. A) Bright-field micrograph of co-cultivated diatoms and bacteria showing cells-producing stalk (S). B) Corresponding

epifluorescence micrograph of DAPI-labelled cell structures showing blue nucleus (N), yellow polyphosphate granules (polyP), yellow frustule (F), and yellow stalks (S). Scale bar: 10 µm.

To investigate the fluorescence spectra of DAPI binding to *A. mimutissimum* structures, DAPI-labelled cells were subjected to confocal laser scanning microscopy (CLSM) using 405 nm excitation and an emission wavelength scanning (lambda scan mode) from 410 to 630 nm (Figure 4. 2A). As shown in Figure 4. 2B, DAPI exhibits different emission spectra according to the labelled structure of the cell. DAPI-DNA complexes show a maximum emission spectrum at 467 nm, emitting a blue colour, which was barely visible in Figure 4. 2A. The faint blue colour results from the use of a higher wavelength of excitation (405 nm instead of 365 nm) which reduces considerably the DNA emission signal contribution and increase the signal of higher emission wavelengths like DAPI-polyP complexes. When bound to polyP granules, DAPI fluorescence emission is shifted, exhibiting a maximum emission spectrum at 540 nm. DAPI also binds to stalks with a maximum emission spectrum similar to the DAPI-polyP complex. In addition, DAPI also binds to cell frustules with a maximum emission spectrum at 521 nm (Figure 4. 2B).

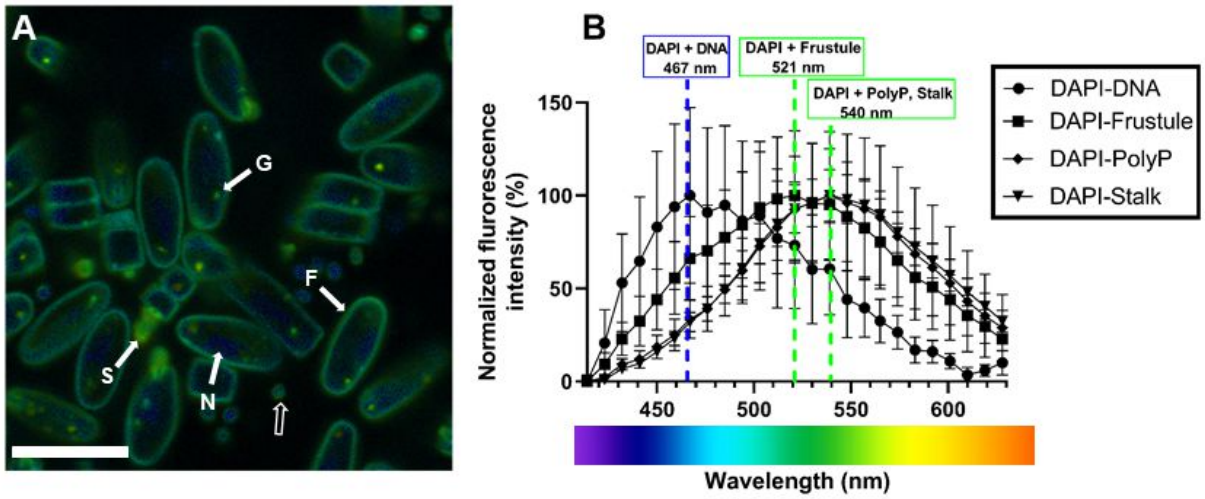

Figure 4. 2: Shifts in DAPI signature emission spectra (excitation: 405 nm) upon binding to DNA or stalks, frustules, and intracellular polyP granules. A) CLSM of co-cultivated *A. minutissimum* and *Dyadobacter* sp. 32 stained with DAPI showing intracellular polyP granules (G), stalks (S), nucleus containing DNA (N), frustule (F). B) Corresponding emission spectra of DAPI bound to DNA, frustules, polyP, or stalks from cells shown in A). Note the shifts in the spectrum when DAPI binds to polyP granules, frustules, or stalks compared to the DAPI-DNA complex. The black arrow shows a DAPI-labelled bacterium. Data in B) represent means of n=3 emission spectra. Error bars indicate standard deviations. Scale bar: 10 µm.

As the CLSM data show a similar DAPI-shifting signal for polyP and stalks, the polyP distribution in the biofilm was mapped using SRS, selecting the Raman band of polyP located at 1161 cm^{-1} (Figure 4. 3B). PolyP was not found to be associated with stalks but only found intracellularly (Figure 4. 3C).

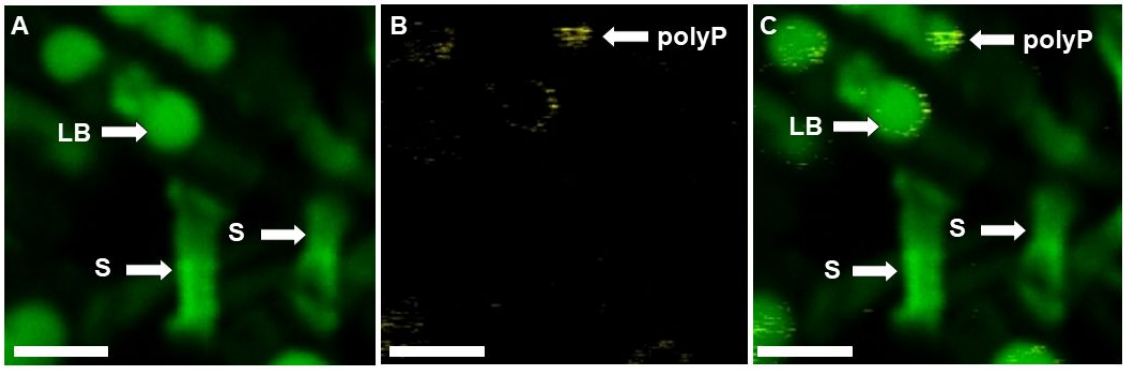

Figure 4. 3: SRS images via stimulated Raman loss detection of *A. minutissimum* co-cultivated with *Dyadobacter* sp.32 showing A) Coherent anti-Stokes Raman scattering (CARS) image displaying stalks (S) and lipid bodies (LB). B) Polyphosphate (polyP) signal at 1661 cm^{-1}. C) Merged images of A) and B). No bright-field micrograph was available using this experimental setup. Scale bar: 10 µm.

Mapping of the atom distribution in *A. minutissimum* using energy-dispersive X-ray (EDX) analysis

To further investigate the elemental composition of the stalks, cells in co-culture were analysed by scanning electron microscope (SEM) coupled with energy-dispersive X-ray (EDX) spectroscopy (Figure 4. 4). Stalk EDX analyses revealed a sulphur (S) hotspot with a wavelength X-ray signature at 2.46 keV (Figure 4. 4A). The S peak in the stalk was associated with iron (Fe) and magnesium (Mg) ions with X-ray signatures at 0,70 and 1,25 keV, respectively, which are not found in the frustule or the silica matrix (Figure 4. 4ABC). S is detected by EDX in the frustule, as well as phosphorous (P) with a wavelength X-ray signature of 2,01 keV (Figure 4. 4B).

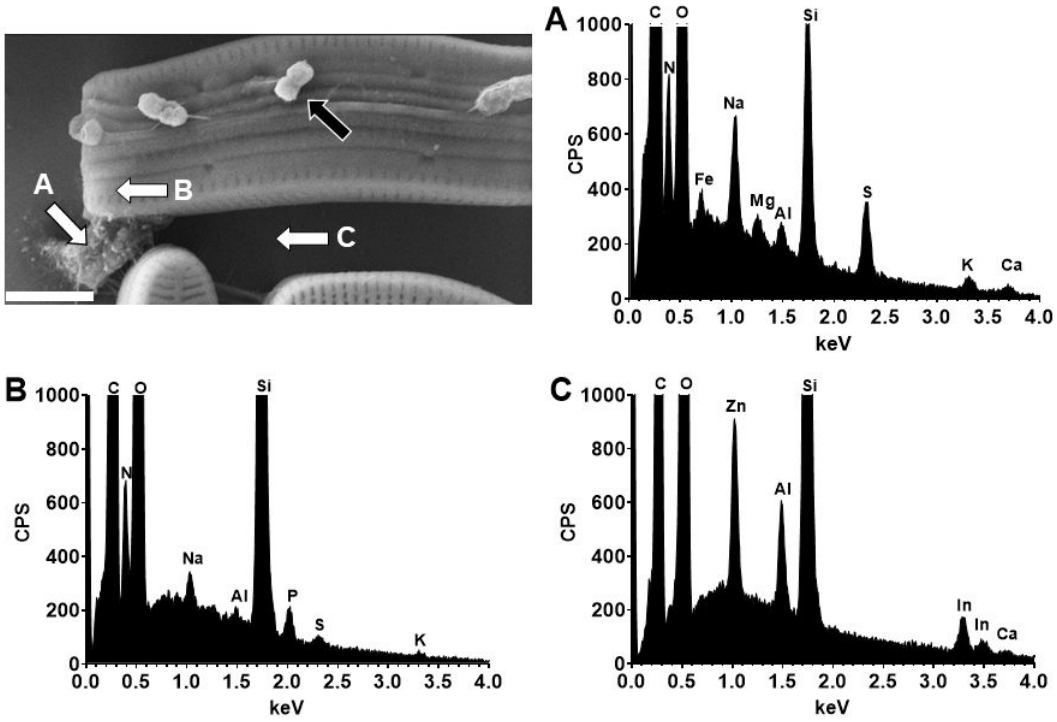

Figure 4. 4: SEM micrograph of *A. minutissimum* co-cultivated with *Dyadobacter* sp. 32 and the EDX spectra from the corresponding spots indicated by the white arrows. A) Stalk (spectra peaks 0,70; 1,25; and 2,46 keV corresponding to iron (Fe), magnesium (Mg) and sulphur (S) respectively. B) Frustule (spectra peak at 2,01 and 2.46 keV indicates phosphorous (P) and S signal. C) Thermanox matrix covered with carbon (C). The black arrow shows a bacterium attached to the diatom's frustule. Scale bar: 1 µm.

DAPI shifting fluorescence

To further understand the wavelength shift of fluorescence emission of DAPI when bound to stalks, we investigated whether the presence of sulfate within the stalk could influence the shift in DAPI fluorescence. For this purpose, we analysed the capacity of DAPI to bind to dextran sulfate (DXS), a polyanionic sulphated glycan. When excited at 405 nm, the presence of DXS induced a shift in DAPI fluorescence with a maximum emission spectrum at 540 nm, similarly to a DAPI-polyP complex (Figure 4. 5).

However, this shift did not occur in presence of non-sulphated dextran (DX), suggesting that DAPI does not bind to the glycan itself but preferentially to the sulphate groups present in the glycan.

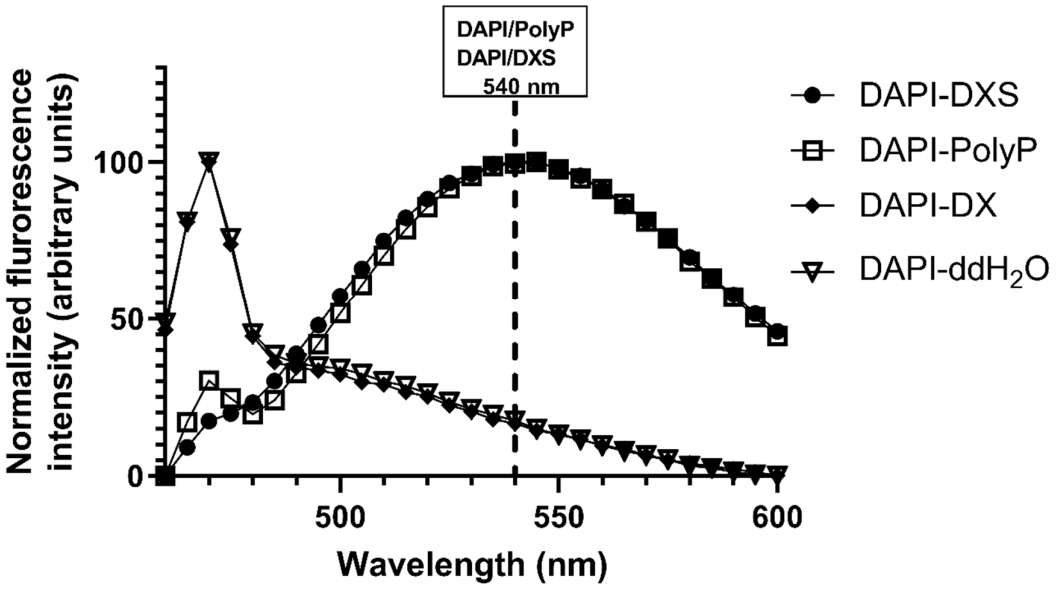

Figure 4. 5: DAPI emission fluorescence (405 nm excitation) spectra upon binding to dextran sulphate (DAPI-DXS), standard polyP (DAPI-polyP), dextran (DAPI-DX) or double distilled water (DAPI-ddH_2O).

Characterization of the stalk ultrastructure in *A. minutissimum*

Electron micrographs of *A. minutissimum*-producing stalks revealed that this adhesive EPS structure is composed of interwoven fine fibrillar material secreted from apical frustule pores (FP). In addition; the stalk does not display any structures like a collar or pad (Figure 4. 6ABC).

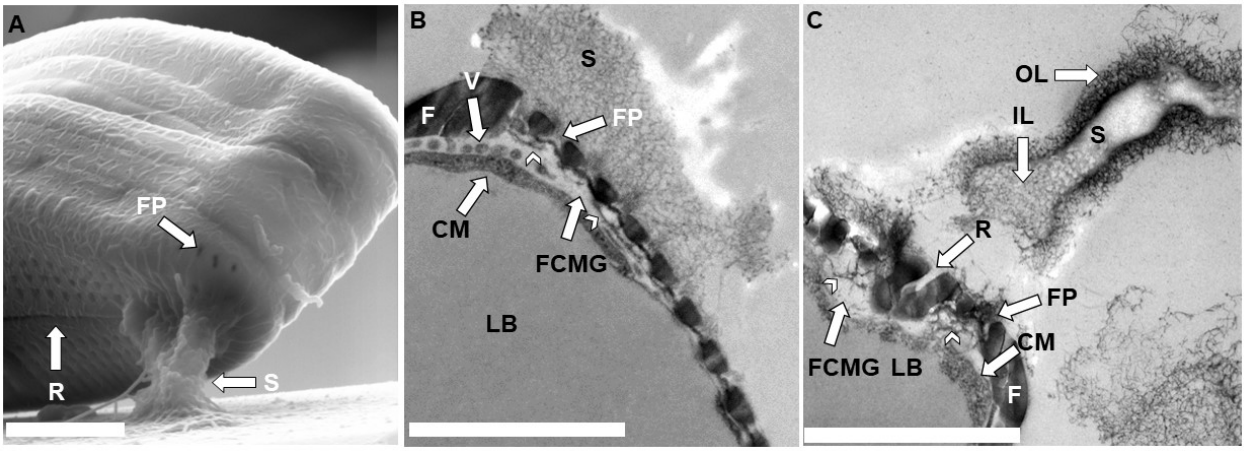

Figure 4. 6. *A. minutissimum* cell and its extracellular adhesives. A) SEM micrograph of the diatom producing a stalk (S) extruding from apical frustule pores (FP). B) TEM micrograph of a longitudinally sectioned cell showing a fibrillar early-stage stalk (S) formation and the production of vesicles (V) and fibrous material (arrowheads) in the frustule-cell membrane gap (FCMG). C) TEM micrograph of a longitudinally sectioned cell showing an elongated stalk displaying fibrillary material arranged in an electron-dense out layer (OL) and a less dense inner layer (IL), and the production of fibrous material (arrowhead) within the FCMG. Note that the basal part of the stalk is missing. LB, lipid body; F, frustule; R, raphe channel. Scale bar: 2.5 µm.

However, stalks appear to be composed of two layers differing in their density in fibrils (Figure 4. 6C). The fibrous material from the outer layer appears more densely interwoven than in the inner layer, which makes the latter less electron-dense. The early-stage stalk formed in Figure 4. 6B does not display a dense outer layer when other cells producing an early-stage stalk possessed one (data not shown).

In contrast, no fibrous material was observed extruded from the raphe channel (Figure 4. 7). Several vesicles, as well as a fibrous material, were visible in the frustule-cell membrane gap (FCMG) (Figure 4. 6BC), with the elongated stalk only displaying fibrous material (Figure 4. 6C). The cell membrane appears denser only at the FCMG located at the stalk production site.

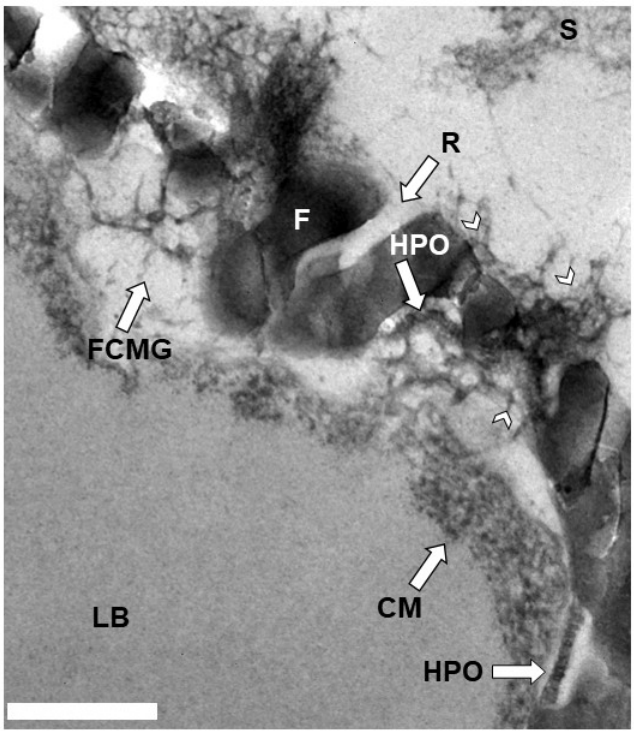

Figure 4. 7: Enlargement of the TEM micrograph shown in Figure 4. 6 C. Intracellular and extracellular fibrous material, presumably the stalk material (white arrowheads) are located close to the inner and outer side of the hymenate pore occlusion (HPO), respectively. HPO is located on the inner side of the frustule. Intracellular fibrous material is located within the frustule-cell membrane gap (FCMG). The cell membrane (CM) is thick, laminate, and granular at the site of stalk production. LB, Lipid body; R, raphe channel; S, stalk. Scale bar: 0.5 µm.

Discussion

Although DAPI is primarily used to stain DNA and cell nuclei, this fluorescent probe is also useful for staining other cellular structures (Bahulikar & Kroth, 2007, Wustman et al., 1997). DAPI can bind electrostatically to DNA by the interaction of its two positively charged end-groups to the phosphate groups of the DNA (Manzini *et al.*, 1983). When bound to DNA, DAPI excited with ≈ 360 nm light has a maximum emission peak at ≈ 460 nm, displaying a typical blue colour (Kapuściński & Skoczylas, 1978). Using a similar excitation, DAPI-polyphosphate (polyP) complexes have been detected with a DAPI fluorescence emission peak shifting to 525

nm, emitting a green-yellow fluorescence (Tijssen *et al.*, 1982). This discovery allows visualization of polyP in microorganisms, and notably, numerous studies have reported the use of DAPI in microalgae (Eixler et al., 2005, Ruiz et al., 2001, Diaz et al., 2008, Wustman et al., 1997, Bahulikar & Kroth, 2007). In our study, granular structures in *A. minutissimum* show yellow or green fluorescence when stained with DAPI, depending on the excitation wavelength, and resemble the polyP granules that are previously described in chapter 3. With a similar fluorescence peak shift, DAPI also labels the stalk, as well as the periphery of the cell. However, via stimulated Raman spectrscopy we could not detect polyP in the stalks, indicating that the biochemical composition of the stalk is different from polyP granules.

In 1997, Wustman et al. described that upon addition of DAPI, stalk as well as frustule of the diatom *Cymbella cistula* fluoresced yellow. Similarly to these observations, we show that the stalk of *A. minutissimum* also contains sulphur and metal ions like Mg as well as Fe. In addition to the DAPI-polyP complex, it was recently shown that the DAPI can also interact with other negatively-charged particles (Omelon et al., 2016). It is a cationic dye and its shift of fluorescence has been attributed to dye-dye electrostatic interactions due to the proximity of each molecule when bound to polyanionic groups (Omelon et al., 2016). It was also demonstrated that heparin, a sulphated glycosaminoglycan, fluoresces at ca. 550 nm when interacting with DAPI (Kolozsvari *et al.*, 2014). Our data indicate that the stalks of *A. minutissimum* are sulphated and thus negatively charged, which therefore attracts DAPI, resulting in the shift of its emission fluorescence. It has been shown that the stalks of *C. cistula* also contain sulphated polysaccharides (Wustman et al., 1997), which likely induce the shift of DAPI fluorescence to yellow, as observed in *A. minutissimum*. Sulphur is an important elemental component of stalks produced by diatoms (Wustman et al., 1997), and was shown to be involved in metal ion adsorption in the stalks of *D. germinata* (Somanader *et al.*, 2022, Wysokowski *et al.*, 2017). The presence of metal ions along with sulphur within stalks was also observed in *C. cistula* (Wustman et al., 1997). Here, metal ions were involved in the cross-linking of the sulphated xylogalactan, which also might be the case in the stalk of *A. minutissimum*. Metal cationic cross-linking may also be involved in the stalk formation of *Achnanthes longipes* and *Amphora coffeaeformis* (Wustman et al., 1997). Although it appears to be a common feature in diatom stalks, the different metals binding of polysaccharides may have more importance for *A. minutissimum* stalk formation, as the diatom is not able to form any structured EPS when *Dyadobacter* sp. 32 is absent from the culture. However, the absence of the bacterium does not impede the secretion of copious amounts of soluble carbohydrates

(CHO) (Windler et al., 2015). It has been shown that addition of EDTA in a biofilm culture of *C. cistula* was completely solubilizing their stalks, suggesting that EDTA was chelating the metal ions cross-linking the polysaccharides and thus disrupting the polysaccharide structure (Gretz & Hoagland, 1997). Therefore, the presence of metal in stalks is crucial for the organization of these adhesive EPS structures. As *A. minutissimum* still secretes soluble CHO in absence of *Dyadobacter* sp. 32, one can hypothesize that the signal molecules produced by the bacterium for inducing the biofilm formation could potentially induce the diatom to organize their CHO via the use of ion metal for cross-linking their polysaccharides resulting in the formation of fine insoluble fibrils.

Stalk ultrastructure in *A. minutissimum* reveals two layers of fibrils. The stalk margin is a layer of tightly interwoven fibrils while the inner part is filled with a loose network of similar fibrils. Diatom stalks have been reported to be an anastomosis of extremely fine fibrils extruded through the siliceous cell wall (Drum, 1969, Gibson, 1979, Blunn & Evans, 1981, Daniel *et al.*, 2007) with a different level of organization. Stalks can display a low level of organization like in *A. minutissimum* or *Gomphonema olivaceum* (Drum, 1969), with stalks made of interwoven fibrils. In contrast, the colonial diatom *D. germinata* possesses stalks displaying multiple and highly structured layers of fibrils. The latter diatom is considered to produce one of the most complex stalks reported so far in diatoms (Aboal *et al.*, 2012). Electron microscopy investigations revealed that the site of stalk secretion in *A. minutissimum* is located at its apical frustule pores (FP). In addition, we do not exclude a secretion at other locations, like the raphe channel nearby the apical FP, although no fibrillary material was observed there. The site of stalk secretion varies amongst diatom species and may be in addition to the apical FP, the raphe, or the mantle edge (Gibson, 1979, Pickett-Heaps *et al.*, 1991, Hoagland et al., 1993, Kooistra *et al.*, 2003). A large number of vesicles containing undefined material were observed in the frustule-cell membrane gap (FCMG) located at the site of stalk excretion. Similar vesicles were observed in the diatom *Amphora veneta* and were attributed to the exocytosis process of extraneous lipid membranes (Daniel *et al.*, 1980). Although the nature and site of production of these vesicles remain unknown, Golgi-derived vesicles in diatoms are believed to be implied in the diatom mucilage secretion (Blunn & Evans, 1981, Daniel et al., 1980). Golgi apparatus was not observable nearby these structures and more data are needed to define the role of these vesicles within the FCMG. However, the presence of dense fibrous material within the FCMG strongly suggests the presence of stalk precursors in the FCMG. These precursors are secreted through a fine siliceous membrane containing nanometre-scale pores, the hymenate pore

occlusion (HPO) (Mann, 1981), which closes the inner side of the frustule pores (FP). Observations of a thicker and laminate cell membrane at the stalk production site suggests an increased activity of the membrane at this location. Diatotepic layers have been found to encapsulate the cell membrane in *A. longipes* and fibrous material was found to be derived from it and extruded through the frustule channel for stalk production (Wang *et al.*, 2000). Such layers were not observable in *A. minutissimum*, which only seemed to exhibit a single layer cell membrane.

Conclusion

Taken together, the results update the knowledge on the biofilm formation of the diatom *A. minutissimum*. DAPI staining is a useful tool for rapidly staining the EPS of the diatom, but care must be taken when using the fluorescent probe for polyP visualization as it produces a similar signal when interacting with other molecules, notably with EPS. Although more detailed biochemical analyses are required, the stalk of *A. minutissimum* resembles the stalk of the common diatom *C. cistula*, made of sulphated polysaccharides associated with metal ions. Further investigations must be conducted focusing on the role of the metal ions (Mg and Fe) which can potentially play an important role in the stalk formation of *A. minutissimum* in response to the *Dyadobacter* sp. 32 info-chemicals.

Acknowledgements

This work was supported by the DFG (Deutsche Forschungsgemeinschaft)-298726046/GRK2272 (RTG R3). We want to thank Brittany Sprecher for the constructive discussions and Antonia Keller for the technical support.

Chapter 5. Effects of varying phosphorus supplies on the resilience and the biofilm formation of the freshwater diatom *A. minutissimum*

Adrien Lapointe, Pengyu Ji and Peter G. Kroth

Manuscript not published

Abstract

The freshwater diatom *A. minutissimum* has been isolated from photoautotrophic biofilms of Lake Constance (Germany). In presence of the bacterium *Dyadobacter* sp. 32, the diatom forms a biofilm by first producing a stalk, which mediates its attachment to solid surfaces, and later forms a capsule. The goal of our study was to monitor the growth of the diatom as well as its biofilm formation under different phosphorus (P) supplies, mimicking a varying environment where P availability may be often limited. For this purpose, we designed an experimental setup where biofilm cultures were grown in various P conditions. At first, axenic diatoms and bacteria were pre-adapted separately for 5 days in P-replete ($P_{(+)}$) or P-deplete ($P_{(-)}$) cultivation medium. Subsequently, diatoms and bacteria pre-adapted in similar conditions were co-cultivated and transferred to a new cultivation medium containing either the same P conditions ($P_{(+/+)}$ or $P_{(-/-)}$) or different ($P_{(+/-)}$ or $P_{(-/+)}$, and cultivated for 12 more days. Only diatoms in $P_{(-/-)}$ and $P_{(+/-)}$ cultures were producing surface-associated alkaline phosphatase (AP), indicating that absence of exogenous P induced a cellular P stress. However, $P_{(+/-)}$ cultures displayed lower AP than the $P_{(-/-)}$ ones, suggesting the use of intracellular P reserves, which buffered the cell in P under $P_{(-)}$ conditions. Usage of intracellular P storage was also suggested by the low impact of the absence of exogenous P on cell division. Biofilm formation differed according to the cellular P status. $P_{(+/+)}$, $P_{(+/-)}$, and $P_{(-/+)}$ cells produced a maximum stalk length of ca. 5 µm whereas they were lengthened by 2 (ca. 10 µm) under $P_{(-/-)}$ conditions, suggesting that limited P reserves after a prolonged period in $P_{(-)}$ conditions induced the stalk elongation. Our results reveal new insights about the strategies used by *A. minutissimum* to resist in P-limited environments.

Keywords: *A. minutissimum*, biofilm, phosphorus supply, intracellular P reserves, stalk, alkaline phosphatase

Introduction

Biofilms are often found in the littoral zones of lakes, streams, and oceans. When sufficient light and water are present, biofilms form a brownish/greenish thin mucous layer on stones or at the surface of the sediments. A biofilm is a community of microorganisms adhering to surfaces and each other by the production of extracellular polymeric substances (EPS), which act as connective tissue between the microorganisms (Flemming & Wingender, 2001, Flemming *et al.*, 2007).

Diatoms are unicellular algae found worldwide in aquatic environments. They are early colonizers of surfaces (Patil & Anil, 2005) and play a major role in the primary productivity of biofilms (Bellinger *et al.*, 2009). EPS produced by diatoms in biofilms are generally composed of insoluble polysaccharides forming cell-bound structures like stalks, tubes, and capsules, allowing the cells attachment to substrata (Hudon & Bourget, 1981, Bahulikar & Kroth, 2007). Production of EPS in biofilm is of ecological importance because it contributes to the 'biostabilization' of sediments (Gerbersdorf & Wieprecht, 2015), but also causes severe economic issues in water industries with the deterioration of submerged objects (Vishwakarma, 2020).

The diatom *Achnanthidium minutissimum* is a dominant benthic diatom in freshwater samples worldwide (Potapova & Hamilton, 2007, Hlúbiková et al., 2011, Rimet *et al.*, 2009) and has colonized the littoral zone of Lake Constance (Windler et al., 2012). The diatom is associated with a variety of satellite bacteria (Bruckner et al., 2008). In presence of its naturally associated bacteria, the xenic diatom produces insoluble carbohydrates (CHO) forming stalks allowing the cell to attach to surfaces. After the removal of bacteria, axenified diatoms no longer form biofilms and grow suspended, but still secrete soluble CHO (Windler et al., 2015). The bacterium *Dyadobacter* sp. 32 was isolated from the same epilithic biofilms as *A. minutissimum* and was shown to excrete unknown bioactive molecules, which in turn induce the stalk production of the diatom. The co-cultivation of both organisms became a model for biofilm quantification studies (Leinweber *et al.*, 2016).

Phosphorus (P) is an essential element for all living organisms. It is involved in several important cellular components such as nucleic acid, phospholipids, and ATP. P is often considered to be the limiting factor in freshwater environments (Hecky & Kilham, 1988). While the biofilm formation of *A. minutissimum* under ideal conditions is well documented (Windler et al., 2015, Leinweber & Kroth, 2015), the impact of nutrient-limited conditions on the diatom

within the biofilm is unknown. This knowledge is crucial to better understand the ecology of the diatom in oligotrophic conditions, such as in Lake Constance where the P concentrations are low (< 0.105 µM) (IGKB 2018). To understand the challenges of living in such an environment, we studied the effects of different P availability on the diatom producing a biofilm, in presence of *Dyadobacter* sp. 32. We mimicked a variable environment by subjecting the biofilm to different P availability, and investigate the subsequent adaptations of the diatom. Our results provide insights into the strategies of *A. minutissimum* to thrive in P-variable habitats.

Material and methods

Organisms and cultivation conditions.

The freshwater diatom *A. minutissimum* (Kützing) Czarnecki (strain MW1), was isolated from photoautotrophic, epilithic biofilms in Lake Constance (47°41´N; 9°11`E, Germany) (Bruckner et al., 2008), and its associated bacteria were removed using the antibiotic imipenem (Windler et al., 2012). Axenic diatoms were cultivated in "*Achnanthidium* medium" (AM, (Windler, 2014)). This medium is a modification of the BM medium "Bacillariophycaean medium" (Schlösser, 1994), lacking the soil extract component. Vitamins, silica, selenate, and trace metals ion solution were supplemented as described for F/2 medium (Guillard, 1975). For the study, different phosphorus (P) contents as inorganic phosphate (P_i) (K_2HPO_4) within AM were used with ca. 53 µM P_i, accounting for P-replete ($P_{(+)}$) conditions, and no addition of K_2HPO_4 accounting for P-deplete ($P_{(-)}$) conditions.

First, a 100 mL cell stock was cultured in $P_{(+)}$ conditions, and half of the culture was exchanged weekly for new AM $P_{(+)}$, to keep cells in the log phase (1.0×10^6 cell/mL). Two tubes containing each 10 mL of the cells in exponential phase were centrifuged (5000 g, 5 min). The supernatant was discarded, and cell pellets were resuspended with either 10 mL of AM $P_{(+)}$ or AM $P_{(-)}$, and transferred in 90 mL of their corresponding medium for a pre-conditioning of 5 days in vented cell culture flasks (Sarstedt, Newton, NC, USA) at 16°C, under a 16:8 day/night cycle at a light intensity of 70 µmol photons m^{-2} s^{-1}. $P_{(+)}$ and $P_{(-)}$ cells were gently shaken daily for 5 s to allow gas exchange within the flask.

Dyadobacter sp. 32 was isolated by Bruckner et al. (2008). This bacterium was enriched from a xenic *Cymbella microcephala* Grunow strain D-32 culture, which originated from photoautotrophic, epilithic biofilms from the same sampling site as *A. minutissimum* (47°410

N; 9°110 E, Germany). Before the beginning of the experiment, a 50 mL bacteria cell stock was originally cultivated at 20 °C in AM $P_{(+)}$ supplemented with 10 mM of glucose with shaking (130 rpm), and bacteria were cultivated until reaching an OD_{600nm} of 0.2. Subsequently, the stock solution was divided into two equal volumes of 25 mL, each transferred into 50 mL tubes, and the tubes were centrifuged (5000 g, 3 min). The supernatant was discarded and the pellets were resuspended in 25 mL of either AM $P_{(+)}$ or AM $P_{(-)}$, both supplemented with 10 mM of glucose, for 5 days of pre-conditioning, at 20 °C with shaking (130 rpm).

Co-cultivation of the diatoms with bacteria in different P supplies.

In the following, *A. minutissimum* together with *Dyadobacter* sp. 32 is termed a "co-culture". At first, 30 vented cell culture flasks (Sarstedt, Newton, NC, USA) were filled with 9 mL of AM $P_{(+)}$ and 30 others with 9 mL of AM $P_{(-)}$. Each $P_{(+)}$ and $P_{(-)}$ pre-conditioned diatom stock was divided into two equal volumes of 50 mL, each transferred into 50 mL tubes, and the tubes were centrifuged (5000 g, 5 min). The supernatant was discarded and one of the two pellets of $P_{(+)}$ cells was suspended in AM $P_{(+)}$ and cell stock was referred to as $P_{(+/+)}$, while the other pellet was suspended in AM $P_{(-)}$ and cell stock was referred to as $P_{(+/-)}$. Similarly, the two pellets of $P_{(-)}$ cell stocks were suspended in either AM $P_{(+)}$ or AM $P_{(-)}$, and cell stocks were referred to as $P_{(-/+)}$ and $P_{(-/-)}$, respectively. Subsequently, 1 mL of $P_{(+/+)}$ cell stock was transferred into 15 vented cell culture flasks containing 9 mL of AM $P_{(+)}$, and 1 mL of $P_{(+/-)}$ cell stock was transferred into 15 vented cell culture flasks containing 9 mL of AM $P_{(-)}$. The same procedure was repeated for $P_{(-/-)}$ transferred in 15 vented cell culture flasks containing 9 mL of AM $P_{(-)}$, and $P_{(-/+)}$ cell stock transferred into 15 vented cell culture flasks containing 9 mL of AM $P_{(+)}$. Thus, the 60 vented cell culture flasks were divided into four groups of 15 flasks containing 10 mL of either $P_{(+/+)}$, $P_{(+/-)}$, $P_{(-/+)}$, and $P_{(-/-)}$ diatom cells. The final diatom cell concentration was 200×10^3 cells/mL.

The OD_{600nm} of the pre-conditioned $P_{(+)}$ and $P_{(-)}$ cultures of *Dyadobacter* sp. 32 were measured. $P_{(+)}$ and $P_{(-)}$ bacteria stocks were split into two parts of 12.5 mL, each transferred into 15 mL tubes, and the tubes were centrifuged (5000 g, 5 min). The supernatant was discarded and one of the two $P_{(+)}$ bacteria pellets was resuspended in AM $P_{(+)}$ without glucose addition to reach a final OD_{600nm}=0.2, and cell stock was referred to as $P_{(+/+)}$. Similarly, the other pellet was suspended in AM $P_{(-)}$ to reach a final OD_{600nm}=0.2, and cell stock was referred to as $P_{(+/-)}$. The same procedure was repeated for the two $P_{(-)}$ bacteria pellets which were suspended in either

AM $P_{(+)}$ or AM $P_{(-)}$ and cell stocks were referred to as $P_{(-/+)}$ and $P_{(-/-)}$, respectively. Subsequently, 300 µL of $P_{(+/+)}$ bacteria stock was transferred in 15 culture flasks containing 10 mL of $P_{(+/+)}$ diatom culture, and 300 µL of $P_{(+/-)}$ bacteria stock were transferred in 15 culture flasks containing 10 mL of $P_{(+/-)}$ diatom culture. The same procedure was repeated for $P_{(-/-)}$ and $P_{(-/+)}$ bacteria stocks.

Co-cultures were cultivated for 12 days at 16°C, under a 16:8 day/night cycle at a light intensity of 70 µmol photons m^{-2} s^{-1}. Cells were gently shaken daily for 5 s to allow gas exchange within the flask. On days 0, 3, 6, 9, and 12, three flasks from each $P_{(-/+)}$, $P_{(-/-)}$, $P_{(+/+)}$, $P_{(+/-)}$ treatments were used for growth measurement, extracellular dissolved phosphate concentration and microscopy analyses. During sampling, each flask was gently shaken, and the spent medium containing non-attached cells was transferred to a 15 mL tube. The empty flasks were immediately resupplied with 10 mL of the corresponding new cultivation medium. After, each flask containing the attached cells was subjected to an ultrasonic bath during 10-20 s (Transsonic T700, Elma, Germany), under gentle shaking to detach and resuspend the cells. Cells were subsequently transferred in a 15 mL tube from where 100 µL was taken for cell counting (Multisizer 4 Coulter cell counter®, Beckman). The tubes containing the spent medium and the attached cells were subsequently centrifuged (5000 g, 5 min). 1 mL of each spent medium sample was taken for dissolved extracellular phosphate measurements and the rest was discarded. The supernatant from the attached cells tubes was lowered to 200 µL and cells were resuspended with it by gently pipetting. Each sample containing the attached cells was split in two, resulting in two tubes containing each 100 µL of $P_{(+/+)}$, $P_{(+/-)}$, $P_{(-/+)}$, or $P_{(-/-)}$ cells which were used for microscopy analyses.

Quantification of dissolved extracellular phosphate

The concentration of dissolved inorganic phosphate (P_i) in the spent medium was measured in a 96 well-plate using the ascorbate-antimony-molybdate assay described by Christ and Blank (2018b). 150 µL of each sample were pipetted in one well of the microplate. 150 µL of K_2HPO_4 in triplicate (0 to 100 µM P_i) were pipetted elsewhere in the microplate and served as a standard for the P calibration curve. Then, 50 µL of P_i detection reagent (more details in chapter 3, quantification of dissolved extracellular phosphate section) was added to each well. After 2 min of incubation at room temperature and gentle mixing, the sample's absorbances were read at 882 nm. The lowest amount of P_i that could be determined with suitable precision and accuracy

was given by the limit of quantitation (LOQ) (ICH Guideline, 1996), see also equation 1 in (chapter 1).

Staining and microscopy

The tubes containing 100 µL of $P_{(+/+)}$, $P_{(+/-)}$, $P_{(-/+)}$, or $P_{(-/-)}$ cells were stained either with crystal violet or ELF-97. Stalks produced by *A. minutissimum* cells in co-cultures were stained with crystal violet.

The first tube from each treatment was briefly centrifuged (5000 g, 1 min), the supernatant was discarded and cells were resuspended with 100 µL of a 1:100 crystal violet solution (Kaplan & Fine, 2002), and let for incubation for 10 min at room temperature. Subsequently, cells were centrifuged (5000 g, 1 min), the supernatant was lowered to 10 µL and cells were resuspended with it. Cells were observed with an upright light microscope under bright-field mode (Olympus BX51; Olympus Europe, Hamburg, Germany). Using the ImageJ software, 50 cells per sample were measured for their stalk- length.

The remaining tubes containing 100 µL of $P_{(+/+)}$, $P_{(+/-)}$, $P_{(-/+)}$, or $P_{(-/-)}$ cells were incubated with 5 µL of ELF-97 (ThermoFisher, Karlsruhe, Germany), for 2h in the dark at room temperature (Yamaguchi *et al.*, 2006). ELF-stained cells were directly observed under the same microscope described above (see chapter 4, DAPI staining for fluorescence microscopy section) Using the software ImageJ, a total of 50 cells per sample replicate were counted and the percentage of ELF-stained cells to the total number of cells was calculated based on the absence or presence of a green fluorescence precipitate, displayed on the cell surface (Yamaguchi et al., 2006). The cells were counted as "fluorescent" even if a small portion of their cell surface was displaying the green precipitate.

Results

A. minutissimum is a benthic diatom growing attached to surfaces by producing a stalk, when co-cultivated with the bacterium *Dyadobacter* sp. 32. We investigated whether varying P conditions would have any impact on the diatom physiology parameters such as the P uptake, growth, the alkaline phosphatase activity, as well as the biofilm formation.

Dissolved extracellular phosphate

No extracellular P was detectable during the experiment in $P_{(-/-)}$ and $P_{(+/-)}$ culture (<LOQ) (Figure 5. 1A and 5. 1D). Starting extracellular P concentrations in $P_{(-/+)}$ and $P_{(+/+)}$ cultures were 50.33 ± 0.07 and 50.00 ± 0.36 µM P_i, respectively (Figure 5. 1B and 5. 1C).

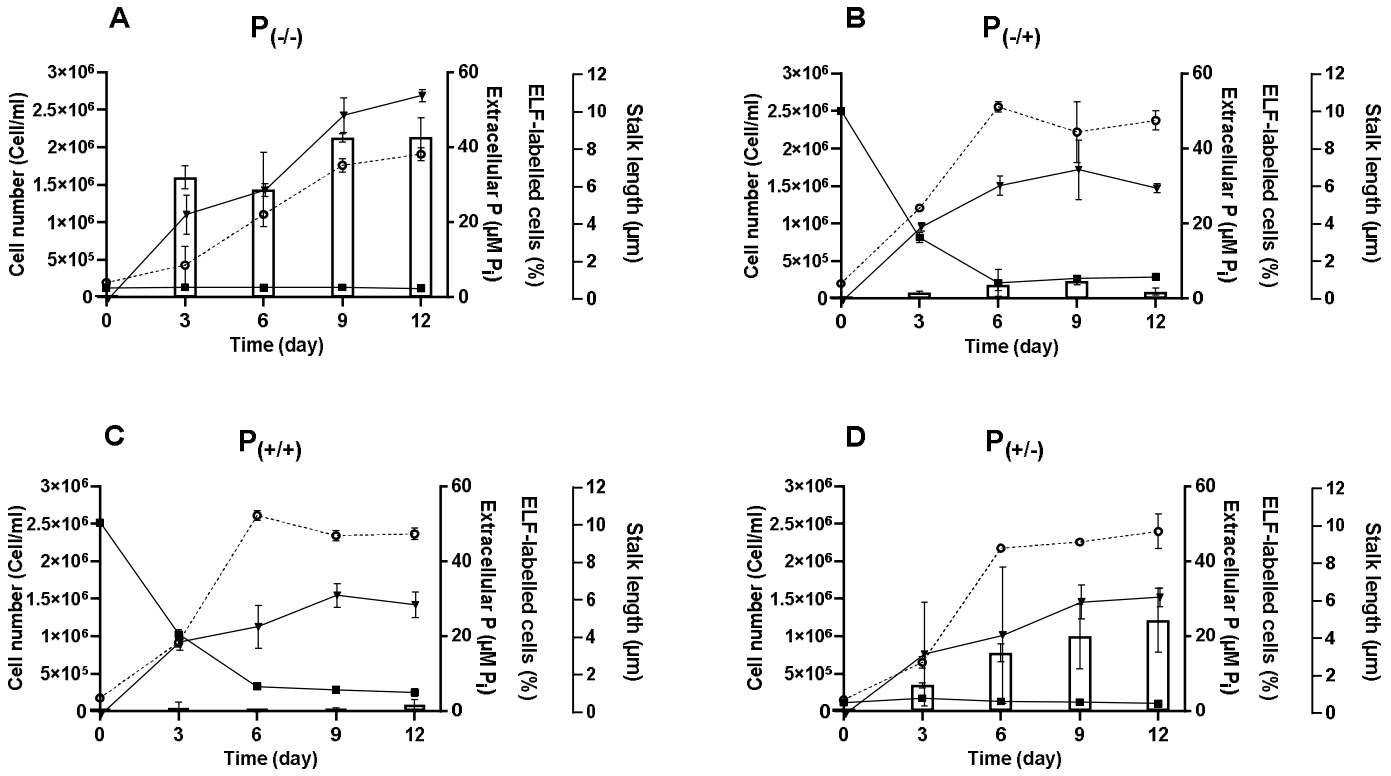

Figure 5. 1: Dynamics of physiological parameters in *A. minutissimum* co-cultivated with the bacterium *Dyadobacter* sp. 32, subjected to different P supplies. Diatom cell densities (Y_1, cell/mL, ○), dissolved extracellular P concentrations (Y_2 axis, µM P_i, ■), percentage of ELF-labelled cells (Y_2 axis, %, open bar) and length of stalks (Y_3 axis, µm, ▼) were measured in A) $P_{(-/-)}$, B) $P_{(-/+)}$, C) $P_{(+/+)}$ and D) $P_{(+/-)}$ cells. Error bars are n=3 replicates. Each replicate of stalk length and ELF-labelled cells was containing 50 cells.

From day 0 to day 3, P uptakes were slightly higher for $P_{(+/+)}$ than $P_{(-/+)}$ with 11.4 ± 0.42 pg P_i/cell/day and 9.78 ± 0.16 pg P_i/cell/day, respectively (Figure 5. 2C and 5. 2B). From day 3 to day 6, the P uptake decreased and were slightly higher for $P_{(+/+)}$ than $P_{(-/+)}$ cells with 1.88 ± 0.17 pg P_i/cell/day and 1.27 ± 0.01 pg P_i /cell/day, respectively. Exogenous P was not detectable in both cultures on day 6 (<LOQ) (Figure 5. 1C and 5. 1B).

Growth of the diatoms in biofilm form

The $P_{(-/-)}$, $P_{(-/+)}$, $P_{(+/+)}$, and $P_{(+/-)}$ cultures were started at cell concentrations of 200×10^3 cell/mL (Figure 5. 1). Cells in $P_{(-/-)}$ cultures were in lag phase during the three first days of the experiment (Figure 5. 1A), while the other cultures were already dividing at day 3 (Figure 5. 1BCD). Final cell densities were 1.2 times lower for $P_{(-/-)}$ cultures with $1.91\times10^6 \pm 8.86\times10^4$ cells/mL (Figure 5. 1A) compared to the other cultures with $2.37 \times10^6 \pm 1.27\times10^5$ cells/mL, $2.36 \times10^6 \pm 7.48\times10^4$ cells/mL, and $2.39 \times10^6 \pm 2.31\times10^5$ cell/mL for $P_{(-/+)}$, $P_{(+/+)}$ and $P_{(+/-)}$, respectively (Figure 5. 1BCD).

All cultures reached the stationary phase on day 6 (Figure 5. 1BCD), except for $P_{(-/-)}$ cultures which continued to grow for 3 more days until day 9 (Figure 5. 1A). Although $P_{(-/-)}$ cultures were depleted in extracellular P, cells continued growing which indicates that cells were having intracellular P reserves even after a 5 days pre-conditioning in $P_{(-)}$ conditions (Figure 5. 1A). In the same manner, $P_{(+/-)}$ cells were growing for 6 days in $P_{(-)}$ conditions supporting that cells stored intracellular P during their pre-adaptation in $P_{(+)}$ conditions, and used it when exogenous P was depleted (Figure 5. 1D). This indicates that the stationary phases in $P_{(-/+)}$, $P_{(+/+)}$ and $P_{(+/-)}$ cultures were not induced by $P_{(-)}$ conditions, but rather another nutrient.

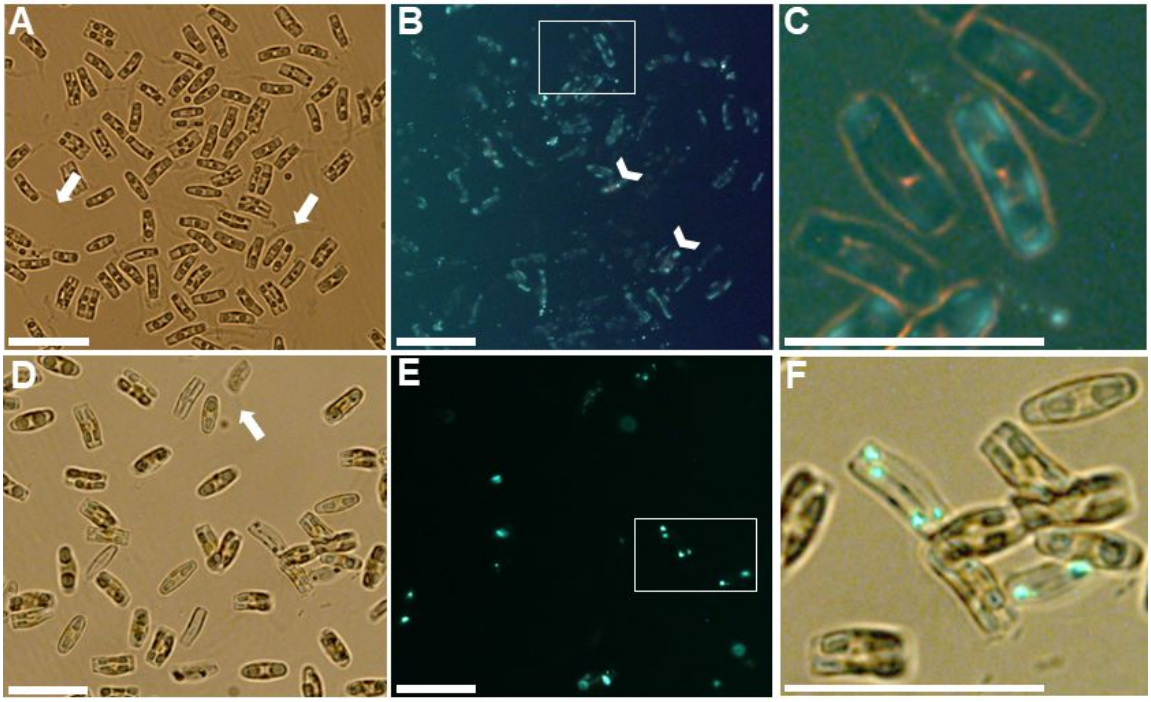

Figure 5. 2: Representative cellular sites of alkaline phosphatase (AP) activity in the diatom *A. minutissimum* labelled with ELF-97. Bright-field micrographs of A) $P_{(-/-)}$ and D) $P_{(+/+)}$ cultures of ELF-97-labelled *A. minutissimum* cells co-cultivated with cultivated *Dyadobacter* sp. 32 at day 12. The corresponding epifluorescent micrographs of ELF-97-labelled cells are shown in B) and E) respectively. Merged micrographs are shown in C) and F). White squares in B) and E) indicate the area of interest corresponding to C) and F) merged micrographs. White arrows in A) and D) indicate stalks and white arrowheads in B) indicate cells showing ELF-97 labeling the periphery as well as intracellular granules. Scale bars: 20 µm.

Percentages of cells ELF-labelled were high and stable during growth for $P_{(-/-)}$ cultures with 31.98 ± 3.13% and 33.71 ± 6.78% of labelled cells on days 3 and 6, respectively (Figure 5. 1A). Later, at the onset of the stationary phase the percentages of cells ELF-labelled in $P_{(-/-)}$ cultures increased with 42.49 ± 1.06% at day 9 and later reached a plateau with 42.65 ± 5.27% at day 12 (Figure 5. 1A). Throughout the experiment, the percentages of cells ELF-labelled in $P_{(-/+)}$ and $P_{(+/+)}$ cultures were low with less than 3% of labelled cells (Figure 5. 1B and 5. 1C respectively). These percentages were higher in $P_{(+/-)}$ cultures compared to $P_{(-/+)}$ and $P_{(+/+)}$ cultures, and they increased during the experiment, starting from 6.92 ± 0.66% on day 3 and reached 24.28 ± 8.57% of labelled cells at day 12. However, the percentages of ELF-labelled cells in $P_{(+/-)}$ cultures were ca 1.75 times lower than those in $P_{(-/-)}$ cultures on day 12 (Figure 5. 1AD).

Stalk length

On day 0, diatoms in $P_{(-/+)}$, $P_{(+/-)}$. $P_{(-/-)}$ and $P_{(+/+)}$ cultures were stained with crystal violet to detect stalks 1h after they were co-cultivated with bacteria, and no stalks were visible (Figure S5. 2). The absence of stalks 1h of cultivation with *Dyadobacter sp. 32* is following previous observations, which indicate a stalk production only after ca. 3h of co-cultivation (data not shown). On day 3, stalks were visible and lengths were increasing similarly in all cultures during growth from day 3 to day 6 with an average length of 3.88 ± 1.37 µm to 5.21 ± 1.85 µm, respectively (two-way ANOVA, $p > 0.05$) (Figure 5. 1ABCD).

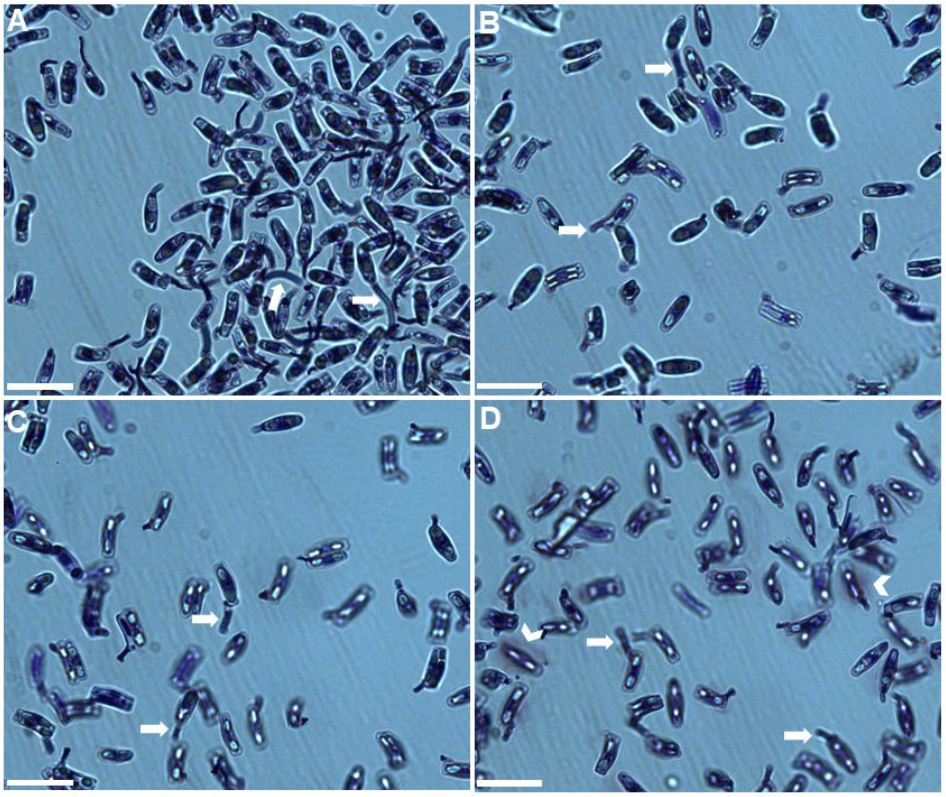

Figure 5. 3: Representative bright-field micrographs of *A. minutissimum* cells producing stalks when co-cultivated with *Dyadobacter* sp. 32 under different P supplies, after 12 d of cultivation. A) $P_{(-/-)}$ B) $P_{(-/+)}$ C) $P_{(+/+)}$ and D) $P_{(+/-)}$. After 12 d, the stalks (white arrows) produced by the $P_{(-/-)}$ diatoms appeared more elongated compared to the other cultures. Some capsular material (white arrowheads) is visible in $P_{(+/-)}$ cultures but was rarely found during the experiment. Scale bars: 15 µm

During the stationary phase on days 9 and 12, stalks were not elongating anymore and lengths were similar to day 6 for all cultures except for $P_{(-/-)}$ cells, where stalks were longer on day 9 (two-way ANOVA, $p < 0.05$) with an average length 9.83 ± 0.92 µm (Figure 5. 1A). At day 12, stalk lengths in $P_{(-/-)}$ cultures remained similar to day 9 and were ca. 2 times longer than the other cultures (Figure 5. 1A and Figure 5. 3AB).

Discussion

Alkaline phosphatase activity: a marker of phosphorus stress in *A. minutissimum*

In $P_{(+/+)}$ and $P_{(+/-)}$ cultures, ELF-treated cells revealed the labelling of intracellular granules. These structures were optically distinct from chlorophyll autofluorescence in the diatom cell. Moreover, although *Dyadobacter sp. 32* is known to attach to *A. minutissimum* cells (Leinweber & Kroth, 2015), we did not find pieces of evidence for the ELF-labelling of bacteria. Since ELF 97 is cell impermeable, it can only penetrate disrupted cells. This is in line with the observation of green fluorescent granules often present in empty cells under bright-field mode observations. The percentage of disrupted cells was low during early growth and raised during the stationary phase when cultures were getting nutrient-limited. We could not resolve the nature of these granules but it is possible that they may contain acid phosphatases playing a role in autophagic processes in dead or dying *A. minutissimum* cells (González-Gil *et al.*, 1998, Schmitter & Jurkiewicz, 1981).

For intact cells, the alkaline phosphatase (AP) activity was localized in the periphery of the cells. Although we cannot rule out that AP activity was associated with the cell wall or the cell membrane, a simple focus up and down the cell showed that the green fluorescence was always localized at the periphery of the cell. AP activity sites of several phytoplankton species have already been shown to be located on the cell surface of *Chaetoceros affinis*, *Chlorella sp.*, *S. costatum,* or *Phaeodactylum tricornutum* (Kuenzler & Perras, 1965, Møller *et al.*, 1975), cultivated in P limited conditions. Cell-surface AP is thought to hydrolyse the extracellular organic P (bound to carbon) sources in the space surrounding immediately the cells when P is limited in the environment (González-Gil et al., 1998, Li *et al.*, 2018). We found that *A. minutissimum* cultures facing P-limited conditions displayed in general more ELF-labelled cells compared to cultures cultivated in $P_{(+)}$ conditions. In addition, the level of cells ELF-labelled appears to be lower for $P_{(+/-)}$ than for $P_{(-/-)}$ cultures. This suggests the existence of intracellular

P pools in *A. minutissimum* built during $P_{(+)}$ conditions, which likely buffer P requirements, delaying the AP activation. The presence of intracellular P pools was also suggested by the fact that $P_{(-/-)}$ cells were continuing to divide, even after 5 days of pre-conditioning in $P_{(-)}$ conditions followed by an additional transfer in $P_{(-)}$ conditions. In total, $P_{(-/-)}$ cells subjected to P-limited conditions were able to divide during 14 days, indicating that cells are highly adapted to thrive in such conditions. AP activity in phytoplankton is known to be regulated by intracellular P pools, increasing when P pools are declining under P limitation (Litchman & Nguyen, 2008, Ou *et al.*, 2020). Thus, the nutritional history of microalgae and their intracellular P pools may determine their P status, as already suggested in previous studies (Dyhrman & Palenik, 1999, Falkner & Falkner, 2003). After 17 days of cultivation in $P_{(-)}$ conditions, the $P_{(-/-)}$ cultures had the highest percentage of cells ELF-labelled with ca. 43%, suggesting an advanced state of intracellular P depletion than in the other cultures. Though, there were no indications of AP activity in the other half of the culture. This could suggest that about half of the cells in these cultures were not P stressed even after 17 days of culture in $P_{(-)}$ conditions, supporting the hypothesis that $P_{(-/-)}$ cells stopped dividing at day 9 because of a lack of a different nutrient. Studies on AP production in phytoplankton showed that AP can also be released as a soluble state in the environment (Lin et al., 2013), and thus cannot be detected by the ELF-97 staining method. Analyses measuring the AP produced at the cellular and the extracellular level would be necessary in future studies to verify whether *A. minutissimum* is also able to secrete soluble AP in P limited conditions.

The role of stalk elongation in *A. minutissimum*

Stalk elongation has already been studied in the marine diatom *Achnanthes longipes*, which elongates its stalk in response to high cell densities (Lewis et al., 2002). In addition, the freshwater diatom *Didymosphenia geminata* elongates extensively its stalk in P-limited conditions when cells do not divide anymore (Kilroy & Bothwell, 2011, Kilroy & Bothwell, 2012). It also has been observed in prokaryotes like the gram-negative bacterium *Caulobacter crescentus* facing P-limited conditions. The ability of *A. minutissimum* to grow in a P-limited environment was hypothesized to originate from its capacity to store intracellular P reserves acquired during $P_{(+)}$ conditions, using e.g. polyphosphate (see chapter 3). Here we confirm the importance of a pre-adaptation of the diatom in $P_{(+)}$ conditions for intracellular P storage, as a pre-requisite for continuing division in $P_{(-)}$ conditions. However, a prolonged period in $P_{(-)}$

conditions, referring to the $P_{(-/-)}$ culture, results in increased intracellular P-stress, demonstrated by an increased AP activity.

Although AP activity in $P_{(-/-)}$ culture was high, stalk elongation only occurred at the onset of the stationary phase when cells stopped dividing. Similarly, the freshwater diatom *D. germinata* elongates its stalk under $P_{(-)}$ conditions, and the elongation is negatively correlated with the frequency of cell division (Kilroy & Bothwell, 2011). Stalks produced by diatoms are composed of extracellular polymeric substances (EPS), mainly composed of carbohydrates (CHO) (Wustman et al., 1997). Photosynthesis is considered as the driving process for EPS production in benthic diatoms (Staats *et al.*, 2000). When nutrients become limited during the stationary phase, an increase in EPS production by diatoms is a known phenomenon (Bhosle *et al.*, 1995). It is believed to be primarily caused by a "photosynthetic overflow" with increasing EPS secretion as the result of excess carbon fixation due to nutrient limitation (Staats et al., 2000, Smith & Underwood, 2000). In a previous study, *A. minutissimum* was shown to increase its extracellular EPS secretions during the stationary phase. However, no stalk elongation was observed during the study, probably because cells were initially cultivated in $P_{(+)}$ conditions and intracellular P pools were replete enough (Windler et al., 2015).

Taken together, this raises questions about the advantages of stalk elongation in *A. minutissimum*. The first obvious ecological function of the stalk is the attachment of the cell to the substrata, which is a well-documented strategy for growth and survival in many marine and aquatic microorganisms, (Wetherbee et al., 1998). The attachment also confers a stable adhesion to the surface in turbulent water, providing the photosynthetic benthic microbes necessary light an soluble nutrient availability (Hoagland et al., 1993). *A. minutissimum* was originally isolated from an epilithic biofilm, composed of naturally associated eukaryotes and prokaryotes microorganisms (Bruckner et al., 2008). Although little is known about the ecology of *A. minutissimum* within natural biofilms, competition for light or nutrients within a biofilm is a known phenomenon (van der Grinten *et al.*, 2005, Koedooder *et al.*, 2019). In a natural environment like the oligotrophic Lake Constance, *A. minutissimum* cells are likely competing with other surface-associated species for P. Elongation of the stalk would allow the diatom to better utilize the vertical dimension, and the height discrepancy would offer a further increase in the availability of nutrients and light (Hudon & Bourget, 1981).

Conclusion

In conclusion, our data show that stalk elongation in the diatom *A. minutissimum* is caused by an intracellular P limitation coupled with the cessation of cell growth. The distinction between extracellular and intracellular P limitation is important in this regard, as only pre-starved cells can elongate their stalks under $P_{(-)}$ conditions. Further work must be conducted on testing whether other nutrients (carbon, nitrogen) or additional abiotic parameters (pH, temperature, oxygen) can also influence the stalk elongation of *A. minutissimum*, to better understand the adaptations of benthic diatoms in a varying environment.

Acknowledgements

This work was supported by the DFG (Deutsche Forschungsgemeinschaft)-298726046/GRK2272 (RTG R3).

Chapter 6. General Discussion

This thesis describes studies regarding the effects of varying phosphorus (P) availability on the intracellular and extracellular adaptations of *A. minutissimum*. Using a combination of Raman spectroscopy and electron microscopy techniques, we identified the presence of polyP reserves in the diatom. We developed a simple and high throughput method to extract and quantify the polyP levels in *A. minutissimum*, allowing us to follow the fate of polyP within the diatom subjected to varying phosphorus (P) conditions. Along with other P reserves, the axenic diatoms were likely using polyP as a P buffer, allowing them to continue dividing in P-limited conditions for several days. Diatoms in biofilm form subjected to P limitation also continued to divide in P-limited conditions. Using different sequences of P availability in the biofilm cultures, we discovered that diatoms were able to modify their biofilm production when subjected to an internal, rather than an extracellular P stress. This thesis proposes to understand the role of P reserves such as polyP in the adaptations of the diatom, in its planktonic as well as in its benthic form, to a succession of different P availability, mimicking a variable environment.

A new method for extraction and quantification of polyP in diatoms: easy-to-use, specific and high throughput

A major goal of this thesis was the development of a method to extract and quantify a major molecule responsible for P storage within microbes: polyphosphates (polyP).

Extraction and quantification of polyP topics in diatoms have been rarely addressed. In 1995, Leitão et al. studied the effects of osmotic stress on the size and dynamic of the polyP produced in *P. tricornutum*. In this study, polyP extraction involved 5 steps to recover three different fractions of polyP, according to their sizes. Although the authors claimed the high recovery of polyP using their method, it does not appear to be suitable for routine measurements involving several replicates. More recently in 2012, Dyhrman et al. investigated the production of polyP within the diatom *T. pseudonana* using solid-state ^{31}P nuclear magnetic resonance (NMR) spectroscopy. The measurement of polyP did not require any extraction but a drying step of the sample at 65°C. ^{31}P NMR is a powerful and non-destructive analytical technique which can detect concentrations of polyP as low as a few millimolar (Christ *et al.*, 2020). However, such a procedure requires specific instrumentation and cannot be performed at high throughput. Therefore, there was a need to find an easy-handling method including only a few steps which would work in high throughput using common analytical instruments. Because of its

polyanionic state, polyP possesses similar electrical properties to the P backbone in DNA. Therefore in chapter 2, we compared published extraction protocols based on nucleic acid extractions in regards to their capacity of extracting polyP from polyP-rich *A. minutissimum*. In addition, we used a simple extraction protocol used for extracting polyP from marine phytoplankton samples based on a brief boiling and proteinase K treatment (Martin & Van Mooy, 2013). We retained the protocol from a DNA kit based on gel filtration purification, allowing us to extract high amounts of polyP and requiring only two steps.

Subsequent quantification of the extracts was another challenge due to the relative impurity of the sample. A method of choice for quantifying polyP in microbes is based on using DAPI staining (Aschar-Sobbi *et al.*, 2008). The method was used to quantify polyP in marine phytoplankton samples after using the extraction protocol described earlier (Martin et al., 2018, Martin & Van Mooy, 2013). Here, the method does not include further purification steps, likely resulting in the presence of different compounds along with polyP. In their study, Martin and Van Mooy (2013) were taking into account the polyP quantification of various matrix effects as well as the presence of nucleic acids occurring in the sample extract, which could lead to large over/underestimates in the final results.

In addition to matrix effects, nucleic acids are known to interfere with the polyP signal using DAPI quantification (Martin & Van Mooy, 2013), we saw in chapter 4 that other polyanions could also have an impact on the DAPI signal, but are not taken into account when using the polyP quantification method based on DAPI fluorescence (Omelon et al., 2016). The soluble and insoluble EPS inherent to planktonic and benthic photoautotrophic microbes (Aslam et al., 2012, Biersmith & Benner, 1998, Bahulikar & Kroth, 2007) may also remain in the sample after the boiling and the proteinase K treatments included in the protocol by Martin and Van Mooy (2013). As shown in chapter 4, dextran sulphate interfered with DAPI signals, and a similar polyanionic saccharide was likely present in the stalk produced by *A. minutissimum*. Sulphated polysaccharides are common amongst the EPS secreted by diatoms, and therefore care must be taken before using the DAPI quantification method as it is not a specific stain for polyP.

To overcome these technical challenges, we quantified based on enzymatic polyP hydrolysis using an exopolyphosphatase (PPX) and subsequent colourimetric inorganic phosphate (orthophosphate) detection (Christ & Blank, 2018b, Werner *et al.*, 2007, Ohtomo *et al.*, 2008, Bru et al., 2016a). PPX allows the specific hydrolysis of polyP to inorganic phosphate unit (P_i) and requires a rather low sample purity. The enzyme was shown to not interact with a wide range of P-containing compounds such as nucleic acids, the polyanionic ATP, but also glucose-

6-phosphate, fructose-1,6-diphosphate or phosphoenolpyruvate (Christ 2018). A drawback of this enzyme is that it is rarely commercially available, which makes it an expensive product. However, 1 mg PPX bought commercially allows producing ca. 1000 reactions. A non-commercial alternative is also possible, since, in 1994, Wurst et al. sequenced the gene encoding for the *Saccharomyces cerevisiae* PPX, allowing the purification of the enzyme by protein expression using an available plasmid (Addgene plasmid # 38327 ; http://n2t.net/addgene:38327 ; RRID:Addgene_38327), (Werner *et al.*, 2005). Another procedure for PPX purification typically yields more than 5 mg of pure enzyme which is enough for ca. 5000 reactions (Pokhrel et al., 2019).

Finally, the subsequent quantification of the released P_i by PPX was performed using a one-reagent P_i detection in a 96-well plate. Two key innovations dictated the choice of a P_i detection method. The introduction of antimony in the ascorbate-molybdate-sulphuric acid decreased the colour development from several minutes to only two (Schelske & Sicko-Goad, 1990), and secondly, the scaling down of the assay to a 96-well plate allowed further automation and the use of a microplate reader (Christ & Blank, 2018b). The resulting assay allowed the rapid processing of several hundreds of polyP extracts generated in chapters 2 and 3 in a fast and automated way. The drawback of the assay is the lower slope of the P_i calibration curve with a 4.7 times lower sensitivity (*i.e.*, the slope of the calibration curve) compared to the malachite green assay (Christ 2018). However, in chapter 3, the depletion of cellular polyP measured using our method coincided with the stimulated Raman spectroscopy (SRS) data and showed an absence of polyP granules within the cells, suggesting that the method of P_i detection using the developed ascorbate-antimony-molybdate assay is sensitive enough for measuring polyP dynamics in diatoms. In the future, it would be interesting to use malachite green instead of ascorbate-antimony-molybdate as a inorganic phosphate detection reagent, which may reveal finer polyP dynamics in the diatom *A. minutissimum*.

Pre-conditioning history: the importance of phosphorus reserves

"The preconditioning environment of a population is important in determining algal response to the old environment and to a new one" said Perry in 1976, for describing the adaptations of *T. pseudonana* to variable phosphorus availabilities. In this study, cells that were pre-cultivated in P-deplete ($P_{(-)}$) and subsequently transferred in a P-replete ($P_{(+)}$) growth medium, displayed higher P uptake and polyP production, than cells having previously experienced $P_{(+)}$ conditions.

This thesis built on this observation from Perry in that the pre-conditioning of cells is of particular importance for the resulting cell division, scavenging behaviour and EPS secretions of *A. minutissimum* under variable P availability.

To explain the importance of pre-conditioning in microalgae, Perry was suggesting that the history of the microalgae population reflected their cellular P concentrations (Perry, 1976). Similarly, in this thesis we saw that the importance of the pre-conditioning step of *A. minutissimum* in a cultivation media lies in the ability of cells for storing or consuming P reserves, determining its nutrient status. PolyP and likely other P reserves like membranes phospholipids (PL) are playing a crucial role in the P status in *A. minutissimum*. For example, the overplus effect, thus the rapid accumulation of exogenous P accompanied by an intense polyP production observed in chapter 3, only occurred after conditioning the diatoms to $P_{(-)}$ conditions and lowering their P reserves, before their transfer to $P_{(+)}$ conditions. A more advanced state of P reserves depletion was required for observing stalk elongation with a first acclimation of 5 days in $P_{(-)}$ conditions, followed by an additional transfer into a new $P_{(-)}$ growth medium. In chapters 3 and 5, P reserves in *A. minutissimum* subjected to $P_{(+)}$ conditions were replenished, with cells producing for example polyP through the luxury uptake of P. The presence of replenished P reserves in these cells allowed them to continue dividing under P limitation by buffering cells in P and delayed the diatom's P-adaptive responses, as is shown in chapter 5 when alkaline phosphatase (AP) activity was strongly decreased in cultures pre-adapted and/or transferred in $P_{(+)}$ conditions. The delay of P-stress adaptive responses in cells having sufficient P reserves was also observed in other microorganisms. For example, in S. *cerevisiae*, the polyP deficient mutant lacking the VTC (vacuolar transporter chaperone) complex genes induced the gene responsible for a phosphatase production in response to cell P stress faster than the wildtype, suggesting that the presence of polyP might buffer internal P concentrations under P limitation (Neef & Kladde, 2003). In *T. pseudonana*, cells initially grown in $P_{(+)}$ and transferred to $P_{(-)}$ conditions first decreased their non-lipid P stocks, possibly including polyP, before increasing the production of membranes betaine lipids and sulfolipids (Hunter et al., 2018), which is typical responses to P-stress in microalgae. Therefore, the length of time until cells induce their P-stress responses depends on the level of their internal P stocks. Hence, parameters such as the previous but also the present availability of extracellular P have an impact on the levels of their P reserves (Werner et al., 2005, Bru et al., 2016b). The level of P reserves differs between taxa, but also within the same taxon. For example, different strains

of cyanobacteria showed different maximum values of polyP when grown under P limitation (Li & Dittrich, 2019).

The quantification of P reserve levels appears to be important for the deduction of the cellular P status. The absence of polyP in *A. minutissimum* cannot account alone for determining an intracellular P limitation, as the polymer quickly disappears after transferring cells in P-limited conditions, and diatoms continue dividing. Following both the dynamic levels of polyP and PL would improve the knowledge of P reserves dynamics within diatoms, but has never been investigated so far. A simple way to evaluate P reserves depletion in cells was given by Droop in 1968, where he calculated the cellular P concentration at which growth ceases (q_0). This parameter is less specific for measuring levels of each P reserve in cells but would give an idea of the limit threshold of intracellular P concentration before the cessation of growth (Perry, 1976). In this thesis, we could not resolve q_0 in *A. minutissimum* because growth ceased most likely due to other nutrients than P.

Our data indicated that *A. minutissimum* cultures freshly transferred to $P_{(-)}$ conditions, continued their division at the expense of their P reserves, and only gradually produced AP. Such adaptive response to a shortage in exogenous P indicates that diatoms privilege their division over scavenging for organic P when possessing enough P reserves. *A. minutissimum* may release extracellular phosphatases in addition to the membrane-associated ones, such as in *P. tricornutum* (Lin et al., 2013). Such enzymes cannot be recovered or recycled meaning they have high energy costs for the cell. Thus, *A. minutissimum* adapts to P-stress conditions by minimizing the unnecessary expression of genes that encode energetically expensive molecules such as phosphatases. Instead, they would favour the investment of energy in their division at the expense of their P reserves acquired when extracellular P was available. However, this fine-tuned balance later may be tilted towards the scavenging of organic P once their intracellular P reserves are too low.

Extra- and intracellular P sensing in *A. minutissimum*?

In chapter 5, levels of *A. minutissimum* cells displaying AP activity increased in cultures subjected to prolonged cultivation in $P_{(-)}$ media, suggesting that the phosphatase activity is rather regulated by the internal P storage than the external P availability. This phenomenon was also suggested in phytoplankton during exogenous P depletion in other laboratory experiments (Elgavish *et al.*, 1982). Moreover, we describe in chapter 3 that polyP is utilized by the cell

when exogenous P is depleted. The diatom *A. minutissimum* may possess a P sensing system, which can discriminate between the exogenous and the intracellular P availability.

In gram-negative bacteria, the regulation of P transport and assimilation is mediated by a two-component signal-transduction system (sensor and regulator) (Stock *et al.*, 2000), that comprises the proteins PhoB-PhoR forming the Pho regulon (Vershinina & Znamenskaya, 2002). PhoR is a transmembrane protein containing extracellular and intracellular P sensing modules (Dick *et al.*, 2011, Stock et al., 2000). Under P limitation (intracellular or intracellular), PhoR senses the external or internal stimuli and transmits the information to the cytosolic PhoB (response regulator). In turn, PhoB binds to the promoters of the Pho regulon, initiating the transcription of genes involved in the synthesis of P_i transporters as well as the scavenging of organic-P compounds through the production of AP. In cyanobacteria, similar regulatory systems were found (Hirani 2001), and in the cyanobacteria *Synechococcus* and *Prochlorococcus*, P limitation induces two-step Pho regulon gene expression, based on the regulation of PtrA (potential transcriptional regulator). Firstly, PhoB induces high-affinity P_i transporters but not the AP gene expression response. If the resulting levels of intracellular P do not rise, PtrA expression is increased, which binds to promoters of AP genes, thus up-regulating the production of AP (Ostrowski *et al.*, 2010). In microalgae, the P threshold concentration for when the signal transduction cascade occurs is not well known and likely is a function of both exogenous and intracellular P pools (Dyhrman, 2016). A transcriptomic study in the plant *Arabidopsis thaliana* showed that 70% of the genes involved in the response to P availability are directly related to the external P concentrations, while the remaining are regulated by the intracellular P concentration (Thibaud *et al.*, 2010). Concerning diatoms, the P-stress signalling cascade is not known and the recent transcriptomic studies only began to describe the molecular mechanisms regulated during exogenous P limitation. The current research on P limitation in diatoms based on omics data is in line with the findings of this thesis, showing upregulation of the metabolic pathways related to the scavenging and P transport (Alipanah et al., 2018, Cruz de Carvalho et al., 2016, Yang et al., 2014), resulting in the production of AP and increased uptake of available P as we saw in this thesis. A comprehensive list of genes involved in P homeostasis in diatoms can be found elsewhere (Lovio-Fragoso *et al.*, 2021). Although *A. minutissimum* displayed adaptive responses to P stress suggesting that it may discriminate between the intra- and extracellular P levels, the molecular evidence of the existence of a P sensing system in diatoms remains to be seen. The identification of such specific molecular markers in diatoms would greatly improve the method for measuring P-

stress in diatoms/phytoplankton populations (Lin et al., 2016). This would allow a better understanding of the fine-tuned balance between extracellular and intracellular P sensing regulatory mechanisms.

The life of *A. minutissimum* in biofilm: "the tallest tree in the forest"

Biofilm formation by *A. minutissimum* can be induced by molecules produced by the bacterium *Dyadobacter* sp. 32 (Dow, 2019). These molecules are supposedly sensed by the diatom, which in turn attaches to surfaces by producing a stalk (Windler et al., 2015). As shown in chapter 4, stalks of *A. minutissimum* are composed of interwoven sulphated polysaccharides. The attached form provides benthic diatoms several advantages over phytoplankton (i.e. stability, optimal light conditions and nutrient access) (Letáková et al., 2018). However, little is known about the benefits (if any) to the bacteria in this inter-kingdom relationship.

Previous works showed that *Dyadobacter* sp. 32 is capable to grow when supplied with carbohydrates (CHO) secreted by diatoms (Windler, 2014), and attaches mostly to diatoms producing EPS structures (stalks and capsules) (Leinweber & Kroth, 2015). One can imagine that bacteria would attach to diatom polysaccharides for nutritional purposes. The ability to process a wide range of polysaccharides is a common property of the Bacteroidetes phylum from which *Dyadobacter sp.32* belongs to. A genomic survey detected 97 putative CHO utilizing gene clusters in the bacterium (Dow *et al.*, 2020a). This value is within the same range of polysaccharides utilizing loci found in other *Dyadobacter* species (Terrapon *et al.*, 2018). The degradation of algal polysaccharides in bacteria is catalysed by CHO-active enzymes (CAZymes) (Lombard *et al.*, 2014). These enzymes allow the hydrolysis of diverse polymers, resulting in a wide range of oligosaccharide exudates available for consumption by bacteria. In Bacteroidetes, CAZymes are co-localized within clusters referred to as polysaccharide utilization loci (PUL), which encode the machinery for polysaccharide detection, hydrolysis and uptake (Grondin *et al.*, 2017). In addition, these PUL were shown to often harbour several sulphatases (Grondin et al., 2017, Mann *et al.*, 2013). In addition, among other free amino acids, concentrations of dissolved free methionine, a sulphur-containing amino acid within *A. minutissimum* culture increased drastically during co-cultivation with *Dyadobacter* sp. 32, suggesting that sulphur in EPS is important for the bacterium (Bruckner *et al.*, 2011). Although the presence of PUL and sulphfatases in *Dyadobacter* sp. 32 remain to be elucidated, the presence of sulphated polysaccharides within the diatom stalks shown in chapter 4 may be a

hint for orientating future investigations focusing on the benefits of the bacteria for inducing the biofilm formation of *A. minutissimum*.

In the presence of sufficient nutrients in its natural environment, attached *A. minutissimum* divides and other microbes further colonize the surface, producing more EPS, which increases the thickness and density of the biofilm community. In 1982, Hoagland et al. described the succession in periphyton communities dominated by diatoms adhering to Plexiglas as "heterogeneous and spatially and temporally dynamic throughout colonization and development". He described the steps of biofilm formation from a first attachment of low physical stature (bacteria and diatoms with short-stalks), to further high stature microorganisms (large diatom rosettes, long-stalked diatoms, filamentous green algae), comparing the development of more complex biofilms to the stature in higher plants (Hoagland *et al.*, 1982). This vertical succession in diatom dominance was suggested to result from competition for space and nutrients in the biofilm (Jackson, 1977, Hoagland et al., 1982). Such nutrient limitation can occur via the diffusive boundary layer surrounding the microbial community, resulting in a difference in chemical conditions between the water column and the benthic community (Riber & Wetzel, 1987). The transfer by molecular diffusion within the water column occurs in several steps: rapid, turbulent transport to and near the bed region, slower transport near and within the periphyton matrices, transfer through the viscous sublayers of the boundary layers, and transport through cell membranes (Larned *et al.*, 2004). These steps can be seen as a sequence of resistors which reduce the chemical exchanges from the column water to the cells, with most of the resistance caused by the thickness of the boundary layers that cover the benthos (Larned, 2010, Riber & Wetzel, 1987).

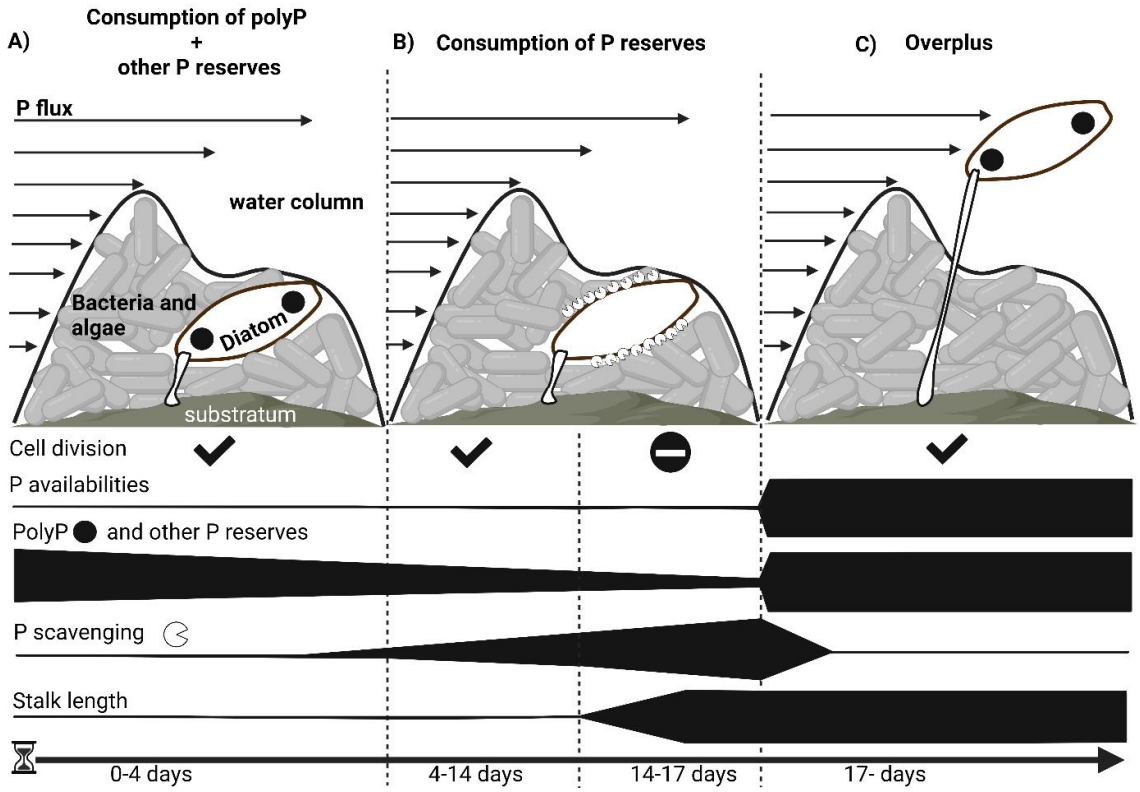

Figure 6. 1: Hypothetical scenario of *A. minutissimum* lifestyle in a freshwater epilithic phototrophic biofilm, based on the data collected during this thesis. Diatoms live attached to the surface of a submerged stone, along with other microorganisms (grey forms surrounding *A. minutissimum*: bacteria, diatoms), forming a biofilm. The boundary layer between the biofilm and the water column limits the nutrient flux within the biofilm, resulting in phosphorus (P) deficient conditions. In this simplified scenario, P is not available within the biofilm but only in the water column. A) In absence of exogenous P, the diatom continues dividing using its P reserves, by consuming polyP (black circles within the cell) as well as unidentified other intracellular resources. B) Following the polyP exhaustion; diatoms can still divide by using their remaining intracellular P reserves. Diatoms start to scavenge for P once their P reserves reach dip below a threshold, by producing phosphatases (ᗡ) located on their surface. Cells may stop dividing due to a prohibitively low intracellular P concentration, or due to another nutrient limitation. Due to an absence of division and low intracellular P reserves, the diatom stalk elongates and elevates the cell above the boundary layer to the water column where more P is available. C) Cell takes high amounts of P and rapidly repletes their intracellular P reserves including polyP, through the overplus response. The availability of extracellular P reduces the scavenging of cells and allows the cells to divide again.

In an epilithic biofilm from an oligotrophic lake such as Lake Constance, the low concentrations of P in the water in addition to the boundary layers of the biofilm might often limit the availability of this nutrient in the microbenthos, leading to competition for it. However, we saw that *A. minutissimum* possesses can use its P reserves for a prolonged P limitation period. If the

phosphorus starvation persists, the advantage of penetrating the boundary layer through vertical extension via stalk elongation is obvious, allowing it to assimilate the P available in the water column. Once more P is available, the diatom may rapidly take up this nutrient, showing an overplus response, replenishing its polyP stocks. Thus, the diatom with the longest stalk in a case of a crowded biofilm layer may lower the competition with the other diatoms and benefit from the presence of nutrients and light from the column water to continue dividing (Hoagland et al., 1982, Passy, 2007, Rimet et al., 2009) (Figure 6. 1). Moreover, one can speculate that stalk elongation may help elevate *A. minutissimum* cells to the surface of the biofilm for facilitating the release of its daughter cell in the water column. The free daughter cell may be transported by the water flow and can in turn colonize new surfaces responding to the molecules secreted by *Dyadobacter* sp. 32 (among other bacteria). To our knowledge, other than *Dydimosphenia germinata*, *A. minutissimum* is the only diatom described in literature elongating its stalk in response to P-stress. Other benthic diatoms are known to produce extensive stalks like *Cymbella affinis* or *Gomphonema olivaceum*, resulting in stalk production of several hundreds of micrometres in lengths (Hoagland et al., 1982, Passy, 2007). However, the reasons for such an elongation have never been investigated in detail. In this thesis, the stalk of the diatom *A. minutissimum* acts as a morphological trait that could maximize nutrient acquisition under severe intracellular P stress and may be a selective advantage for the success of the diatom under variable environmental conditions.

Conclusions and perspectives

In aquatic systems (marine and freshwater), photoautotrophic biofilms are a complex consortium of prokaryotic and eukaryotic microorganisms interacting together and with their environments. Diatoms are eukaryotic photosynthetic microalgae playing a major role in the primary production within these biofilms. Disentangling the interactions between the microorganisms and their environment reveals to be challenging in such a dense consortium. With the co-culture of the benthic freshwater diatom *A. minutissimum*, and the bacterium *Dyadobacter* sp. 32 as a model for biofilm formation, recent studies allowed to unravel new phenotypes and molecular processes occurring within a biofilm via genomic, physiological and structural analyses (Windler et al., 2015, Leinweber & Kroth, 2015, Leinweber et al., 2016, Dow *et al.*, 2020b).

The data of this thesis gives new insights into understanding the complex mechanisms of intracellular and extracellular adaptations of diatoms in biofilm lifestyle for defying environmental changes. PolyP, a phosphorus (P) reserve found in all life forms was found in *A. minutissimum* and was produced in presence of extracellular P. The polymer was shown to be consumed under P-limited conditions, along with other P reserves, acting as a buffer during P starvation and allowing the diatoms to thrive in its environment for several days. Therefore, polyP may be a crucial component contributing to the P homeostasis within diatoms. Future works must focus on the characterization of the different P reserves existing in diatoms, including polyP but also the membranes phospholipids for example, and the sequence to which they are used under P limited conditions. The presence of polyP reserves within the diatom was unambiguously revealed by using stimulated Raman spectroscopy (SRS) when other techniques like DAPI fluorescence also suggested that the diatom stalk might also contain this polymer. Hence, the SRS technique is precious for revealing the presence of molecules without disrupting cell content and may be useful to unravel novel nutrient reserves compartments in diatoms, as the technique was recently used for detecting nitrogen reserves in a variety of microalgae (Mojzes *et al.*, 2020).

The presence of intracellular phosphorus reserves in *A. minutissimum* impacted its EPS secretions as well as its P uptake when a minimum threshold of intracellular P reserves is reached; depending on its previous exposure to exogenous P. The presence of these P reserves acquired during past exposure to P may act as some sort of a "memory" that regulates the activity of the cell P uptake system as well as its P reserve accumulation. Therefore, further investigations need to be conducted to elucidate the molecular mechanisms underlying P sensing in diatoms.

Like diatoms, P limitation has also multiple effects on bacteria and can impact the secretion of metabolites involved in interspecies interactions (Santos-Beneit, 2015). This thesis focused on the diatom adaptations to P limitation but further works need to be conducted to investigate whether *Dyadobacter* sp.32 would also be impacted by P limitation, hence having a broader picture of the impact of P limitation on the interspecies interactions within the biofilm. Further studies may for example investigate whether P limitation has an impact on the secretions of *Dyadobacter* sp. 32, notably in the biofilm-forming info-chemicals production.

The intracellular P limitation impacted the stalk formation of the diatom, and further studies on other benthic stalk-producing diatom species must be conducted to unravel whether P intracellular availability, rather than exogenous P, is a driver for stalk elongation. This would

help to better understand the processes underlying the extensive stalk production of *D. germinata*, from which unprecedented nuisance blooms have been reported in rivers worldwide (Bray et al., 2017, Ellwood & Whitton, 2007).

Acknowledgements

A PhD rimes with a journey, and it is a (long) journey. A journey where I learnt so many new things, a journey where I met so many people, and a journey where I travelled so many times. It is also a journey where I learnt a lot about myself through the bad as well as the good times. Jean d'Ormesson said: "Life is not a perpetual party. Thank you for the roses, thank you also for the thorns".

Through these acknowledgements, I want to thank the following persons who accompanied me during this adventure.

First, I want to thank my two supervisors Pr. Dr. Peter Kroth and Pr. Dr Dieter Spiteller who offered me this PhD project. I want to thank them for their guidance and for the countless hours of "FPD" discussing the project advancements as well as providing ideas for developing it. I want to thank Peter also for allowing me to fulfil my dream of being a rockstar on a stage. Long life to PMF band! "Shall we talk on Friday?"

My lab/office life would not have been that great without my two favourites "pipelettes", Shvaita and Masha. Thank you so much for helping a French guy abroad to improve his poor English skills. Thanks to you; I am not anymore angry when I am hungry. Thank you for your kindness and for always listening. "Taki taki!"

I want to warmly thank my "mate" Lachlan who took me under his wing the first day I arrived in the lab. You showed me everything to start my PhD in the best conditions. Thank you for your time and for the relevant scientific discussions and advice, which helped me a lot in starting the project. "Yeasts!"

A huge thank you to Tony and Crispy! Thank you for your hard work! You were my best "polyPadawans!"

Thank you, Niccolo and Ruqian, my two bandmates aka the "gold fingers" and "angel voice". Thank you for the countless laughs and good vibes that we shared. From the karaoke nights to the PMF concerts, it was an honour to share these moments, and many others with you. "We should start a fire!"

Thank you to Rugby Club Konstanz. I found there a second family. Especially Lorenz and David, my brothers of blood on the rugby fields. Thank you for the countless laughs during all these years. "Tchou tchou!"

Many thanks to my gym buddy Maike. You were always a source of motivation to give my best at the gym and on the rugby field. Thank you also for all your efforts to keep me on the boat for all the administration papers. Thank you for your smile and your teasings. “Dan Carter is the best!”

Thank you to Enzo, you became during these five years a real little brother. Little because you are younger and smaller than I, you know that. Countless memories with you my eternal flatmate from Rimouski to the Seezeit student's dorms and to Rosmarin WG. You were always here during the good and the bad moments and I am very grateful for that. “Welcome to Rosmarinheideweg 11!”.

I would like to thank my life cheerleader, Laura. Even if sometimes it was not easy after a bad day of work, you were always supportive during the difficult times and I am very grateful for that. You definitely deserve more flowers; you deserve all the flowers in the world. “Weiss hallo!”.

Finally, I would like to thank my little family, Camille, Louis, Jean-Marc, Mum and mamie Moissac. You were always so supportive. I know it was long and that we couldn’t see each other as often as we wanted. If I became who I am today, it is in major part thanks to you. I hope I make you proud.

Author contributions

Chapter 2

The study was conceptualized by Adrien Lapointe, Dieter Spiteller and Peter G. Kroth. The methodology was designed by Adrien Lapointe, Dieter Spiteller and Peter G. Kroth. The investigations were done by Adrien Lapointe. Visualization of data was done by Adrien Lapointe. Interpretation of the results was performed by Adrien Lapointe, Dieter Spiteller and Peter G. Kroth. Adrien Lapointe took the lead in writing the manuscript and all co-authors contributed to the revision and editing process.

Chapter 3

The study was conceptualized by Adrien Lapointe, Dieter Spiteller and Peter G. Kroth. The methodology was designed by Adrien Lapointe, Dieter Spiteller and Peter G. Kroth. The investigation was performed by Adrien Lapointe. Preparation of the samples was carried out by Adrien Lapointe, Imaiyan Chitra Ragupathy, Paavo Bergman, Michael Laumann and Mustafa Kocademir. The visualization of the data was performed by Adrien Lapointe, Imaiyan Chitra Ragupathy, Paavo Bergman, Michael Laumann and Mustafa Kocademir. Adrien Lapointe, Imaiyan Chitra Ragupathy, Paavo Bergman, Mustafa Kocademir, Dieter Spiteller, Andreas Zumbush and Peter G. Kroth contributed to the interpretation of the results. Adrien Lapointe took the lead in writing the manuscript, and all co-authors contributed to the revision process.

Chapter 4

The study was conceptualized by Adrien Lapointe and Peter G. Kroth. The methodology was designed by Adrien Lapointe and Peter G. Kroth. The investigation was performed by Adrien Lapointe. Preparation of the samples was carried out by Adrien Lapointe, Paavo Bergman, Michael Laumann, Imaiyan Chitra Ragupathy, and Mustafa Kocademir. The visualization of the data was performed by Adrien Lapointe, Paavo Bergman, Michael Laumann, Imaiyan Chitra Ragupathy and Mustafa Kocademir. Adrien Lapointe, Imaiyan Chitra Ragupathy, Paavo Bergman, Mustafa Kocademir, Dieter Spiteller, Andreas Zumbush and Peter G. Kroth contributed to the interpretation of the results. Adrien Lapointe took the lead in writing the manuscript, and all co-authors contributed to the revision process.

Chapter 5

The study was conceptualized by Adrien Lapointe and Peter G. Kroth. The methodology was designed by Adrien Lapointe. The investigation was performed by Adrien Lapointe.

Preparation of the samples was carried out by Adrien Lapointe and Pengyu Ji. The visualization of the data was performed by Adrien Lapointe and Pengyu Ji. Adrien Lapointe interpreted the results. Adrien Lapointe took the lead in writing the manuscript, and Peter G. Kroth contributed to the revision process.

Supporting information

Chapter 2. High throughput method for extracting polyphosphates from diatoms

Table S2. 1: Comparison of the polyP determination methods: List of chemicals and organisms used as well as the number of steps and the duration (min) for extracting polyP using different approaches.

PolyP extraction protocol	Chemicals used for extraction	Organism used in protocol	Number of steps	Duration of extraction and purification
Method 1 "Nexttec DNA isolation 1-Step™"	Lysis buffer Proteinase k	Tissues and cells	2	ca. 60
Method 2 (Bru *et al*. 2016)	Phenol Chloroform Nucleases	Yeast	5	ca. 300
Method 3 (Christ and Blank 2018a)	Phenol Chloroform	Yeast	1	ca. 20
Method 4 Adapted from Martin and Van Mooy (2013)	Tris Proteinase K	Environmental plankton	2	ca. 140
Method 5 (Pokhrel *et al*. 2020)	GITC	Bacteria	3	ca. 15

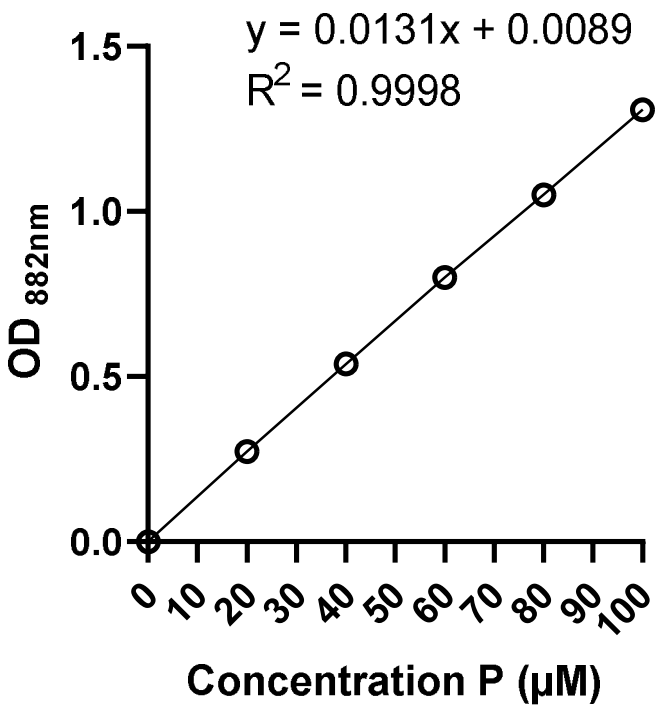

Figure S2. 1**:** Standard curve of the OD 882 nm vs the concentration of phosphate (P). Data represent means, and standard deviations are given as error bar of n = 3 replicates. The error bars are not visible due to too small standard deviation (≤ 0.01).

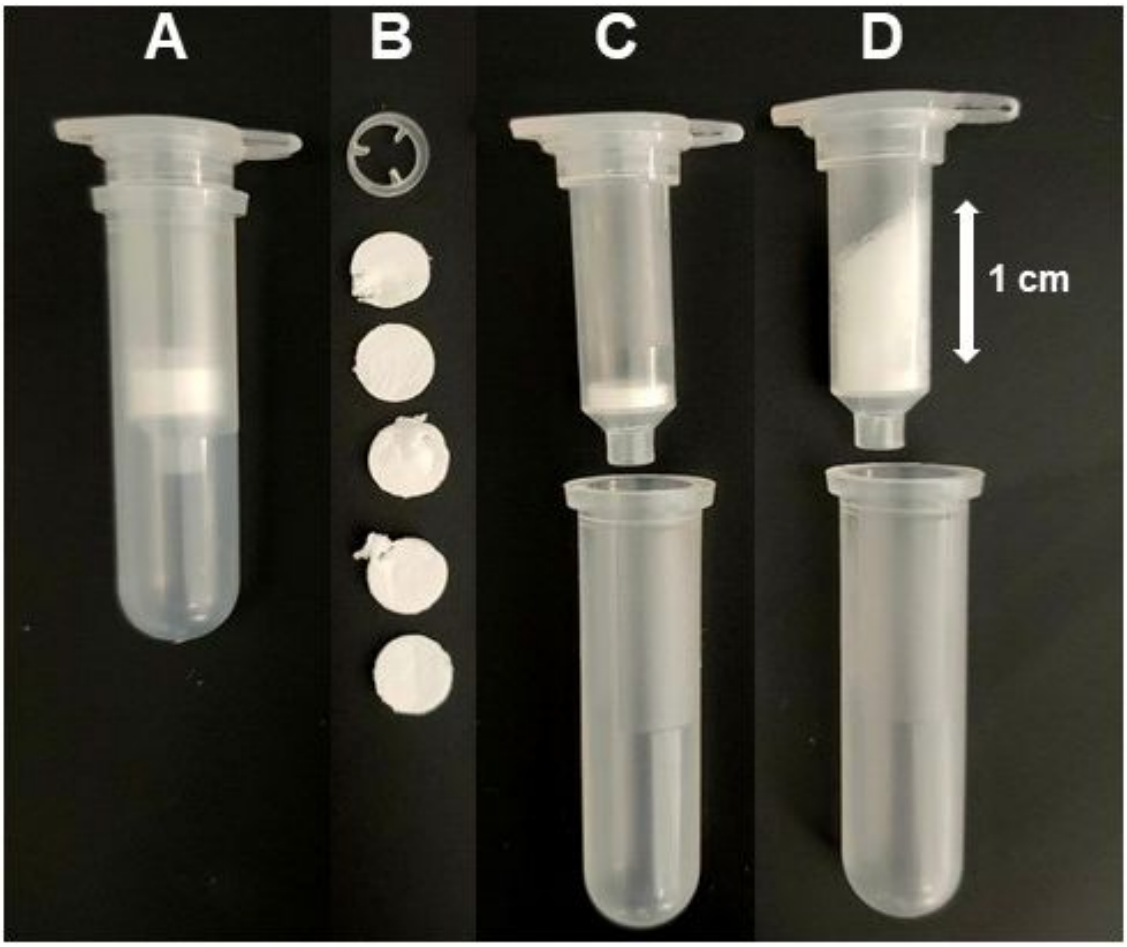

Figure S2. 2: Preparation of self-made gel filtration columns using empty commercial spin columns. (A) Used commercial spin column from GENECLEAN®. (B) The upper plastic ring stopper and the membrane discs are removed using tweezers. (C) The remaining lower filter disc is left for supporting the gel filtration resin. (D) Gel filtration resin is added until reaching a height of 1 cm.Preparation of self-made gel filtration columns using empty commercial spin columns. A) Used commercial spin column from GENECLEAN®. B) The upper plastic ring stopper and the membrane discs s are removed using tweezers. C) The remaining lower filter disc is left for supporting the gel filtration resin. D) Gel filtration resin is added until reaching a height of 1 cm.

Chapter 3. Characterization of polyphosphate dynamics in the widespread freshwater diatom *A. minutissimum* under varying phosphorus supplies.

Table S3. 1: Protocol for cell fixation and embedding for SEM visualization. "RT" is room temperature.

Chemical/Substance		°C	Time
Sample preparation	Sucking pellet in cellulose capillary by capillary forces. Capillaries containing cells are sectioned with a scalpel every 0.2 – 0.3 cm to seal each edge, avoiding cell losses. Put cellulose capillaries in an Eppendorf cup containing 0.5 mL of new AM $P_{(+)}$.	RT	
Pre-Fixation	Add to cell suspension in proportion 1:1 with AM $P_{(+)}$: 4% glutaraldehyde in Na-HEPES buffer (0.2 M Na-HEPES, 0.01 M $CaCl_2$, 0.02 M $MgCl_2$, pH = 7.0).	on ice	15 min
Fixation I	Remove the supernatant carefully and add ca. 1 mL of 2% glutaraldehyde in Na-HEPES buffer (0.05 M Na-HEPES buffer, 0.01 M $CaCl_2$, 0.01 M $MgCl_2$, pH = 7.0).	on ice	2 x 30 min
Washing	Remove carefully the supernatant and add 1 mL of Na-HEPES buffer (0.05 M Na-HEPES buffer, 0.01 M $CaCl_2$, 0.01 M $MgCl_2$, pH = 7.0).	on ice	3 x 10 min
Fixation II	Remove carefully the supernatant and add 1% OSO_4 in 0.1 M Na-HEPES buffer.	on ice	75 min
Washing	Remove carefully the supernatant and add 0.1 M Na-HEPES.	on ice	3 x 10 min
Dehydration (ethanol)	Remove carefully the supernatant and add ca.1 mL of 30% ethanol.	on ice	10 min
	Remove carefully the supernatant and add 50% ethanol.	on ice	15 min
	Remove carefully the supernatant and add 70% ethanol.	on ice	Overnight
	Remove carefully the supernatant and add 80% ethanol.	RT	3 x 10min
	Remove carefully the supernatant and add 90% acetone.	RT	3 x 10min

Dehydration (acetone)	Remove carefully the supernatant and add 96% acetone.	RT	3 x 10min
	Remove carefully the supernatant and add 100% absolute acetone.	RT	3 x 10min
Intermedium	Remove carefully the supernatant and add 100% absolute acetone.	RT	30 min
Infiltration	Remove carefully the supernatant and add 12.5% SPURR in absolute acetone.	RT	60 min
	Remove carefully the supernatant and add 33% SPURR in absolute acetone.	RT	60 min
	Remove carefully the supernatant and add 50% SPURR in absolute acetone.	RT	60 min
	Remove carefully the supernatant and add 75% SPURR in absolute acetone.	RT	Overnight
Embedding	Remove carefully the supernatant and add 100% SPURR.	RT	3 x 2 h
Polymerization	Transfer cellulose capillaries in TAAB-capsules or silicone moulds and fill up with 100% SPURR in the oven.	65°C	48 h
Cooling	Remove TAAB capsules or silicone moulds from the oven and put them in a flow cabinet.	RT	4 h

Table S3. 2: Final cell densities of *A. minutissimum* (in cells/mL) after 15 days of cultivation together with the growth rates (μ, d^{-1}) during the exponential growth phase under $P_{(+)}$ and $P_{(-)}$ conditions before medium resupply. Data represent means and standard deviations of n= 4 replicates. Values in the same column with different superscript letters present significant statistical differences ($p < 0.05$).

	Cell density (10^6 cells · mL^{-1})	Growth rate (d^{-1})	Growth rate (d^{-1})	Growth rate (d^{-1})	Growth rate (d^{-1})
Time (d)	15	2 to 4	4 to 6	6 to 8	8 to 10
$P_{(+)}$	2.85 ± 0.83^a	0.74 ± 0.09^a	0.36 ± 0.02^a	0.29 ± 0.04^a	0.09 ± 0.02^a
$P_{(-)}$	1.24 ± 0.04^b	0.65 ± 0.07^a	0.26 ± 0.05^b	0.25 ± 0.03^a	0.11 ± 0.01^a

Table S3. 3: Final cell densities of *A. minutissimum* (cell/mL) after 18 days of cultivation, and growth rates (μ, d^{-1}) at exponential phase under $P_{(+/+)}$ or $P_{(-/+)}$ conditions after resupplying with AM $P_{(+)}$ medium at day 15. Data represent means and standard deviations of n= 4 replicates. Values in the same column with different superscript letters indicate significant statistical differences ($p < 0.05$).

	Cell density (10^6 cells · mL^{-1})	Growth rate (d^{-1})	Growth rate (d^{-1})
Time (d)	18	16 to 17	17 to 18
$P_{(+/+)}$	3.02 ± 0.23^a	0.95 ± 0.07^a	0.62 ± 0.05^a
$P_{(-/+)}$	2.41 ± 0.19^b	0.76 ± 0.05^b	0.71 ± 0.03^b

Table S3. 4: Rate of polyP synthesis and degradation (pg Pi/cell/day), before media resupply for $P_{(+)}$ cultures, and after medium resupply at d 15 for $P_{(+/+)}$ cultures. (N/A) means that there are no data because polyP is not detectable.

Time (d)	0 to 2	2 to 4	4 to 6	6 to 8	8 to 10
$P_{(+)}$	0.21 ± 0.15	0.30 ± 0.01	-0.56 ± 0.02	-0.12 ± 0.06	$5.02\times10^{-3} \pm 1.00\times10^{-3}$
Time (d)	10 to 12	12 to 15	15 to 16	16 to 17	17 to 18
$P_{(+)}$	N/A	N/A	0.43 ± 0.11	$0.32 \pm 0,13$	-0.73 ± 0.20

Table S3. 5: Rate of polyP synthesis and degradation (pg Pi/cell/day), before media resupply for $P_{(-)}$ cultures, and after medium resupply at d 15 for $P_{(-/+)}$ cultures. (N/A) means that there are no data because polyP is not detectable.

Time (d)	0 to 2	2 to 4	4 to 6	6 to 8	8 to 10
$P_{(-)}$	-0.07 ± 0.03	-0.16 ± 0.03	N/A	N/A	N/A
Time (d)	10 to 12	12 to 15	15 to 16	16 to 17	17 to 18
$P_{(-)}$	N/A	N/A	1.78 ± 0.34	-0.24 ± 0.03	-1.25 ± 0.25

Table S3. 6: Exogenous P_i uptake allocated to polyP synthesis (%), before media resupply for $P_{(+)}$ and $P_{(-)}$ cells, and after medium resupply at d 15 for $P_{(+/+)}$ and $P_{(-/+)}$ cells. (N/A) means that there is no polyP synthesis.

Time (d)	0 to 2	2 to 4	4 to 6	15 to 16	16 to 17	17 to 18
$P_{(+)}$	7.55 ± 2.71	20.40 ± 4.00	N/A	18.00 ± 0.50	10.19 ± 0.55	N/A
$P_{(-)}$	N/A	N/A	N/A	26.00 ± 7.00	N/A	N/A

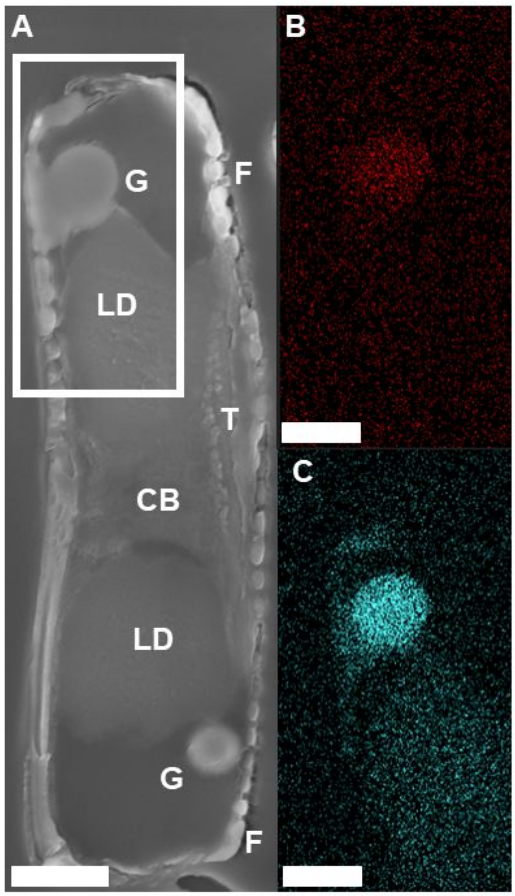

Figure S3. 1: Ultrastructural SEM image of an *A. minutissimum* cell taken from the same sample containing the cell shown in Figure 3. 1A. A) SEM picture of *A. minutissimum* containing a cytoplasmic bridge (CB), thylakoids (T), lipid droplets (LD), electron-dense granule (G), and (F) frustule. The area delimited by the white square in A) was subjected to energy-dispersive X-ray spectroscopy (EDX). EDX elemental mapping for B) calcium and C) phosphorous. These data are representative of cells cultivated in P-replete ($P_{(+)}$) conditions. Scale bar: scanning electron micrograph: 1 µm, elemental maps: 2.5 µm.

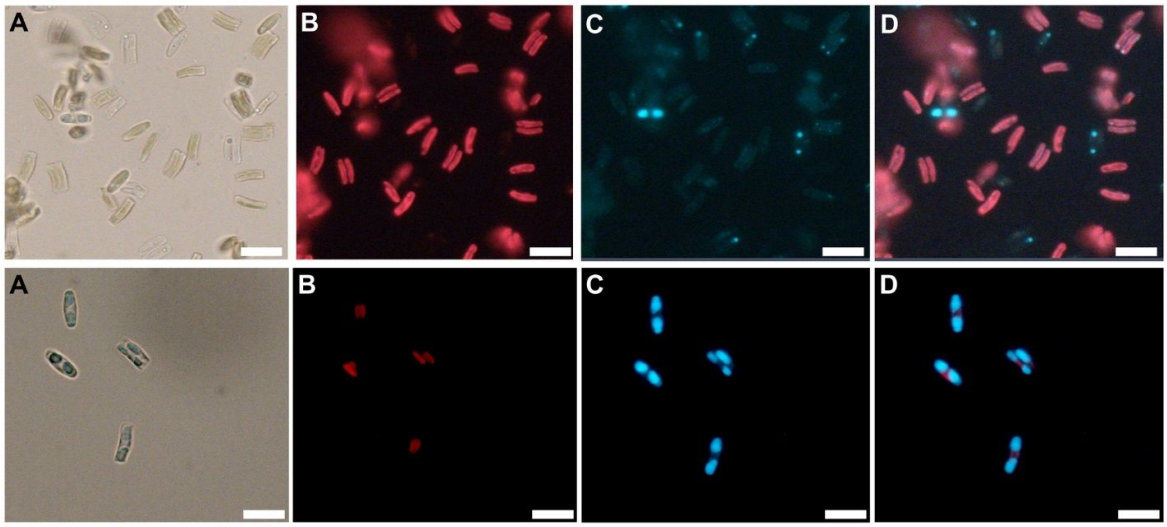

Figure S3. 2. *A. minutissimum* cells cultivated in $P_{(+)}$ condition. Diatom cells cultivated in $P_{(+)}$ conditions for 3 days (upper row) and 6 days (lower row). A) Bright-field micrographs. B) Chlorophyll fluorescence. C) BODIPY staining. D) Merged picture from B) and C).

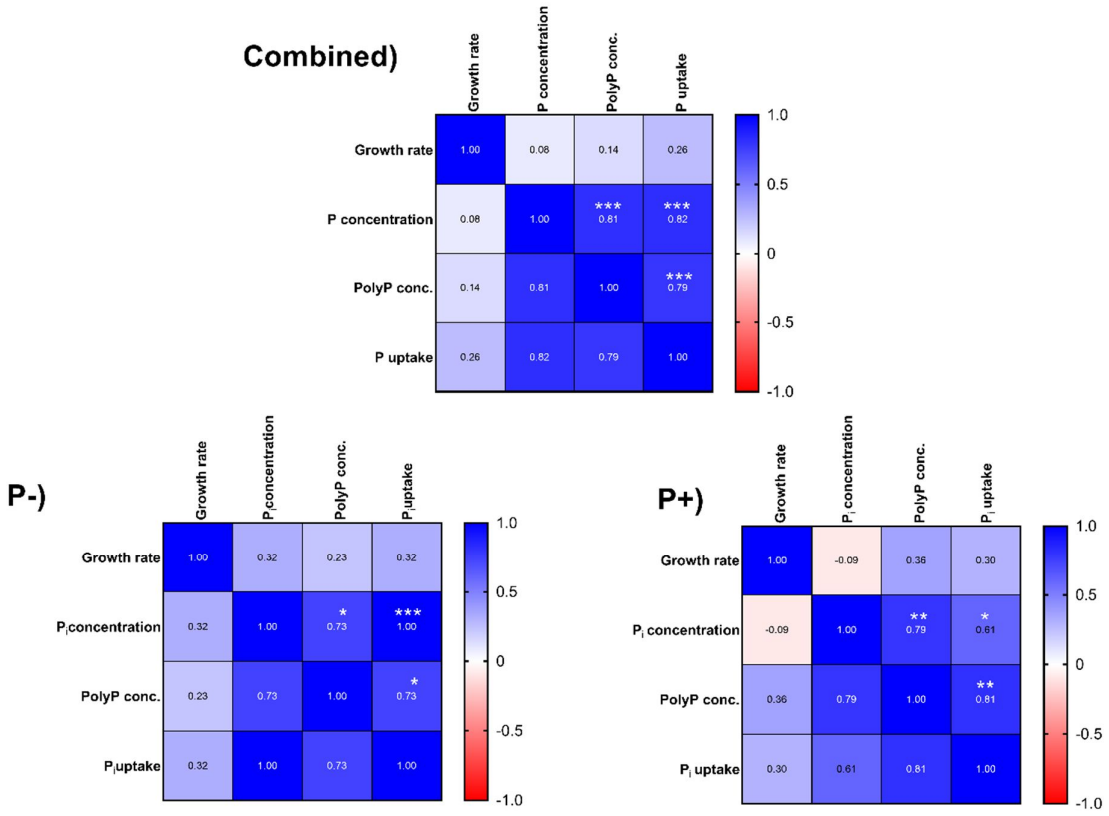

Figure S3. 3. Correlation matrices of cell growth rate, extracellular P, polyP amount and

cellular P uptake in A) $P_{(-)}$ and $P_{(+)}$ combined datasets B) in $P_{(-)}$ dataset and C) in $P_{(+)}$ dataset. Correlations marked with an asterisk are significant (*, $p<0.033$; **, $p<0.02$, ***, $p<0.001$).

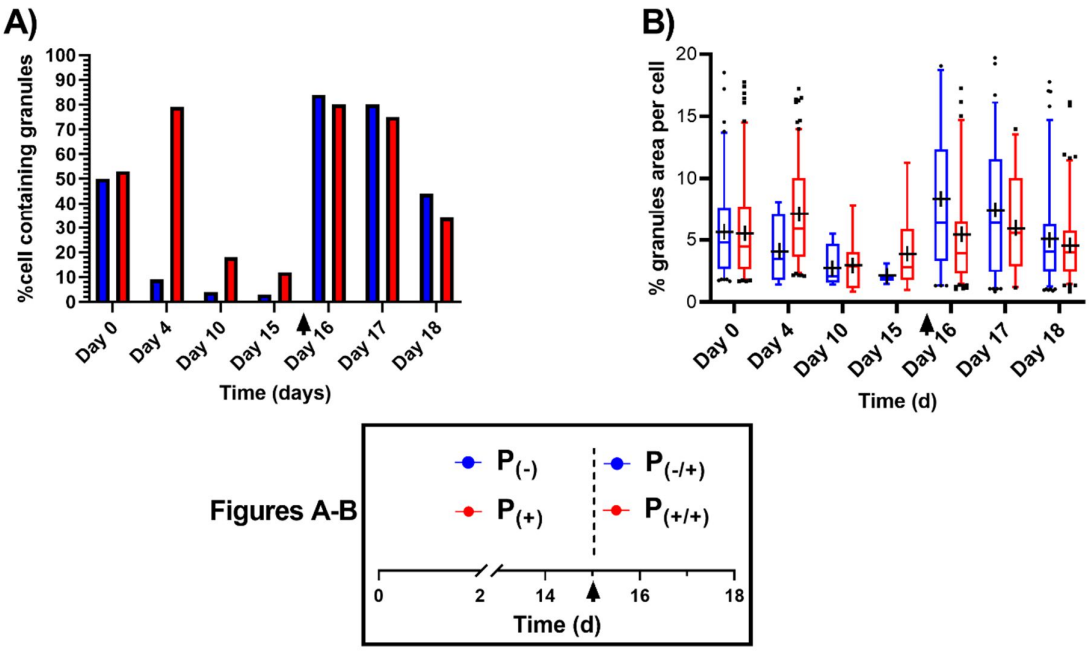

Figure S3. 4. Dynamics of the polyP granules in *A. minutissimum* in different P availabilities. A) Percentage of cells containing at least one granule visible using SRS imaging, before and after resupply with AM $P_{(+)}$ cultivation medium. B) SRS data analysis of the dynamics of the area occupied by polyP granules per cell containing at least one granule, before and after resupply with AM $P_{(+)}$ cultivation medium. Black arrows represent the time point at day 15 of resupply with $P_{(+)}$ cultivation medium in $P_{(+)}$ and $P_{(-)}$ cultures, and cells were annotated $P_{(+/+)}$ and $P_{(-/+)}$, respectively. On day 15, data correspond to before the resupply in $P_{(+)}$ cultivation medium. Data represent n= 1 replicate.

Chapter 5. Effects of varying phosphorus supplies on the resilience and the biofilm formation of the freshwater diatom *A. minutissimum*

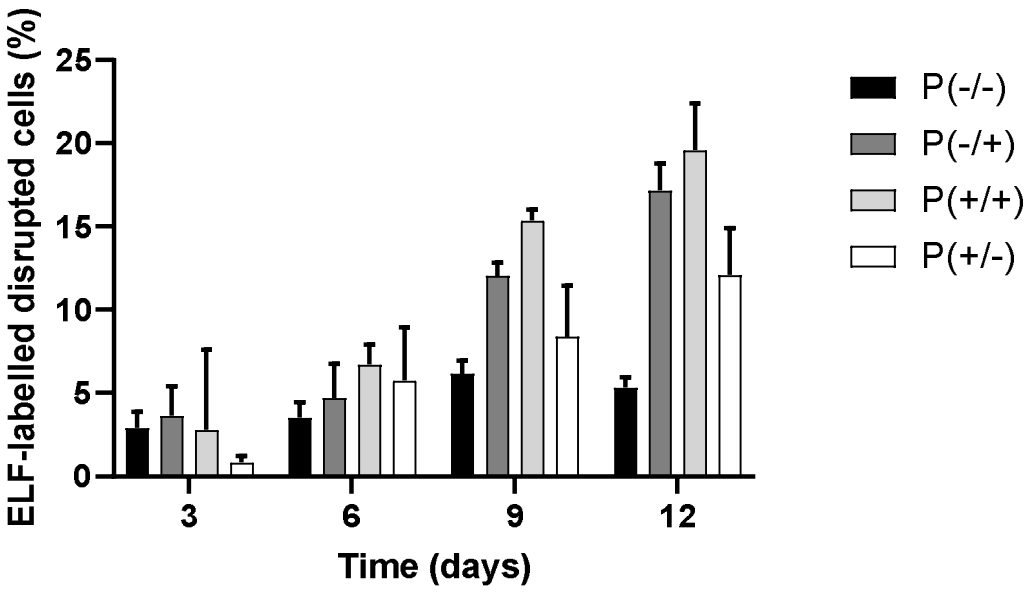

Figure S5. 1: Percentage of disrupted cells labelled by ELF-97 in $P_{(-/-)}$ (black bars), $P_{(-/+)}$ (dark grey bars), $P_{(+/+)}$ (light grey bars), and $P_{(+/-)}$ (white bars) cultures during 12 days. Error bars are n=3 replicates containing 50 cells labelled by ELF-97 for each replicate.

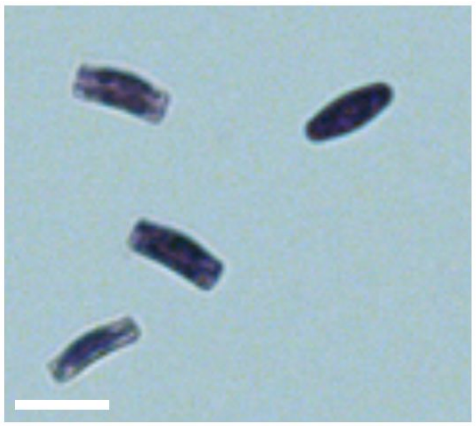

Figure S5. 2. Representative micrograph of $P_{(-/-)}$, $P_{(-/+)}$, $P_{(+/+)}$ or $P_{(+/-)}$ cells stained by crystal violet after 1h of cultivation with *Dyadobacter sp. 32* . Scale bar: 10µm.

List of publications

Dow, L., Stock, F., Peltekis, A., Szamosvari, D., Prothiwa, M., Lapointe, A., Bottcher, T., Bailleul, B., Vyverman, W., Kroth, P. G. & Lepetit, B.

The Multifaceted Inhibitory Effects of an Alkylquinolone on the Diatom *Phaeodactylum tricornutum*

Published in Chembiochem, 2020

DOI: 10.1002/cbic.201900612

Lapointe, A., Spiteller, D. & Kroth, P. G.

Chapter 2. High throughput method for extracting polyphosphates from diatoms

Published in Endocytobiosis and Cell Research, 2022

https://zs.thulb.uni-jena.de/receive/jportal_jparticle_01216927

Lapointe, A., Chitra Ragupathy, I., Bergmann, P., Laumann, M., Spiteller, D., Kocademir, M., Zumbusch, A. & Kroth, P. G.

Chapter 3. Characterization of polyphosphate dynamics in the widespread freshwater diatom *Achnanthidium minutissimum* under varying phosphorus supplies

Published in the Journal of Phycology, 2024

DOI: 10.1111/jpy.13423

References

Aboal, M., Marco, S., Chaves, E., Mulero, I. & García-Ayala, A. 2012. Ultrastructure and function of stalks of the diatom *Didymosphenia geminata*. *Hydrobiologia* **695**:17-24.

Aitchison, P. & Butt, V. 1973. The relation between the synthesis of inorganic polyphosphate and phosphate uptake by *Chlorella vulgaris*. *J Exp Bot* **24**:497-510.

Alipanah, L., Winge, P., Rohloff, J., Najafi, J., Brembu, T. & Bones, A. M. 2018. Molecular adaptations to phosphorus deprivation and comparison with nitrogen deprivation responses in the diatom *Phaeodactylum tricornutum*. *PLoS One* **13**:e0193335.

Armbrust, E. V. 2009. The life of diatoms in the world's oceans. *Nature* **459**:185-92.

Armbrust, E. V., Berges, J. A., Bowler, C., Green, B. R., Martinez, D., Putnam, N. H., Zhou, S., Allen, A. E., Apt, K. E. & Bechner, M. 2004. The genome of the diatom *Thalassiosira pseudonana*: ecology, evolution, and metabolism. *Science* **306**:79-86.

Aschar-Sobbi, R., Abramov, A. Y., Diao, C., Kargacin, M. E., Kargacin, G. J., French, R. J. & Pavlov, E. 2008. High sensitivity, quantitative measurements of polyphosphate using a new DAPI-based approach. *J Fluoresc* **18**:859-66.

Aslam, S. N., Cresswell-Maynard, T., Thomas, D. N. & Underwood, G. J. 2012. Production and Characterization of the Intra- and Extracellular Carbohydrates and Polymeric Substances (EPS) of Three Sea-Ice Diatom Species, and Evidence for a Cryoprotective Role for EPS. *J Phycol* **48**:1494-509.

Ault-Riche, D., Fraley, C. D., Tzeng, C. M. & Kornberg, A. 1998. Novel assay reveals multiple pathways regulating stress-induced accumulations of inorganic polyphosphate in Escherichia coli. *J Bacteriol* **180**:1841-7.

Bahulikar, R. A. & Kroth, P. G. 2007. Localization of EPS components secreted by freshwater diatoms using differential staining with fluorophore-conjugated lectins and other fluorochromes. *Eur J Phycol* **42**:199-208.

Barcytė, D., Pilátová, J., Mojzeš, P. & Nedbalová, L. 2020. The arctic Cylindrocystis (Zygnematophyceae, Streptophyta) green algae are genetically and morphologically diverse and exhibit effective accumulation of polyphosphate. *J Phycol* **56**:217-32.

Becker, B., Hoef-Emden, K. & Melkonian, M. 2008. Chlamydial genes shed light on the evolution of photoautotrophic eukaryotes. *BMC Evol Biol* **8**:1-18.

Bellinger, B., Underwood, G., Ziegler, S. & Gretz, M. 2009. Significance of diatom-derived polymers in carbon flow dynamics within estuarine biofilms determined through isotopic enrichment. *Aquat Microb Ecol* **55**:169-87.

Benitez-Nelson, C. R. 2000. The biogeochemical cycling of phosphorus in marine systems. *Earth-Sci Rev* **51**:109-35.

Benning, C., Huang, Z.-H. & Gage, D. A. 1995. Accumulation of a novel glycolipid and a betaine lipid in cells of *Rhodobacter sphaeroides* grown under phosphate limitation. *Arch Biochem Biophys* **317**:103-11.

Bhosle, N., Sawant, S., Garg, A. & Wagh, A. 1995. Isolation and partial chemical analysis of exopolysaccharides from the marine fouling diatom *Navicula subinflata*.

Biersmith, A. & Benner, R. 1998. Carbohydrates in phytoplankton and freshly produced dissolved organic matter. *Marine Chemistry* **63**:131-44.

Blunn, G. & Evans, L. 1981. Microscopical observations on Achnanthes subsessilis, with particular reference to stalk formation.

Bowler, C., Allen, A. E., Badger, J. H., Grimwood, J., Jabbari, K., Kuo, A., Maheswari, U., Martens, C., Maumus, F. & Otillar, R. P. 2008. The *Phaeodactylum* genome reveals the evolutionary history of diatom genomes. *Nature* **456**:239-44.

Bray, J., Kilroy, C., Gerbeaux, P. & Harding, J. S. 2017. Ecological eustress? Nutrient supply, bloom stimulation and competition determine dominance of the diatom *Didymosphenia geminata*. *Freshwater Biol* **62**:1433-42.

Brembu, T., Muhlroth, A., Alipanah, L. & Bones, A. M. 2017. The effects of phosphorus limitation on carbon metabolism in diatoms. *Philos Trans R Soc Lond B Biol Sci* **372**.

Brinck, J. W. 2009. World resources of phosphorus. *Ciba foundation symposium.* pp. 23-48.

Brown, M. R. & Kornberg, A. 2004. Inorganic polyphosphate in the origin and survival of species. *P Natl A Sci* **101**:16085-87.

Bru, S., Jimenez, J., Canadell, D., Arino, J. & Clotet, J. 2016a. Improvement of biochemical methods of polyP quantification. *Microb Cell* **4**:6-15.

Bru, S., Martinez-Lainez, J. M., Hernandez-Ortega, S., Quandt, E., Torres-Torronteras, J., Marti, R., Canadell, D., Arino, J., Sharma, S., Jimenez, J. & Clotet, J. 2016b. Polyphosphate is involved in cell cycle progression and genomic stability in *Saccharomyces cerevisiae*. *Mol Microbiol* **101**:367-80.

Bru, S., Samper-Martin, B., Quandt, E., Hernandez-Ortega, S., Martinez-Lainez, J. M., Gari, E., Rafel, M., Torres-Torronteras, J., Marti, R., Ribeiro, M. P. C., Jimenez, J. & Clotet, J. 2017. Polyphosphate is a key factor for cell survival after DNA damage in eukaryotic cells. *DNA Repair (Amst)* **57**:171-78.

Bruckner, C. G., Bahulikar, R., Rahalkar, M., Schink, B. & Kroth, P. G. 2008. Bacteria associated with benthic diatoms from Lake Constance: phylogeny and influences on diatom growth and secretion of extracellular polymeric substances. *Appl Environ Microbiol* **74**:7740-9.

Bruckner, C. G., Rehm, C., Grossart, H. P. & Kroth, P. G. 2011. Growth and release of extracellular organic compounds by benthic diatoms depend on interactions with bacteria. *Environ Microbiol* **13**:1052-63.

Caceres, C., Spatharis, S., Kaiserli, E., Smeti, E., Flowers, H. & Bonachela, J. A. 2019. Temporal phosphate gradients reveal diverse acclimation responses in phytoplankton phosphate uptake. *ISME J* **13**:2834-45.

Carpenter, S. R., Caraco, N. F., Correll, D. L., Howarth, R. W., Sharpley, A. N. & Smith, V. H. 1998. Nonpoint pollution of surface waters with phosphorus and nitrogen. *Ecol Appl* **8**:559-68.

Cembella, A. D., Antia, N. J., Harrison, P. J. & Rhee, G.-Y. 1984. The utilization of inorganic and organic phosphorous compounds as nutrients by eukaryotic microalgae: a multidisciplinary perspective: part 2. *CRC Cr Rev Microbiol* **11**:13-81.

Chiovitti, A., Dugdale, T. M. & Wetherbee, R. 2006. Diatom adhesives: molecular and mechanical properties. *Biological adhesives.* Springer, pp. 79-103.

Christ, J. J. & Blank, L. M. 2018a. Analytical polyphosphate extraction from *Saccharomyces cerevisiae*. *Anal Biochem* **563**:71-78.

Christ, J. J. & Blank, L. M. 2018b. Enzymatic quantification and length determination of polyphosphate down to a chain length of two. *Anal Biochem* **548**:82-90.

Christ, J. J., Willbold, S. & Blank, L. M. 2020. Methods for the analysis of polyphosphate in the life sciences. *Anal Chem* **92**:4167-76.

Cooksey, B. & Cooksey, K. E. 1988. Chemical signal-response in diatoms of the genus Amphora. *J Cell Sci* **91**:523-29.

Cotner Jr, J. B. & Wetzel, R. G. 1992. Uptake of dissolved inorganic and organic bphosphorus compounds by phytoplankton and bacterioplankton. *Limnol Oceanogr* **37**:232-43.

Crawford, R. M. 1973. The protoplasmic ultrastructure of the vegetative cell of *Melosira varians*. *J Phycol* **9**:50-61.

Cruz de Carvalho, M. H., Sun, H. X., Bowler, C. & Chua, N. H. 2016. Noncoding and coding transcriptome responses of a marine diatom to phosphate fluctuations. *New Phytol* **210**:497-510.

Daniel, G., Chamberlain, A. & Jones, E. 1980. Ultrastructural observations on the marine fouling diatom *Amphora*. *Helgoländer Meeresuntersuchungen* **34**:123-49.

Daniel, G. F., Chamberlain, A. H. L. & Jones, E. B. G. 2007. Cytochemical and electron microscopical observations on the adhesive materials of marine fouling diatoms. *Brit Phycol J* **22**:101-18.

Davis, B. D. 1958. On the importance of being ionized. *Arch Biochem Biophys* **78**:497-509.

Dell'Aquila, G. & Maier, U. G. 2020. Specific acclimations to phosphorus limitation in the marine diatom *Phaeodactylum tricornutum*. *Biol Chem* **401**:1495-501.

Denning, E. J. & MacKerell Jr, A. D. 2011. Impact of arsenic/phosphorus substitution on the intrinsic conformational properties of the phosphodiester backbone of DNA investigated using ab initio quantum mechanical calculations. *J Am Chem Soc* **133**:5770-72.

Diaz, J., Ingall, E., Benitez-Nelson, C., Paterson, D., de Jonge, M. D., McNulty, I. & Brandes, J. A. 2008. Marine polyphosphate: a key player in geologic phosphorus sequestration. *Science* **320**:652-5.

Dick, C. F., Dos-Santos, A. L. & Meyer-Fernandes, J. R. 2011. Inorganic phosphate as an important regulator of phosphatases. *Enzyme Res* **2011**:103980.

Docampo, R., de Souza, W., Miranda, K., Rohloff, P. & Moreno, S. N. 2005. Acidocalcisomes conserved from bacteria to man. *Nat Rev Microbiol* **3**:251-61.

Dow, L., Morrissey, K. L., Willems, A. & Kroth, P. G. 2020a. Complete genome sequence of *Dyadobacter* sp. 32, isolated from a culture of the freshwater diatom *Cymbella microcephala*. *Mar Genomics* **52**:100720.

Dow, L. E. 2019. Interactions between the freshwater benthic diatom *Achnanthidium minutissimum* and the bacterium *Dyadobacter* sp. 32. University of Konstanz.

Droop, M. R. 1968. Vitamin B12 and marine ecology. IV. The kinetics of uptake, growth and inhibition in *Monochrysis lutheri*. *J Mar Biol Assoc UK* **48**:689-733.

Drum, R. W. 1969. Electron microscope observations of diatoms. *Österreichische Botanische Zeitschrift* **116**:321-30.

Dyhrman, S. T. 2016. Nutrients and their acquisition: phosphorus physiology in microalgae. *The Physiology of Microalgae.* pp. 155-83.

Dyhrman, S. T., Jenkins, B. D., Rynearson, T. A., Saito, M. A., Mercier, M. L., Alexander, H., Whitney, L. P., Drzewianowski, A., Bulygin, V. V., Bertrand, E. M., Wu, Z., Benitez-Nelson, C. & Heithoff, A. 2012. The transcriptome and proteome of the diatom *Thalassiosira pseudonana* reveal a diverse phosphorus stress response. *PLoS One* **7**:e33768.

Dyhrman, S. T. & Palenik, B. 1999. Phosphate stress in cultures and field populations of the dinoflagellate *Prorocentrum minimum* detected by a single-cell alkaline phosphatase assay. *Appl Env Microb* **65**:3205-12.

Ehrlich, H., Motylenko, M., Sundareshwar, P. V., Ereskovsky, A., Zgłobicka, I., Noga, T., Płociński, T., Tsurkan, M. V., Wyroba, E., Suski, S., Bilski, H., Wysokowski, M., Stöcker, H., Makarova, A., Vyalikh, D., Walter, J., Molodtsov, S. L., Bazhenov, V. V., Petrenko, I., Langer, E., Richter, A., Niederschlag, E., Pisarek, M., Springer, A., Gelinsky, M., Rafaja, D., Witkowski, A., Meyer, D. C., Jesionowski, T. & Kurzydłowski, K. J. 2016. Multiphase biomineralization: enigmatic invasive siliceous diatoms produce crystalline calcite. *Adv Funct Mater* **26**:2503-10.

Eixler, S., Karsten, U. & Selig, U. 2019. Phosphorus storage in *Chlorella vulgaris* (Trebouxiophyceae, Chlorophyta) cells and its dependence on phosphate supply. *Phycologia* **45**:53-60.

Eixler, S., Selig, U. & Karsten, U. 2005. Extraction and detection methods for polyphosphate storage in autotrophic planktonic organisms. *Hydrobiologia* **533**:135-43.

Elgavish, A., Halmann, M. & Berman, T. 1982. A comparative study of phosphorus utilization and storage in batch cultures of *Peridinium cinctum*, Pediastrum duplex and Cosmarium sp., from Lake Kinneret (Israel). *Phycologia* **21**:47-54.

Ellwood, N. T. W. & Whitton, B. A. 2007. Importance of organic phosphate hydrolyzed in stalks of the lotic diatom *Didymosphenia geminata* and the possible impact of atmospheric and climatic changes. *Hydrobiologia* **592**:121-33.

Elser, J. J. 2012. Phosphorus: a limiting nutrient for humanity? *Curr Opin Biotechnol* **23**:833-8.

Falciatore, A., Jaubert, M., Bouly, J. P., Bailleul, B. & Mock, T. 2020. Diatom molecular research comes of age: model species for studying phytoplankton biology and diversity. *Plant Cell* **32**:547-72.

Falkner, G. & Falkner, R. 2011. The complex regulation of the phosphate uptake system of cyanobacteria. *Bioenergetic Processes of Cyanobacteria.* pp. 109-30.

Falkner, R. & Falkner, G. 2003. Distinct adaptivity during phosphate uptake by the cyanobacterium *Anabaena variabilis* reflects information processing about preceding phosphate supply. *J Trace Microprobe T* **21**:363-75.

Field, C. B., Behrenfeld, M. J., Randerson, J. T. & Falkowski, P. 1998. Primary production of the biosphere: integrating terrestrial and oceanic components. *science* **281**:237-40.

Fisher, K. A. 1971. Polyphosphate in a chlorococcalean alga. *Phycologia* **10**:177-82.

Flemming, H.-C., Neu, T. R. & Wozniak, D. J. 2007. The EPS matrix: the "house of biofilm cells". *J Bacteriol* **189**:7945-47.

Flemming, H.-C. & Wingender, J. 2001. Relevance of microbial extracellular polymeric substances (EPSs)-Part I: Structural and ecological aspects. *Water Sci Technol* **43**:1-8.

Flynn, K., Öpik, H. & Syrett, P. 1986. Localization of the alkaline phosphatase and 5′-nucleotidase activities of the diatom *Phaeodactylum tricornutum*. *Microbiology* **132**:289-98.

Flynn, K. J., Clark, D. R. & Xue, Y. 2008. Modeling the release of dissolved organic matter by phytoplankton. *J Phycol* **44**:1171-87.

Gerbersdorf, S. & Wieprecht, S. 2015. Biostabilization of cohesive sediments: revisiting the role of abiotic conditions, physiology and diversity of microbes, polymeric secretion, and biofilm architecture. *Geobiology* **13**:68-97.

Gibson, R. A. 1979. Observations of stalk production by *Pseudohimantidium pacificum* Hust. & Krasske (Bacillariophyceae: Protoraphidaceae). *Nova Hedwigia* **31**:899-915.

Gleick, P. H. & Schneider, S. 1996. Encyclopedia of climate and weather. *Water Resour* **2**:817-23.

González-Gil, S., Keafer, B. A., Jovine, R. V., Aguilera, A., Lu, S. & Anderson, D. M. 1998. Detection and quantification of alkaline phosphatase in single cells of phosphorus-starved marine phytoplankton. *Mar Ecol Prog Ser* **164**:21-35.

Gordon, R., Losic, D., Tiffany, M. A., Nagy, S. S. & Sterrenburg, F. A. 2009. The Glass Menagerie: diatoms for novel applications in nanotechnology. *Trends Biotechnol* **27**:116-27.

Gretz, M. R. & Hoagland, K. D. 1997. Molecular and Physiological Mechanisms of Diatom Fouling Phenomena. Michigan Technological Univ Houghton.

Grondin, J. M., Tamura, K., Déjean, G., Abbott, D. W. & Brumer, H. 2017. Polysaccharide utilization loci: fueling microbial communities. *J Bacteriol* **199**:e00860-16.

Groussman, R. D., Parker, M. S. & Armbrust, E. V. 2015. Diversity and evolutionary history of iron metabolism genes in diatoms. *PLoS One* **10**:e0129081.

Guillard, R. R. 1975. Culture of phytoplankton for feeding marine invertebrates. *Culture of marine invertebrate animals.* Springer, pp. 29-60.

Hamm, C. E., Merkel, R., Springer, O., Jurkojc, P., Maier, C., Prechtel, K. & Smetacek, V. 2003. Architecture and material properties of diatom shells provide effective mechanical protection. *Nature* **421**:841-43.

Harold, F. 1964. Enzymic and genetic control of polyphosphate accumulation in *Aerobacter aerogenes*. *Microbiology* **35**:81-90.

Harold, F. M. 1966. Inorganic polyphosphates in biology: structure, metabolism, and function. *Bacteriol Rev* **30**:772-94.

Harris, G. 2003. Ecological Stoichiometry: Biology of elements from molecules to the biosphere. Sterner, RW and Elser, JJ (2002) Princeton University Press, Princeton, NJ, USA. ISSN 0-691-07491-7. Oxford University Press.

Hartmann, J. & Nümann, W. 1977. Percids of Lake Constance, a lake undergoing eutrophication. *Journal of the Fisheries Board of Canada* **34**:1670-77.

Hecky, R. & Kilham, P. 1988. Nutrient limitation of phytoplankton in freshwater and marine environments: a review of recent evidence on the effects of enrichment 1. *Limnol Oceanogr* **33**:796-822.

Hlúbiková, D., Ector, L. & Hoffmann, L. 2011. Examination of the type material of some diatom species related to *Achnanthidium minutissimum* (Kutz.) Czarn. (Bacillariophyceae). *Algological Studies* **136-137**:19-43.

Hoagland, K. D., Roemer, S. C. & Rosowski, J. R. 1982. Colonization and community structure of two periphyton assemblages, with emphasis on the diatoms (Bacillariophyceae). *Am J of Boty* **69**:188-213.

Hoagland, K. D., Rosowski, J. R., Gretz, M. R. & Roemer, S. C. 1993. Diatom extracellular polymeric substances: function, fine structure, chemistry, and physiology. *J Phycol* **29**:537-66.

Hothorn, M., Neumann, H., Lenherr, E. D., Wehner, M., Rybin, V., Hassa, P. O., Uttenweiler, A., Reinhardt, M., Schmidt, A., Seiler, J., Ladurner, A. G., Herrmann, C., Scheffzek, K. & Mayer, A. 2009. Catalytic core of a membrane-associated eukaryotic polyphosphate polymerase. *Science* **324**:513-6.

Huang, B., Marchand, J., Blanckaert, V., Lukomska, E., Ulmann, L., Wielgosz-Collin, G., Rabesaotra, V., Moreau, B., Bougaran, G., Mimouni, V. & Morant-Manceau, A. 2019. Nitrogen and phosphorus limitations induce carbon partitioning and membrane lipid remodelling in the marine diatom *Phaeodactylum tricornutum*. *Eur J Phycol* **54**:342-58.

Huang, W., Rio Bartulos, C. & Kroth, P. G. 2016. Diatom Vacuolar 1,6-beta-Transglycosylases can Functionally Complement the Respective Yeast Mutants. *J Eukaryot Microbiol* **63**:536-46.

Hudon, C. & Bourget, E. 1981. Initial colonization of artificial substrate: community development and structure studied by scanning electron microscopy. *Can J of Fish and Aquat Sci* **38**:1371-84.

Hunter, J. E., Brandsma, J., Dymond, M. K., Koster, G., Moore, C. M., Postle, A. D., Mills, R. A. & Attard, G. S. 2018. Lipidomics of *Thalassiosira pseudonana* under phosphorus stress reveal underlying phospholipid substitution dynamics and novel Diglycosylceramide Substitutes. *Appl Environ Microbiol* **84**.

Jackson, J. 1977. Competition on marine hard substrata: the adaptive significance of solitary and colonial strategies. *The American Naturalist* **111**:743-67.

Kamerlin, S. C., Sharma, P. K., Prasad, R. B. & Warshel, A. 2013. Why nature really chose phosphate. *Q Rev Biophys* **46**:1-132.

Kaplan, J. B. & Fine, D. H. 2002. Biofilm dispersal of Neisseria subflava and other phylogenetically diverse oral bacteria. *Appl Environ Microbiol* **68**:4943-50.

Kapuscinski, J. 1995. DAPI: a DNA-specific fluorescent probe. *Biotech Histochem* **70**:220-33.

Kapuściński, J. & Skoczylas, B. 1978. Fluorescent complexes of DNA with DAPI 4′, 6-diamidine-2-phenyl indole 2HCl or DCI 4′, 6-dicarboxyamide-2-pnenyl indole. *Nucleic Acids Res* **5**:3775-800.

Kilroy, C. & Bothwell, M. 2011. Environmental control of stalk length in the bloom-forming, freshwater benthic diatom *Didymosphenia geminata* (Bacillariophyceae)(1). *J Phycol* **47**:981-9.

Kilroy, C. & Bothwell, M. L. 2012. *Didymosphenia geminata* growth rates and bloom formation in relation to ambient dissolved phosphorus concentration. *Freshwater Biol* **57**:641-53.

Koedooder, C., Stock, W., Willems, A., Mangelinckx, S., De Troch, M., Vyverman, W. & Sabbe, K. 2019. Diatom-bacteria interactions modulate the composition and productivity of benthic diatom biofilms. *Front Microbiol* **10**:1255.

Kolozsvari, B., Parisi, F. & Saiardi, A. 2014. Inositol phosphates induce DAPI fluorescence shift. *Biochem J* **460**:377-85.

Kooistra, W. H., De Stefano, M., Mann, D. G., Salma, N. & Medlin, L. K. 2003. Phylogenetic position of *Toxarium*, a pennate-like lineage within centric diatoms (bacillariophyceae) 1. *J Phycol* **39**:185-97.

Kornberg, A., Kornberg, S. & Simms, E. S. 1956. Metaphosphate synthesis by an enzyme from *Escherichia coli*. *Biochimica et biophysica acta* **20**:215-27.

Koski-Vähälä, J. & Hartikainen, H. 2001. Assessment of the risk of phosphorus loading due to resuspended sediment. *J Environ Qual* **30**:960-66.

Kroth, P. G., Chiovitti, A., Gruber, A., Martin-Jezequel, V., Mock, T., Parker, M. S., Stanley, M. S., Kaplan, A., Caron, L. & Weber, T. 2008. A model for carbohydrate metabolism in the diatom *Phaeodactylum tricornutum* deduced from comparative whole genome analysis. *PloS one* **3**:e1426.

Kuenzler, E. J. & Perras, J. P. 1965. Phosphatases of marine algae. *The Biological Bulletin* **128**:271-84.

Kuhl, A. 1974. Phosphorus In: Stewart WDP, editor. Algal Physiology and Biochemistry. Oxford: Blackwell Scientific.

Kulaev, I. S., Vagabov, V. & Kulakovskaya, T. 2004. *The biochemistry of inorganic polyphosphates.* John Wiley & Sons.

Lachnit, M., Buhmann, M. T., Klemm, J., Kroger, N. & Poulsen, N. 2019. Identification of proteins in the adhesive trails of the diatom *Amphora coffeaeformis*. *Philos Trans R Soc Lond B Biol Sci* **374**:20190196.

Lapointe, A., Spiteller, D. & Kroth, P. G. 2022. High throughput method for extracting polyphosphates from diatoms. *Endocyt Cell Res* **31**:29-38.

Larned, S. T. 2010. A prospectus for periphyton: recent and future ecological research. *J N Am Benthol Soc* **29**:182-206.

Larned, S. T., Nikora, V. I. & Biggs, B. J. 2004. Mass-transfer-limited nitrogen and phosphorus uptake by stream periphyton: A conceptual model and experimental evidence. *Limnol Oceanogr* **49**:1992-2000.

Lee, W. D., Gawri, R., Shiba, T., Ji, A. R., Stanford, W. L. & Kandel, R. A. 2018. Simple silica column-based method to quantify inorganic polyphosphates in cartilage and other tissues. *Cartilage* **9**:417-27.

Leinweber, K. & Kroth, P. G. 2015. Capsules of the diatom *Achnanthidium minutissimum* arise from fibrillar precursors and foster attachment of bacteria. *PeerJ* **3**:e858.

Leinweber, K., Muller, S. & P, G. K. 2016. A semi-automated, KNIME-based workflow for biofilm assays. *BMC Microbiol* **16**:61.

Leitão, J. M., Lorenz, B., Bachinski, N., Wilhelm, C., Müller, W. E. & Schröder, H. C. 1995. Osmotic-stress-induced synthesis and degradation of inorganic polyphosphates in the alga *Phaeodactylum tricornutum*. *Mar Ecol Prog Ser* **121**:279-88.

Letáková, M., Fránková, M. & Poulíčková, A. 2018. Ecology and Applications of Freshwater Epiphytic Diatoms — Review. *Cryptogamie Algol* **39**:3-22.

Levasseur, M., Thompson, P. A. & Harrison, P. J. 1993. Physiological acclimation of marine phytoplankton to different nitrogen sources 1. *J Phycol* **29**:587-95.

Levitan, O., Dinamarca, J., Zelzion, E., Lun, D. S., Guerra, L. T., Kim, M. K., Kim, J., Van Mooy, B. A., Bhattacharya, D. & Falkowski, P. G. 2015. Remodeling of intermediate metabolism in the diatom *Phaeodactylum tricornutum* under nitrogen stress. *P Natl A Sci* **112**:412-17.

Lewis, R. J., Johnson, L. M. & Hoagland, K. D. 2002. Effects of cell density, temperature, and light intensity on growth and stalk production in the biofouling diatom *Achnanthes longipes* (Bacillariophyceae) 1. *J Phycol* **38**:1125-31.

Li, J. & Dittrich, M. 2019. Dynamic polyphosphate metabolism in cyanobacteria responding to phosphorus availability. *Environ Microbiol* **21**:572-83.

Li, J., Plouchart, D., Zastepa, A. & Dittrich, M. 2019. Picoplankton accumulate and recycle polyphosphate to support high primary productivity in coastal Lake Ontario. *Sci Rep* **9**:19563.

Li, T., Guo, C., Zhang, Y., Wang, C., Lin, X. & Lin, S. 2018. Identification and expression analysis of an atypical alkaline phosphatase in *Emiliania huxleyi*. *Front Microbiol* **9**:2156.

Lieberman, L. 1890. Detection of metaphosphoric acid in the nuclein of yeast. *Pflugers Arch* **47**:155-60.

Lin, H. Y., Shih, C. Y., Liu, H. C., Chang, J., Chen, Y. L., Chen, Y. R., Lin, H. T., Chang, Y. Y., Hsu, C. H. & Lin, H. J. 2013. Identification and characterization of an extracellular alkaline phosphatase in the marine diatom *Phaeodactylum tricornutum*. *Mar Biotechnol (NY)* **15**:425-36.

Lin, S., Litaker, R. W. & Sunda, W. G. 2016. Phosphorus physiological ecology and molecular mechanisms in marine phytoplankton. *J Phycol* **52**:10-36.

Liss, E. & Langen, P. 1962. Experiments on polyphosphate overcompensation in yeast cells after phosphate deficiency. *Archiv fur Mikrobiologie* **41**:383-92.

Litchman, E. & Nguyen, B. L. 2008. Alkaline phosphatase activity as a function of internal phosphorus concentration in freshwater phytoplankton. *J Phycol* **44**:1379-83.

Lombard, V., Golaconda Ramulu, H., Drula, E., Coutinho, P. M. & Henrissat, B. 2014. The carbohydrate-active enzymes database (CAZy) in 2013. *Nucleic Acids Res* **42**:D490-D95.

Lovio-Fragoso, J. P., de Jesus-Campos, D., Lopez-Elias, J. A., Medina-Juarez, L. A., Fimbres-Olivarria, D. & Hayano-Kanashiro, C. 2021. Biochemical and molecular aspects of phosphorus limitation in diatoms and their relationship with biomolecule accumulation. *Biology (Basel)* **10**.

Mackey, K. R. M., Van Mooy, B., Cade-Menun, B. J. & Paytan, A. 2019. Phosphorus dynamics in the environment. *Reference Module in Life Sciences.*

Malviya, S., Scalco, E., Audic, S., Vincent, F., Veluchamy, A., Poulain, J., Wincker, P., Iudicone, D., de Vargas, C., Bittner, L., Zingone, A. & Bowler, C. 2016. Insights into global diatom distribution and diversity in the world's ocean. *Proc Natl Acad Sci U S A* **113**:E1516-25.

Mann, A. J., Hahnke, R. L., Huang, S., Werner, J., Xing, P., Barbeyron, T., Huettel, B., Stüber, K., Reinhardt, R. & Harder, J. 2013. The genome of the alga-associated marine flavobacterium *Formosa agariphila* KMM 3901T reveals a broad potential for degradation of algal polysaccharides. *Appl Env Microb* **79**:6813-22.

Mann, D. 1985. In vivo observations of plastid and cell division in raphid diatoms and their relevance to diatom systematics. *Ann Bot-London* **55**:95-108.

Mann, D. G. 1981. Sieves and flaps: siliceous minutiae in the pores of raphid diatoms. *Proceedings of the 6th Symposium on Recent and Fossil Diatoms.* O. Koeltz Koenigstein, pp. 279-300.

Manzini, G., Barcellona, M., Avitabile, M. & Quadrifoglio, F. 1983. Interaction of diamidino-2-phenylindole (DAPI) with natural and synthetic nucleic acids. *Nucleic Acids Res* **11**:8861-76.

Martin, P., Dyhrman, S. T., Lomas, M. W., Poulton, N. J. & Van Mooy, B. A. 2014. Accumulation and enhanced cycling of polyphosphate by Sargasso Sea plankton in response to low phosphorus. *Proc Natl Acad Sci U S A* **111**:8089-94.

Martin, P., Lauro, F. M., Sarkar, A., Goodkin, N., Prakash, S. & Vinayachandran, P. N. 2018. Particulate polyphosphate and alkaline phosphatase activity across a latitudinal transect in the tropical Indian Ocean. *Limnol Oceanogr* **63**:1395-406.

Martin, P. & Van Mooy, B. A. 2013. Fluorometric quantification of polyphosphate in environmental plankton samples: extraction protocols, matrix effects, and nucleic acid interference. *Appl Environ Microbiol* **79**:273-81.

Martin, P., Van Mooy, B. A., Heithoff, A. & Dyhrman, S. T. 2011. Phosphorus supply drives rapid turnover of membrane phospholipids in the diatom *Thalassiosira pseudonana*. *ISME J* **5**:1057-60.

Martiny, A. C., Lomas, M. W., Fu, W., Boyd, P. W., Chen, Y.-l. L., Cutter, G. A., Ellwood, M. J., Furuya, K., Hashihama, F. & Kanda, J. 2019. Biogeochemical controls of surface ocean phosphate. *Science advances* **5**:eaax0341.

McKew, B. A., Taylor, J. D., McGenity, T. J. & Underwood, G. J. 2011. Resistance and resilience of benthic biofilm communities from a temperate saltmarsh to desiccation and rewetting. *ISME J* **5**:30-41.

Michael Beman, J., Arrigo, K. R. & Matson, P. A. 2005. Agricultural runoff fuels large phytoplankton blooms in vulnerable areas of the ocean. *Nature* **434**:211-14.

Mojzes, P., Gao, L., Ismagulova, T., Pilatova, J., Moudrikova, S., Gorelova, O., Solovchenko, A., Nedbal, L. & Salih, A. 2020. Guanine, a high-capacity and rapid-turnover nitrogen reserve in microalgal cells. *Proc Natl Acad Sci U S A* **117**:32722-30.

Molino, P. J. & Wetherbee, R. 2008. The biology of biofouling diatoms and their role in the development of microbial slimes. *Biofouling* **24**:365-79.

Møller, M., Myklestad, S. & Haug, A. 1975. Alkaline and acid phosphatases of the marine diatoms *Chaetoceros affinis* var. willei (Gran) Hustedt and *Skeletonema costatum* (Grev.) Cleve. *Journal of Experimental Marine Biology and Ecology* **19**:217-26.

Morin, S., Duong, T. T., Dabrin, A., Coynel, A., Herlory, O., Baudrimont, M., Delmas, F., Durrieu, G., Schafer, J., Winterton, P., Blanc, G. & Coste, M. 2008. Long-term survey of heavy-metal pollution, biofilm contamination and diatom community structure in the Riou Mort watershed, South-West France. *Environ Pollut* **151**:532-42.

Moudrikova, S., Sadowsky, A., Metzger, S., Nedbal, L., Mettler-Altmann, T. & Mojzes, P. 2017. Quantification of polyphosphate in microalgae by raman microscopy and by a reference enzymatic assay. *Anal Chem* **89**:12006-13.

Murata, K., Hagiwara, S., Kimori, Y. & Kaneko, Y. 2016. Ultrastructure of compacted DNA in cyanobacteria by high-voltage cryo-electron tomography. *Sci Rep* **6**:34934.

Neef, D. W. & Kladde, M. P. 2003. Polyphosphate loss promotes SNF/SWI-and Gcn5-dependent mitotic induction of PHO5. *Molecular and cellular biology* **23**:3788-97.

Nielsen, E. S. & Rochon, T. 1976. The Influence of extremely high concentrations of inorganic P at varying pH on the growth and photosynthesis of unicellular algae. *Internationale Revue der gesamten Hydrobiologie und Hydrographie* **61**:407-15.

Ogawa, N., DeRisi, J. & Brown, P. O. 2000. New components of a system for phosphate accumulation and polyphosphate metabolism in *Saccharomyces cerevisiae* revealed by genomic expression analysis. *Molecular biology of the cell* **11**:4309-21.

Ohtomo, R., Sekiguchi, Y., Kojima, T. & Saito, M. 2008. Different chain length specificity among three polyphosphate quantification methods. *Anal Biochem* **383**:210-6.

Omelon, S., Georgiou, J. & Habraken, W. 2016. A cautionary (spectral) tail: red-shifted fluorescence by DAPI-DAPI interactions. *Biochem Soc Trans* **44**:46-9.

Orchard, E. D., Benitez-Nelson, C. R., Pellechia, P. J., Lomas, M. W. & Dyhrman, S. T. 2010. Polyphosphate in *Trichodesmium* from the low-phosphorus Sargasso Sea. *Limnol Oceanogr* **55**:2161-69.

Ostrowski, M., Mazard, S., Tetu, S. G., Phillippy, K., Johnson, A., Palenik, B., Paulsen, I. T. & Scanlan, D. J. 2010. PtrA is required for coordinate regulation of gene expression during phosphate stress in a marine *Synechococcus*. *ISME J* **4**:908-21.

Ou, L., Qin, X., Shi, X., Feng, Q., Zhang, S., Lu, S. & Qi, Y. 2020. Alkaline phosphatase activities and regulation in three harmful *Prorocentrum* species from the coastal waters of the East China Sea. *Microb Ecol* **79**:459-71.

Passy, S. I. 2007. Diatom ecological guilds display distinct and predictable behavior along nutrient and disturbance gradients in running waters. *Aquat Bot* **86**:171-78.

Patil, J. S. & Anil, A. C. 2005. Biofilm diatom community structure: influence of temporal and substratum variability. *Biofouling* **21**:189-206.

Paytan, A. & McLaughlin, K. 2007. The oceanic phosphorus cycle. *Chem Rev* **107**:563-76.

Perry, M. 1976. Phosphate utilization by an oceanic diatom in phosphorus-limited chemostat culture and in the oligotrophic waters of the central North Pacific 1. *Limnol Oceanogr* **21**:88-107.

Petri, M. 2006. Water quality of lake constance. *The rhine*:127-38.

Pickett-Heaps, J., Hill, D. R. & Blaze, K. L. 1991. Active gliding motility in an araphid marine diatom, *Ardissonea* (formerly *synedra*) *crystallina*. *J Phycol* **27**:718-25.

Pierella Karlusich, J. J., Ibarbalz, F. M. & Bowler, C. 2020. Phytoplankton in the Tara ocean. *Annu Rev Mar Sci* **12**:233-65.

Pinseel, E., Vanormelingen, P., Hamilton, P. B., Vyverman, W., Van de Vijver, B. & Kopalova, K. 2017. Molecular and morphological characterization of the *Achnanthidium minutissimum* complex (Bacillariophyta) in Petuniabukta (Spitsbergen, High Arctic) including the description of *A. digitatum* sp. nov. *Eur J Phycol* **52**:264-80.

Plouviez, M., Fernandez, E., Grossman, A. R., Sanz-Luque, E., Sells, M., Wheeler, D. & Guieysse, B. 2021. Responses of *Chlamydomonas reinhardtii* during the transition from P-deficient to P-sufficient growth (the P-overplus response): The roles of the vacuolar transport chaperones and polyphosphate synthesis. *J Phycol* **57**:988-1003.

Pokhrel, A., Lingo, J. C., Wolschendorf, F. & Gray, M. J. 2019. Assaying for inorganic polyphosphate in bacteria. *J Vis Exp*.

Potapova, M. & Hamilton, P. B. 2007. Morphological and Ecological Variation within the *Achnanthidium minutissimum* (Bacillariophyceae) Species Complex. *J Phycol* **43**:561-75.

Rao, N. N., Gomez-Garcia, M. R. & Kornberg, A. 2009. Inorganic polyphosphate: essential for growth and survival. *Annu Rev Biochem* **78**:605-47.

Rao, N. N., Liu, S. & Kornberg, A. 1998. Inorganic polyphosphate in *Escherichia coli*: the phosphate regulon and the stringent response. *J Bacteriol* **180**:2186-93.

Rashid, M. H., Rumbaugh, K., Passador, L., Davies, D. G., Hamood, A. N., Iglewski, B. H. & Kornberg, A. 2000. Polyphosphate kinase is essential for biofilm development, quorum sensing, and virulence of *Pseudomonas aeruginosa*. *P Natl A Sci* **97**:9636-41.

Reyes-Prieto, A., Hackett, J. D., Soares, M. B., Bonaldo, M. F. & Bhattacharya, D. 2006. Cyanobacterial contribution to algal nuclear genomes is primarily limited to plastid functions. *Curr Biol* **16**:2320-25.

Rhee, G. Y. 1973. A continuous culture study of phosphate uptake, growth rate and polyphosphate in *Scenedesmus* sp. 1. *J Phycol* **9**:495-506.

Riber, H. H. & Wetzel, R. G. 1987. Boundary-layer and internal diffusion effects on phosphorus fluxes in lake periphyton 1. *Limnol Oceanogr* **32**:1181-94.

Rier, S. T., Kinek, K. C., Hay, S. E. & Francoeur, S. N. 2016. Polyphosphate plays a vital role in the phosphorus dynamics of stream periphyton. *Freshw Sci* **35**:490-502.

Rimet, F., Ector, L., Cauchie, H.-M. & Hoffmann, L. 2009. Changes in diatom-dominated biofilms during simulated improvements in water quality: implications for diatom-based monitoring in rivers. *Eur J Phycol* **44**:567-77.

Romann, J., Valmalette, J.-C., Røyset, A. & Einarsrud, M.-A. 2015. Optical properties of single diatom frustules revealed by confocal microspectroscopy. *Opt lett* **40**:740-43.

Round, F. E. 2004. pH scaling and diatom distribution. *Diatom* **20**:9-12.

Ruiz, F. A., Marchesini, N., Seufferheld, M., Govindjee & Docampo, R. 2001. The polyphosphate bodies of *Chlamydomonas reinhardtii* possess a proton-pumping pyrophosphatase and are similar to acidocalcisomes. *J Biol Chem* **276**:46196-203.

Santos-Beneit, F. 2015. The Pho regulon: a huge regulatory network in bacteria. *Front Microbiol* **6**:402.

Sanz-Luque, E., Bhaya, D. & Grossman, A. R. 2020. Polyphosphate: a multifunctional metabolite in cyanobacteria and algae. *Front Plant Sci* **11**:938.

Schelske, C. L. & Sicko-Goad, L. 1990. Effect of chelated trace metals on phosphorus uptake and storage in natural assemblages of Lake Michigan phytoplankton. *J Great Lakes Res* **16**:82-89.

Schlösser, U. G. 1994. SAG-Sammlung von Algenkulturen at the University of Göttingen Catalogue of Strains 1994. *Botanica Acta* **107**:113-86.

Schmitter, R. E. & Jurkiewicz, A. J. 1981. Acid phosphatase localization in PAS-bodies of Gonyaulax. *J Cell Sci* **51**:15-23.

Sforza, E., Calvaruso, C., La Rocca, N. & Bertucco, A. 2018. Luxury uptake of phosphorus in *Nannochloropsis salina* : Effect of P concentration and light on P uptake in batch and continuous cultures. *Biochem Eng J* **134**:69-79.

Sicko-Goad, L. & Lazinsky, D. 1986. Quantitative ultrastructural changes associated with lead-coupled luxury phosphate uptake and polyphosphate utilization. *Arch Environ Conand Tox* **15**:617-27.

Sicko-Goad, L. & Jensen, T. E. 1976. Phosphate metabolism in blue-green algae. II. Changes in phosphate distribution during starvation and the “polyphosphate overplus” phenomenon in *Plectonema boryanum*. *Am J Bot* **63**:183-88.

Smirnov, A., Suzina, N., Kulakovskaia, T. & Kulaev, I. 2002. Magnesium orthophosphate, a new form of reserve phosphates in the halophilic archaeon *Halobacterium salinarium*. *Mikrobiologiia* **71**:786-93.

Smith, D. J. & Underwood, G. J. 2000. The production of extracellular carbohydrates by estuarine benthic diatoms: the effects of growth phase and light and dark treatment. *J Phycol* **36**:321-33.

Smith, S. A. & Morrissey, J. H. 2007. Sensitive fluorescence detection of polyphosphate in polyacrylamide gels using 4',6-diamidino-2-phenylindol. *Electrophoresis* **28**:3461-5.

Smith, S. A., Wang, Y. & Morrissey, J. H. 2018. DNA ladders can be used to size polyphosphate resolved by polyacrylamide gel electrophoresis. *Electrophoresis* **39**:2454-59.

Solovchenko, A., Gorelova, O., Karpova, O., Selyakh, I., Semenova, L., Chivkunova, O., Baulina, O., Vinogradova, E., Pugacheva, T., Scherbakov, P., Vasilieva, S., Lukyanov, A. & Lobakova, E. 2020. Phosphorus feast and famine in cyanobacteria: is luxury uptake of the nutrient just a consequence of acclimation to its shortage? *Cells* **9**.

Somanader, E., Sreenivas, R., Siavash, G., Rodriguez, N., Gao, T., Ehrlich, H. & Rahman, M. A. 2022. Polysaccharide Stalks in *Didymosphenia geminata* Diatom: real world applications and strategies to combat its spread. *Polysaccharides* **3**:83-94.

Šponer, J., Mládek, A., Šponer, J. E., Svozil, D., Zgarbová, M., Banáš, P., Jurečka, P. & Otyepka, M. 2012. The DNA and RNA sugar–phosphate backbone emerges as the key player. An overview of quantum-chemical, structural biology and simulation studies. *Phys Chem Cheml Phys* **14**:15257-77.

Staats, N., Stal, L. J., de Winder, B. & Mur, L. R. 2000. Oxygenic photosynthesis as driving process in exopolysaccharide production of benthic diatoms. *Mar Ecol Prog Ser* **193**:261-69.

Steele, D. J., Franklin, D. J. & Underwood, G. J. 2014. Protection of cells from salinity stress by extracellular polymeric substances in diatom biofilms. *Biofouling* **30**:987-98.

Stock, A. M., Robinson, V. L. & Goudreau, P. N. 2000. Two-component signal transduction. *Annu Rev Biochem* **69**:183-215.

Sutherland, I. W. 1988. Bacterial surface polysaccharides: structure and function. *Int Rev Cyt* **113**:187-231.

Terrapon, N., Lombard, V., Drula, E., Lapébie, P., Al-Masaudi, S., Gilbert, H. J. & Henrissat, B. 2018. PULDB: the expanded database of Polysaccharide Utilization Loci. *Nucleic Acids Res* **46**:D677-D83.

Thibaud, M. C., Arrighi, J. F., Bayle, V., Chiarenza, S., Creff, A., Bustos, R., Paz-Ares, J., Poirier, Y. & Nussaume, L. 2010. Dissection of local and systemic transcriptional responses to phosphate starvation in *Arabidopsis*. *Plant J* **64**:775-89.

Thienpont, J. R., Johnson, D., Nesbitt, H., Kokelj, S. V., Pisaric, M. F. J. & Smol, J. P. 2012. Arctic coastal freshwater ecosystem responses to a major saltwater intrusion: A landscape-scale palaeolimnological analysis. *The Holocene* **22**:1451-60.

Tijssen, J., Beekes, H. & Van Steveninck, J. 1982. Localization of polyphosphates in *Saccharomyces fragilis*, as revealed by 4′, 6-diamidino-2-phenylindole fluorescence. *Biochimica et Biophysica Acta (BBA)-Molecular Cell Research* **721**:394-98.

Tilman, D., Fargione, J., Wolff, B., D'antonio, C., Dobson, A., Howarth, R., Schindler, D., Schlesinger, W. H., Simberloff, D. & Swackhamer, D. 2001. Forecasting agriculturally driven global environmental change. *science* **292**:281-84.

Trilisenko, L., Kulakovskaya, E. & Kulakovskaya, T. 2017. The cadmium tolerance in *Saccharomyces cerevisiae* depends on inorganic polyphosphate. *J Basic Microbiol* **57**:982-86.

Tyrrell, T. 1999. The relative influences of nitrogen and phosphorus on oceanic primary production. *Nature* **400**:525-31.

Underwood, G. & Kromkamp, J. 2000. Primary production by phytoplancton and microphytoplancton in estuaries. *Estuaries, advances in ecological research. Academic Press, London*:93-153.

Underwood, G. J. & Paterson, D. M. 2003. The importance of extracellular carbohydrate production by marine epipelic diatoms. *Advs Bot Res* **40**:183-240.

van der Grinten, E., Janssen, A. P. H. M., de Mutsert, K., Barranguet, C. & Admiraal, W. 2005. Temperature- and light-dependent performance of the cyanobacterium *Leptolyngbya Foveolarum* and the diatom *Nitzschia perminuta* in mixed biofilms. *Hydrobiologia* **548**:267-78.

Van Mooy, B. A., Fredricks, H. F., Pedler, B. E., Dyhrman, S. T., Karl, D. M., Koblizek, M., Lomas, M. W., Mincer, T. J., Moore, L. R., Moutin, T., Rappe, M. S. & Webb, E. A. 2009. Phytoplankton in the ocean use non-phosphorus lipids in response to phosphorus scarcity. *Nature* **458**:69-72.

Vershinina, O. & Znamenskaya, L. 2002. The Pho regulons of bacteria. *Microbiology* **71**:497-511.

Vishwakarma, V. 2020. Impact of environmental biofilms: Industrial components and its remediation. *J Basic Microbiol* **60**:198-206.

Wang, Y., Chen, Y., Lavin, C. & Gretz, M. R. 2000. Extracellular matrix assembly in diatoms (Bacillariophyceae). iv. ultrastructure of *Achnanthes longipes* and *Cymbella cistula* as revealed by high-pressure freezing/freeze substituton and cryo-field emission scanning electron microscopy. *J Phycol* **36**:367-78.

Weeks, M. E. 1933. The discovery of the elements. XXI. Supplementary note on the discovery of phosphorus. *Journal of Chemical Education* **10**:302.

Werner, T. P., Amrhein, N. & Freimoser, F. M. 2005. Novel method for the quantification of inorganic polyphosphate (iPoP) in *Saccharomyces cerevisiae* shows dependence of iPoP content on the growth phase. *Arch Microbiol* **184**:129-36.

Werner, T. P., Amrhein, N. & Freimoser, F. M. 2007. Inorganic polyphosphate occurs in the cell wall of *Chlamydomonas reinhardtii* and accumulates during cytokinesis. *BMC Plant Biol* **7**:51.

Westheimer, F. H. 1987. Why nature chose phosphates. *Science* **235**:1173-78.

Wetherbee, R., Lind, J. L., Burke, J. & Quatrano, R. S. 1998. Minireview—the first kiss: establishment and control of initial adhesion by raphid diatoms. *J Phycol* **34**:9-15.

Whitton, B. A., Ellwood, N. T. W. & Kawecka, B. 2009. Biology of the freshwater diatom *Didymosphenia*: a review. *Hydrobiologia* **630**:1-37.

Windler, M. 2014. Bacterial Influence on Diatoms from Photoautotrophic Freshwater Biofilms. University of Konstanz.

Windler, M., Gruber, A. & Kroth, P. G. 2012. Purification of benthic diatoms from associated bacteria using the antibiotic imipenem. *Journal of Endocyt Cell Res* **22**:62-65.

Windler, M., Leinweber, K., Bartulos, C. R., Philipp, B. & Kroth, P. G. 2015. Biofilm and capsule formation of the diatom *Achnanthidium minutissimum* are affected by a bacterium. *J Phycol* **51**:343-55.

Wustman, B. A., Gretz, M. R. & Hoagland, K. D. 1997. Extracellular matrix assembly in diatoms (Bacillariophyceae)(I. A model of adhesives based on chemical characterization and localization of polysaccharides from the marine diatom *Achnanthes longipes* and other diatoms). *Plant Physiology* **113**:1059-69.

Wysokowski, M., Bartczak, P., Żółtowska-Aksamitowska, S., Chudzińska, A., Piasecki, A., Langer, E., Bazhenov, V. V., Petrenko, I., Noga, T. & Stelling, A. L. 2017. Adhesive stalks of diatom *Didymosphenia geminata* as a novel biological adsorbent for hazardous metals removal. *CLEAN–Soil, Air, Water* **45**:1600678.

Xie, L. & Jakob, U. 2019. Inorganic polyphosphate, a multifunctional polyanionic protein scaffold. *J Biol Chem* **294**:2180-90.

Xu, Y., Ma, B. & Nussinov, R. 2012. Structural and functional consequences of phosphate–arsenate substitutions in selected nucleotides: DNA, RNA, and ATP. *The Journal of Physical Chemistry B* **116**:4801-11.

Yamaguchi, H., Yamaguchi, M. & Adachi, M. 2006. Specific-detection of alkaline phosphatase activity in individual species of marine phytoplankton. *Plankton and Benthos Research* **1**:214-17.

Yang, Z. K., Zheng, J. W., Niu, Y. F., Yang, W. D., Liu, J. S. & Li, H. Y. 2014. Systems-level analysis of the metabolic responses of the diatom *Phaeodactylum tricornutum* to phosphorus stress. *Environ Microbiol* **16**:1793-807.

Yoon, H. S., Hackett, J. D., Ciniglia, C., Pinto, G. & Bhattacharya, D. 2004. A molecular timeline for the origin of photosynthetic eukaryotes. *Mol Biol Evol* **21**:809-18.

Young, C. L. & Ingall, E. D. 2010. Marine Dissolved Organic Phosphorus Composition: Insights from Samples Recovered Using Combined Electrodialysis/Reverse Osmosis. *Aquat Geochem* **16**:563-74.

Zhang, X., Roeffaers, M. B., Basu, S., Daniele, J. R., Fu, D., Freudiger, C. W., Holtom, G. R. & Xie, X. S. 2012. Label-free live-cell imaging of nucleic acids using stimulated Raman scattering microscopy. *Chemphyschem* **13**:1054-9.